CO$_2$ wettability of seal and reservoir rocks and the implications for carbon geo-sequestration

Stefan Iglauer[1], C. H. Pentland[2], and A. Busch[2]

[1]Department of Petroleum Engineering, Curtin University, Kensington, Western Australia, [2]Shell Global Solutions International B.V., Rijswijk, Netherlands

Abstract We review the literature data published on the topic of CO$_2$ wettability of storage and seal rocks. We first introduce the concept of wettability and explain why it is important in the context of carbon geo-sequestration (CGS) projects, and review how it is measured. This is done to raise awareness of this parameter in the CGS community, which, as we show later on in this text, may have a dramatic impact on structural and residual trapping of CO$_2$. These two trapping mechanisms would be severely and negatively affected in case of CO$_2$-wet storage and/or seal rock. Overall, at the current state of the art, a substantial amount of work has been completed, and we find that:

- Sandstone and limestone, plus pure minerals such as quartz, calcite, feldspar, and mica are strongly water wet in a CO$_2$-water system.

- Oil-wet limestone, oil-wet quartz, or coal is intermediate wet or CO$_2$ wet in a CO$_2$-water system.

- The contact angle alone is insufficient for predicting capillary pressures in reservoir or seal rocks.

- The current contact angle data have a large uncertainty.

- Solid theoretical understanding on a molecular level of rock-CO$_2$-brine interactions is currently limited.

- In an ideal scenario, all seal and storage rocks in CGS formations are tested for their CO$_2$ wettability.

- Achieving representative subsurface conditions (especially in terms of the rock surface) in the laboratory is of key importance but also very challenging.

1. Introduction

The storage of greenhouse gases in the earth's subsurface, a process known as carbon geo-sequestration (CGS), is currently considered as a method to limit anthropogenic greenhouse gas emissions to the atmosphere. In CGS, it is proposed that carbon dioxide (CO$_2$), the most important greenhouse gas, is collected from large point-source emitters such as coal-fired power stations, purified, compressed, and injected deep underground into geological storage formations [*IPCC*, 2005]. To date, CGS has been applied on an industrial scale for natural gas separation [e.g., *Arts et al.*, 2008; *Ringrose et al.*, 2009], while application to other industries is progressing. However, CGS is a relatively new technology that is still pending demonstration on a wider industrial level. Potential associated risks with CGS result in negative public perception or high regulatory hurdles to an extent that projects have been stopped in different stages of planning, such as the Barendrecht project in the Netherlands [*Brunsting et al.*, 2011] or the Altmark project in Germany [*Kuehn et al.*, 2012].

The main risk considered for CGS is the leakage of CO$_2$ through natural (e.g., faults, fractures) or man-made (e.g., wells) routes to the atmosphere: CO$_2$ is buoyant and flows upward at given storage conditions. To prevent leakage and mitigate upward migration, several physicochemical storage mechanisms have been proposed and investigated, and these include: structural trapping [e.g., *Hesse et al.*, 2008], residual trapping [e.g., *Juanes et al.*, 2006], dissolution trapping [e.g., *Iglauer*, 2011], and mineral trapping [e.g., *Gaus*, 2010]. An additional proposed way of storing CO$_2$ in clay-rich sandstone formations is by physical adsorption of CO$_2$ on clay surfaces and in clay interlayers [e.g., *Busch et al.*, 2008; *Giesting et al.*, 2012]. Generally, careful

selection of the storage formation is required to ensure that the above mechanisms are effective and prevent any movement of CO_2 back to the surface.

In a nutshell, residual trapping in a reservoir is a process through which micrometer scale CO_2 bubbles are immobilized by capillary forces within the complex pore morphology of the storage rock [*Iglauer et al.*, 2011a]. Here the magnitude of the capillary force equals or exceeds the buoyancy force rendering the CO_2 clusters motionless when CO_2 dissolution or mineralization are not considered. In dissolution trapping, CO_2 dissolves into the water already present in the storage formation. As dissolution proceeds, the water phase density will increase [*Li et al.*, 2004], resulting in downward convective flow of CO_2 saturated water [*Lindeberg and Wessel-Berg*, 1997]. Finally, chemical reactions between CO_2, water, ions dissolved in the water, and formation minerals can result in CO_2 being permanently stored as a solid mineral phase; a process termed mineral trapping.

Structural trapping is considered as the principal storage mechanism. Residual and dissolution processes can be significant too, especially during the injection phase which can typically last for tens of years. In structural trapping, impermeable (or low permeability) rocks such as mudrocks, anhydrite, halite, or tight carbonates act as a barrier to the upward buoyant migration of CO_2, resulting in the retention of CO_2 within a storage formation. This is also the typical process witnessed in hydrocarbon and nonhydrocarbon gas accumulations [*Berg*, 1975; *Watts*, 1987]. These geological settings have been observed many times over the last 100 years, and the associated reservoir fluid statics and dynamics are well understood and routinely predicted with reservoir simulators in hydrocarbon recovery scenarios.

However, there is one important but poorly understood physicochemical factor which highly influences the trapping processes (especially structural and residual trapping), namely the wettability of geologic minerals in the presence of CO_2 and formation brines [*Tokunaga and Wan*, 2013]. Wettability of rock is, in essence, the preference of one fluid over another to be in contact with the rock's surface. Although the definition is simple, the expression of wettability at reservoir-scale—or even in a standard core plug—is complex because of the highly convoluted interplay of surface free energies of the phases, complex pore morphologies, and general heterogeneities of these parameters in the reservoir at various length scales. This text addresses wettability in the CGS context to raise awareness of this phenomenon. We first discuss the physicochemical background of wettability and its influence on CO_2 trapping, including experimental methods to measure wettability. This is followed by an overview of transport and residual trapping of CO_2 in reservoir rocks as well as structural CO_2 trapping below geological seal formations. We then review all available relevant literature data to provide an informed guide for reservoir flow predictions and risk assessments.

In oil-water systems, it has been shown that wettability deviating from water-wet can result in higher amounts of mobile compared to trapped oil [*Anderson*, 1987a; *Jadhunandan and Morrow*, 1995]. If the same behavior were to occur in CO_2-water systems then CO_2 plumes would be extended (e.g., in an open aquifer where a structural trap is missing) if the system were to be less water-wet. In case of a structural trap more mobile CO_2 will result in potentially higher CO_2 column heights and therefore increased pressures acting on the caprock. This again might increase the risk of exceeding either the fracturing or the capillary entry pressure of the formation with possible consequences on shallow saline or drinking water aquifers. Both cases should be considered and risks assessed using adequate reservoir modeling tools.

1.1. Wettability in Geological Carbon Storage

In a three-phase system comprising rock, an aqueous phase liquid and a nonaqueous phase liquid (NAPL), the terms hydrophilic and hydrophobic are commonly used to denote the preference of the aqueous phase to cover, or not to cover, the rock surface, respectively. Wettability directly and strongly influences important variables such as residual NAPL saturations [e.g., *Morrow*, 1990; *Pentland et al.*, 2011; *Chaudhary et al.*, 2013; *Jadhunandan and Morrow*, 1995; *Iglauer et al.*, 2012a], morphology and interfacial areas of fluids [*Iglauer et al.*, 2012a; *Pentland et al.*, 2012], relative permeability [*McCaffery and Bennion*, 1974; *Morrow*, 1990], and the relationship ($p_c[S_w]$) between capillary pressure p_c and aqueous phase saturation S_w which governs the static distribution of reservoir fluids in capillary-buoyancy force equilibrium [*Alam and Donaldson*, 2008; *Jackson et al.*, 2005]. Wettability is therefore a first-order parameter which needs to be appreciated in detail, even though this introduces major physicochemical complexities. In terms of CGS, wettability directly impacts injectivity, containment security, structural and residual trapping capacities, and indirectly
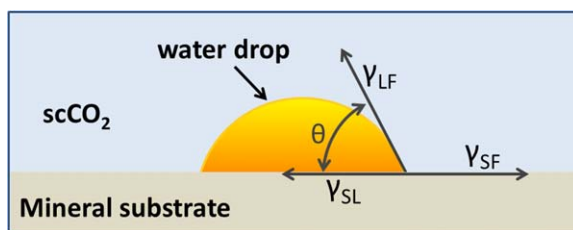
IGLAUER ET AL.   730

Figure 1. Force field acting on a water droplet sitting on a mineral substrate (e.g., single mineral system, seal rock) surrounded by scCO$_2$.

dissolution and mineral trapping capacities (via liquid-liquid and liquid-mineral interface areas)—it is thus crucial that this parameter is assessed sufficiently for risk assessments and storage capacity estimations.

In an immiscible fluid-fluid system such as equilibrated supercritical (sc)CO$_2$-brine, intermolecular forces lead to the typically rapid separation of (hypothetically) molecularly homogenized individual fluid phases (*Atkins and dePaula* [2010] define: "a phase is a form of matter that is uniform throughout in chemical composition and physical state"; this definition of phase is used throughout this text. It should be noted here that depending on salinity and thermophysical conditions up to ∼3 mass % of CO$_2$ dissolve in brine [*Bando et al.*, 2003], and up to ∼1 mol % water dissolves in CO$_2$, [*Sabirzyanov et al.*, 2002]. In addition to such separation, the phases seek to minimize their interfacial areas; this is again caused by intermolecular forces [*Adamson and Gast*, 1997], which can be quantified by the CO$_2$-brine interfacial tension γ. For detailed thermodynamic considerations, please refer to *Atkins and de Paula* [2010] or similar textbooks for a general overview. Following CO$_2$ injection into a reservoir, three immiscible phases (brine, CO$_2$, minerals) interact with each other. In this case, three separate interfacial tensions γ need to be considered: the interfacial tension between the two fluids (in this case CO$_2$ and brine), and each of the two fluids and the solid (mineral phases, e.g., quartz representing a clean sandstone). These three interfacial tensions induce three separate forces which pull the matter into different directions (Figure 1); because all forces are active at the same time (assuming that all other external forces, such as viscous or buoyancy forces, are absent) the resultant force vectors determine the exact fluid configuration on the solid surface, and this configuration is determined by the angle θ between all three phases (Figure 1). This angle is commonly referred to as the contact angle and it is experimentally usually measured through the denser fluid phase (brine in our scenario; note that $\theta = 180 - \alpha$; where α is the contact angle measured through the less dense phase). It is important to understand that this ultimate equilibrium configuration (i.e., the final value of θ) is caused by intermolecular forces. The contact angle can attain any value between [0°; 180°], entirely dependent on the intermolecular force balance. This force balance can be expressed macroscopically by Young's equation (1) [*Young*, 1805]:

$$\cos\theta = \frac{\gamma_{SL} - \gamma_{SF}}{\gamma_{LF}} \tag{1}$$

where γ is the interfacial tension for the liquid-fluid (brine-CO$_2$) (LF), solid-fluid (mineral/rock-CO$_2$) (SF), or solid-liquid (mineral/rock-brine) (SL) interfaces, respectively. γ_{LF} is a function of the molecular interactions which are determined by the chemistry of the fluid and liquid and the thermophysical conditions (pressure, temperature) and is typically quite well understood. The other interfacial forces (γ_{SF} and γ_{SL}) are, however, often not measurable [*Butt et al.*, 2006], and only available through indirect or theoretical approaches (e.g., molecular dynamics or semiempirical equations) [*Good and Girifalco*, 1960], so that θ can usually not simply be calculated via equation (1), but has to be determined experimentally.

This review is dedicated to the discussion of wettability, and in particular θ, in much greater depth, and how it depends on the fluid-liquid system, thermophysical conditions and the rock material itself. In the Petroleum Engineering literature [cf. *Dake*, 1978; *Treiber and Owens*, 1972] three wettabilities based on contact angle are often classified (Figure 2 and Table 1). Such classifications can also be applied to the CO$_2$-brine-rock system with the term oil-wet replaced by the term CO$_2$-wet. These classifications should be compared with the definitions in Physical Chemistry [*Adamson and Gast*, 1997; *Atkins and de Paula*, 2010], where complete wetting or spreading occurs when $\theta = 0°$, partial wetting or spreading happens in the range $0 < \theta < 180°$, and complete nonwetting occurs for $\theta = 180°$. To avoid confusion and to be most precise, the CO$_2$-brine-rock classification tabulated in Table 2 is used in this text.

Note that in the water-wet, intermediate-wet, and CO$_2$-wet cases there is still partial wetting of water. In the case of a low or zero valued θ, the affinity of the water spreading on the solid surface is higher than that of
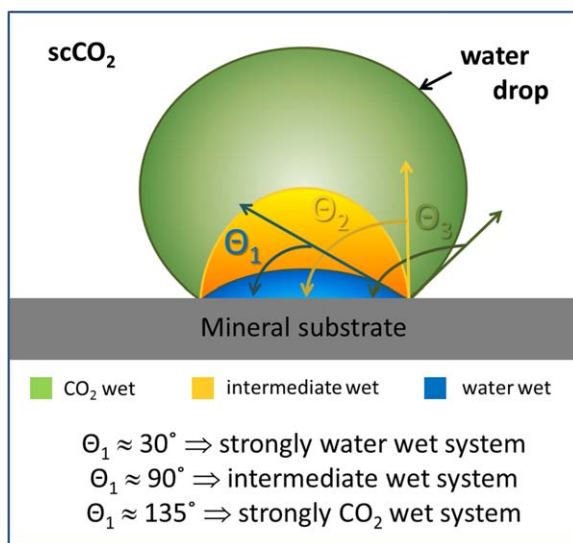
Figure 2. Water, scCO$_2$, and mineral surface system illustrating different contact angles measured through the water phase: strongly water-wet (blue), intermediate-wet (yellow), and CO$_2$-wet (green).

Table 1. Wettabilities Based on Contact Angle From the Petroleum Engineering Literature

Wettability	Treiber and Owens [1972]	Dake [1978]
Water-wet	$0° \leq \theta < 75°$	$0° \leq \theta < 90°$
Intermediate-wet	$75° \leq \theta < 105°$	$\theta = 90°$
Oil-wet	$105° \leq \theta \leq 180°$	$90° < \theta \leq 180°$

the CO$_2$. This affinity can be influenced by variations in pressure, temperature, chemical composition, or entropy. We distinguish the wetting states defined in Table 2 from the term mixed-wet which is used to describe contact angle heterogeneity on the pore-scale, which in turn is influenced by pore-scale mineral heterogeneity. By reviewing contact angles on a mineral by mineral basis in section 2, we aim to provide the basis for a quantitative understanding of mixed-wettabilities when the data are combined with pore-scale mineral heterogeneity mapping techniques [e.g., *Golab et al.*, 2012].

1.2. How the Wettability Phenomenon Influences CO$_2$ Trapping and Retention

1.2.1. Structural Trapping

Wettability directly or indirectly influences all of the processes that trap CO$_2$ in the subsurface. In structural trapping wettability controls the ability of CO$_2$ to enter overlying low permeability strata. Consider the following physical scenario: a buoyant fluid phase exerts a force from below a seal barrier onto both the solid seal rock and the fluids within; the orientation of this buoyancy force is antiparallel to the gravity force and pushes all volumes which have a lower density than the fluids in the seal rock upward, this is schematically illustrated in Figure 3.

Apart from a location near the injection well, where mass transfer can lead to a dry-out effect [e.g., *Pruess and Müller*, 2009; *Berg et al.*, 2013a], CO$_2$ and brine coexist within the pore space of the reservoir into which CO$_2$ has entered; and, on a macroscopic level, a discontinuity in pressure exists across the interface that separates the two fluid phases, this is termed the capillary pressure (p_c):

$$p_c = p_{nw} - p_w \tag{2}$$

where p_{nw} and p_w are the nonwetting and wetting phase pressures, respectively. On a microscopic level (∼1–2 nm for water or n-tridecane) [*Butt et al.*, 2006; *Chang et al.*, 2001], however, the density between the phases changes along the distance of several molecules, corresponding to the size of nanopores; we will not discuss this effect in this article although it may be relevant for the smallest pores in a caprock. The capillary pressure is related to fluid-fluid interface curvature by the Young-Laplace equation [*Laplace*, 1806; *Young*, 1805]:

$$p_c = \gamma \left(\frac{1}{r_1} + \frac{1}{r_2} \right) = \gamma C \tag{3}$$

where γ is the interfacial tension between the immiscible phases and r_1 and r_2 are the principal radii of curvature at any point on the surface (r_1 and r_2 are conventionally defined as positive with respect to the nonwetting phase). C is the curvature of the surface: $C = 1/r_1 + 1/r_2$. When $r_1 = r_2 = r^*$ equation (3) becomes

Table 2. Wettabilities Based on Contact Angle for CO$_2$-Brine-Mineral Systems

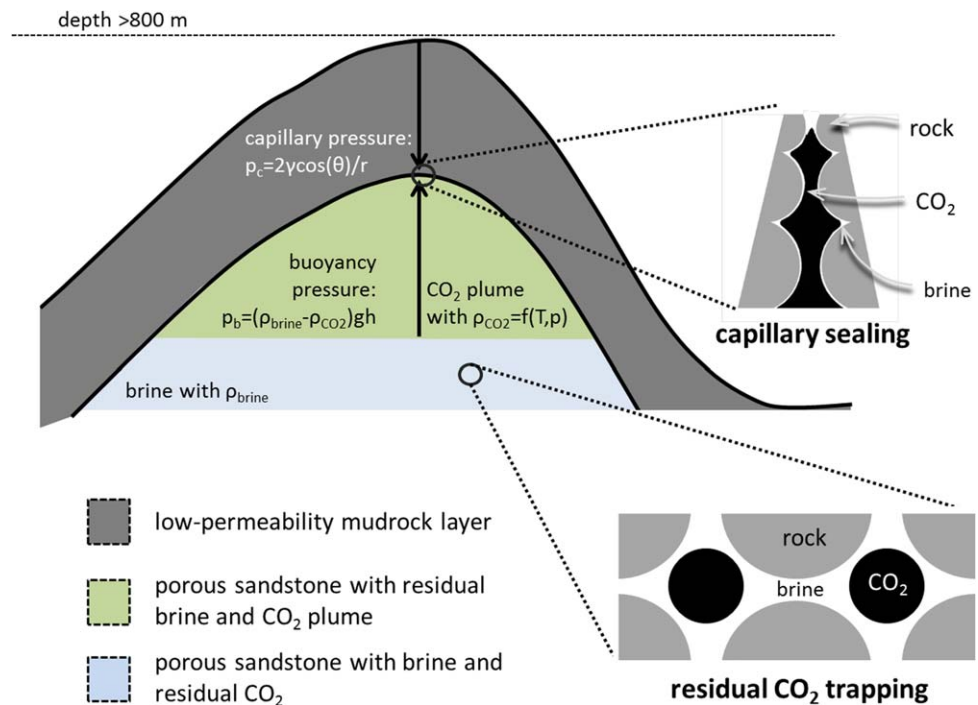| Wettability State	Water Contact Angle θ (°)
Complete wetting or spreading of water	0
Strongly water-wet	0–50
Weakly water-wet	50–70
Intermediate-wet	70–110
Weakly CO$_2$-wet	110–130
Strongly CO$_2$-wet	130–180
Complete nonwetting of water	180

Figure 3. Pressures acting on a fluid column at the reservoir-seal interface for structural trapping. If CO_2 has migrated upward through the underlying water column then a fraction of the CO_2 is residually trapped in the pore space of the reservoir rock. Note that at depths below $\sim$800 m CO_2 is in the supercritical state. The insets on the right side schematically illustrate the pore-scale fluid configurations for a water-wet condition.

$$p_c = \frac{2\gamma}{r^*} \quad (4)$$

However, describing an average p_c arising from interface curvature within a reservoir rock or caprock is highly complex due to the complicated pore morphology. To simplify the description, idealized models are often adopted; one such model being that of a single cylindrical capillary tube with constant cross-sectional inner diameter and ideal surface (i.e., no surface roughness and perfectly homogeneous surface chemistry).

When the curved interface described in equation (4) resides within a cylindrical capillary tube, the radius of the capillary (r') is equal to the product of the radius of the sphere (r^*) and the cosine of the contact angle (θ) between capillary surface and interface ($r' = r^*\cos\theta$) [*Dake*, 1978], thus:

$$p_c = \frac{2\gamma\cos\theta}{r'} \quad (5)$$

note that the interface between the fluid phases is a portion of the surface of a sphere. From equation (5), we see that p_c and r' are inversely proportional: as p_c increases an interface between the two phases can reside in progressively smaller cylindrical tubes of radius r'. This dependency of interface entry into small pores on p_c is the essence of structural trapping where porous shales with very small pores prevent the upward migration of an immiscible buoyant nonwetting phase.

However, the capillary forces acting to prevent the entry of the nonwetting phase are in competition with buoyancy forces. Since structurally trapped CO_2 and brine coexist in the pore space of the invaded rock they maintain pore-scale hydraulic connectivity over the full height of a CO_2 plume (Figure 3 inset). At typical CGS conditions, there will be a density difference between the phases (typically of the order 300–400 kg m^{-3}) resulting in a difference in phase pressures (p_b) caused by buoyancy. p_b is equal to the capillary pressure present in the pore system, between the CO_2 and the brine; p_b increases with CO_2 plume height h and can be described by equation (6):

$$p_b = p_c = \Delta\rho g h \quad (6)$$

where $\Delta\rho$ is the density difference between CO_2 and brine and g is the acceleration due to gravity. When substituting the capillary pressure derived for the circular capillary tube (equation (5)) into equation (6), we obtain:

$$\frac{2\gamma \cos \theta}{r'} = \Delta \rho g h \qquad (7a)$$

$$\Longleftrightarrow \quad h = \frac{2\gamma \cos\theta}{\Delta \rho g r'} \qquad (7b)$$

Equation (7a) gives a first approximation of CO_2 storage capacities by structural trapping when rearranged to equation (7b); however, as mentioned above, the pore morphology of caprock is significantly more complex than a simple circular capillary tube or a bundle of capillary tubes (capillaries with different diameters) [*Dullien*, 1991]. Other pore geometries can be considered in order to appreciate this complexity, e.g., pore network models have been developed (cp. for instance, *Fatt* [1956] or *Ebrahimi et al.* [2013] or direct imaging of the pore space with 3-D X-ray microtomography is now possible [*Blunt et al.*, 2013; *Wildenschild and Sheppard*, 2013]).

1.2.1.1. Risk Scenarios

Since loss of containment is the main risk in CGS, it is reasonable to touch upon consequences of wettability on potential leakage scenarios, i.e., loss of containment. Numerous studies discuss implications of CO_2 leakage on drinking water aquifers or land surface environments in case leakage would occur [e.g., *Birkholzer and Zhou*, 2009; *Pruess*, 2008a, 2008b; *Wang and Clarens*, 2012]. Main leakage scenarios considered, however, are along faults and abandoned wells or hydrodynamic leakage in case of an open aquifer. As discussed earlier, capillary leakage through the caprock is an important aspect but less of a concern than along faults and abandoned wells. Even if wettability would allow the capillary entry pressure to be exceeded, two-phase permeability would be low, resulting in long time scales until CO_2 breakthrough at the top of the caprock would occur [*Busch et al.*, 2010]. Depending on the caprock thickness gas breakthrough will likely only occur after thousands of years. Even then leakage rates can be considered low, with limited hazard to overlying saline aquifers or shallow drinking water horizons. One unknown in this scenario, however, is whether CO_2 percolating into and residing in caprock has any secondary effects, e.g., a geo-chemical or geo-mechanical impact.

1.2.2. Residual Trapping

Residual trapping occurs when clusters of a nonwetting phase are held in place by capillary forces within the confines of the pore space (Figure 3 inset). It takes place primarily during imbibition when the capillary pressure is decreasing, for example, when water is injected into an oil reservoir to enhance recovery or at the trailing edge of a rising CO_2 plume where formation water reinvades the pore space previously occupied by CO_2. Entrapment takes place through the competition between the imbibition processes of piston-like advance and snap-off [*Berg et al.*, 2013b; *Roof*, 1970]. During piston advance pores and throats are filled sequentially with water advancing from one region of pore space to the next. In water-wet systems water can also move through wetting films on the surface of the rock and in crevices. Via this route, it can move ahead of a piston front, which is impeded upon reaching a wide pore, and enter a nearby throat where the wetting films can swell resulting in instability in the nonwetting phase which can lead to rapid disconnection.

This competition is contact angle dependent; snap-off and hence residual trapping of the nonwetting phase are shown to be suppressed for more neutrally wet systems [*Yu and Wardlaw*, 1986], a phenomenon also predicted by network model simulations [*Spiteri et al.*, 2008]. Specifically, wettability influences which phase forms films adjacent to the rock surface [cp. e.g., *Iglauer et al.*, 2012a], thus influencing snap-off processes.

1.2.3. Dissolution and Mineral Trapping

Both dissolution and mineral trapping depend upon the pore-scale configuration of the CO_2 and aqueous phase volumes which is in turn controlled by wettability. For dissolution trapping, the pore-scale configuration of the phases governs the phase interface area [*Pentland et al.*, 2012], which influences the rate of dissolution and thus the transport routes for dissolved CO_2 species [*Iglauer*, 2011]. Once dissolution proceeds the water phase density increases [*Li et al.*, 2004] resulting in a downward convective flow of CO_2 saturated water [*Lindeberg and Wessel-Berg*, 1997], which promotes dissolution trapping. Geochemical reactions will also consequently depend upon the pore-scale configuration of the fluid phases as the configuration determines chemical potentials of the different species in the different phases, e.g., through surface areas and concentration gradients. Furthermore, the distribution of exposed mineral surfaces within the pore space
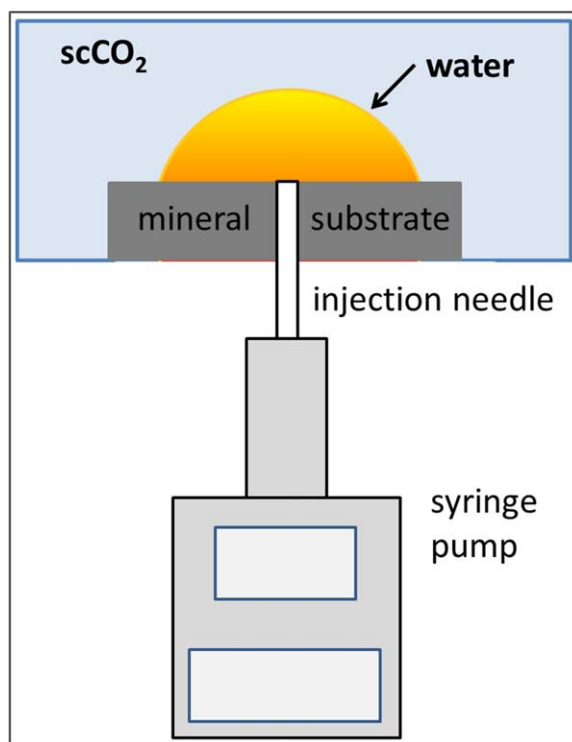
Figure 4. Schematic diagram of a high temperature/high pressure contact angle measurement apparatus used for measuring CO_2/water/mineral contact angles (redrawn from *Kwok and Neumann* [1999]). Note that the precise design of such an apparatus can vary substantially.

affects the kinetics of the reactions. These are complex coupled phenomena, and they remain an area of active research [e.g., *Landrot et al.*, 2012; *Waldmann et al.*, 2014].

1.3. Contact Angle Measurement

We have shown above that the contact angle provides a direct quantification of wettability. There are a number of methods to measure and interpret contact angles and a comprehensive review has been provided previously by *Kwok and Neumann* [1999], the reader is referred to this article for details. Here we only provide a brief overview on the common methods employed in the relevant studies discussed in this review. Moreover, we cover less direct methods to quantify or infer wettability when discussing caprock and reservoir rock, because such additional methodologies are required as contact angle measurements have serious limitations with respect to caprock wettability measurements, this is discussed in more detail below.

1.3.1. Direct Visualization

Most direct methods for measuring contact angles are based on the telescope-goniometer method published by *Bigelow et al.* [1946] and summarized by *Yuan and Lee* [2013]. This direct method brings a droplet (e.g., CO_2) in contact with a mineral surface, which is immersed in a second fluid (e.g., water). This setup is typically housed in a high pressure (HP) cell, and within this cell, pressure, temperature, droplet size, and water salinity can be controlled in order to study the influence of these parameters on the contact angle. Because such HP cells are usually noncommercial setups, their designs, related size, and setups vary. In the literature, the most prominent geometric setups used for determining CO_2/water/mineral contact angles are the sessile or captive drop methods. In the sessile drop method, a water droplet is placed on top of a mineral surface surrounded by a less dense CO_2 atmosphere. This is similar to the captive bubble technique where the fluid droplet (e.g., CO_2) is placed underneath the mineral surface surrounded by water, *Butt et al.* [2006]. In the former case, the contact angle is measured through the wetting phase (water), in the latter case through the nonwetting phase (CO_2), respectively. Both methods are static procedures [e.g., *Bikkina*, 2011; *Dickson et al.*, 2006; *Espinoza and Santamarina*, 2010; *Plug and Bruining*, 2007; *Siemons et al.*, 2006; *Wesch et al.*, 1997; *Yang et al.*, 2008], and strictly speaking such droplets may only be metastable—due to surface roughness and chemical heterogeneity of the surface (this is the reason that contact angles can vary substantially between receding and advancing state); however, it is commonly assumed that they reached true equilibrium so that subsequently the results can be quantified and associated conclusions can be drawn. Experimentally, a drop of fluid is brought in contact with the mineral surface using a small diameter needle connected to a HP pump and an image of the drop is recorded with a camera after a specified equilibration time of the system (cf. Figure 4 for a schematic representation of the sessile drop technique).

Improved methods to the sessile drop technique can vary the drop volume during the measurement. This allows the recording of advancing and receding contact angles (e.g., captive-drop or captive-bubble method) [*Broseta et al.*, 2012; *Chiquet et al.*, 2007; *Shah et al.*, 2008; *Tonnet et al.*, 2010; *Yuan and Lee*, 2013; *Iglauer et al.*, 2014]. Rather common to both methods is the evaluation of the image and the gathering of the contact angle: the macroscopic triple point of contact between the mineral surface, the water and the

CO_2 are located either manually (prone to user-dependent uncertainties) or using image analysis, where a tangent is positioned along the triple line (prone to machine error). We also note here that microscopically the triple point occurs more outward of the macroscopic triple line as the wetting fluid forms a thin tongue (<100 nm thick) on the solid surface [e.g., compare *Hardy*, 1919; *Butt et al.*, 2006], but this phenomenon is outside the scope of the presented discussion.

This experimental method and the associated sample preparation have several limitations including:

1. Sample choice and sample preparation are important. The typical mineral phases considered are calcite, quartz, and mica, while assuming that these are representative of carbonate and siliciclastic reservoirs as well as of clay-rich caprocks, respectively. For quartz, commercial materials are available with a very smooth surface (smooth to an atomic level) that has negligible surface roughness. Other materials are usually naturally occurring ones and a surface is created by cleaving these minerals (e.g., calcite or mica), followed by polishing with extra fine silicon carbide or diamond dust to reduce surface roughness. It is well established that surface roughness can significantly change contact angle and a thorough surface preparation and quantification of surface roughness are crucial for representative results [e.g., *Joanny and de Gennes*, 1984; *Wenzel*, 1949].

2. Cross-equilibration of the fluids in the system CO_2/brine is important to avoid measuring artifacts resulting from the equilibration process. When bringing either a water or a CO_2 droplet in contact with the mineral substrate, the fluids should either be preequilibrated or contact angle should be measured once the system is fully equilibrated (i.e., when contact angle remains constant over time). This, however, will not eliminate any short-term mineralogical changes (e.g., when carbonates are present) that could impact surface properties.

3. Strictly speaking there are no ideal surfaces: surfaces have a certain roughness and may be chemically heterogeneous. As a consequence, the Young's contact angle (which assumes an ideal flat and homogeneous surface) can be measured only with significant uncertainty as it is likely that a metastable droplet is created and observed [*Butt et al.*, 2006]. As a result, typically, the advancing and receding contact angles are reported, and the surface roughness should also be measured to provide meaningful information; generally it is, however, recognized that surface roughness lowers the contact angle (if wetting) and increases the contact angle (if nonwetting) [*Butt et al.*, 2006]. Furthermore, a usual assumption is that the surface is chemically homogeneous; in this context, it is vital that surface contamination is avoided as this can significantly change the contact angle [*Adamson and Gast*, 1997].

4. The droplet for which the contact angle is measured must be sufficiently small (its radius must be smaller than the capillary length) so that gravitational forces do not distort the drop and change the contact angle [*DeGennes et al.*, 2004].

5. If dynamic contact angle measurements (e.g., the Wilhelmy plate method, see below) are conducted one has to take care that the droplet velocity is sufficiently small so that viscous forces do not distort the droplet and change the contact angle [*Elliott and Riddiford*, 1967].

Other direct methods, such as the tilting plate, the Wilhelmy balance, capillary bridge, or other methods, are summarized in *Yuan and Lee* [2013]; these methods have not been used for CGS related measurements.

1.4. Mineralogical and Petrophysical Properties of CO_2 Storage Reservoir and Seal Rocks

We briefly summarize certain parameters indicative of the injection and sealing horizons of currently used CO_2 storage sites (for a detailed geological description standard textbooks can be referred to, e.g., *Folk* [1980]). In addition, we provide some basic characteristics of "standard" sandstones and shales that are discussed in the literature. These data are summarized in Table 3, which provides an overview of these specific rocks. We also note that carbonate reservoirs, which are also considered for CO_2 storage, are mainly composed of calcite and dolomite and usually overlain by tight anhydrite or even halite. A good approximation of carbonate reservoirs is a monomineralic system, and in this sense they are much less complex compared to siliciclastic reservoirs, where five or more dominant mineral phases may occur. The impact of different mineral types on wettability will be discussed in much more detail in the following section 2.

2. CO_2-Wettability of Caprock and Storage Rock Minerals

As outlined in section 1, caprocks, and to a lesser extent storage rocks, can consist of a fairly large variety of minerals (Table 3). At the same time, each mineral is expected to have a different influence on wettability.

Table 3. Mineralogical and Petrophysical Properties of Rocks From Industrial and Demonstration CGS Projects Worldwide and Selected "Standard" Sandstone and Mudrock Samples, Widely Used in the Literature[a]

		Rocks Used in CGS Projects							Rocks Widely Characterized in Literature				
		Sleipner, Norway		In-Salah, Algeria		Ketzin, Germany		Frio, USA	Berea	Bentheimer	Opalinus	Callovo-Oxfordian	Indiana Limestone
		sst	shale	sst	shale	sst	shale	sst	sst	sst	shale	shale	car
		Audigane et al. [2005]	Gaus et al. [2005]	Carroll et al. [2011]	Armitage et al. [2011, 2010]	Norden et al. [2010] and Zemke et al. [2010]	Boulin et al. [2011] and Foerster et al. [2009]	Xu et al. [2010]	Maloney et al. [1990]	Maloney et al. [1990]	Amann-Hildenbr and et al. [2013a, 2013b]	Wenk et al. [2008]	El-Maghraby and Blunt [2013]
Mineralogy													
Clays	Di-octahedral Muscovite/Illite	5.2	24.7	12.0	44.0	17.8	46.7	1.0			26.31	33.9	
	Smectite		8.8					3.9			29.88	1.85	
	I/S mixed layer		1.4										
	Kaolinite	1.3	18.0	2.0	4.0	3.0	2.6	2.0	2.0	0.5	9.7	3.3	
	Tri-octahedral Chlorite		4.1	13.0	30.0		4.7	4.6			5.31	3.8	
Feldspar	Plagioclase	3.0	12.3		2.0	16.9	1.4	19.8	3.0	2.0	3.1	3.85	
	K-Feldspar	6.9	2.1			3.9	13.5	8.2			1.94		
Quartz		76.2	21.5	65.0	20.0	35.2		57.9	94.0	97.5	14.7	24.0	0.8
Carbonate	Calcite	6.7	1.0					1.9			4.61	24.3	97.2
	Siderite			3.0	0.8						1.04		
	Dolomite		1.6		0.8	0.3					0.37		
	Ankerite						19.3					3.45	
	Magnesium carbonate												
Other Minerals	Pyrite		2.8	1.0		0.3					1.76	1.3	
	Anhydrite/gypsum					8.7	15.6				1.43		
	Halite						1						
	Hematite												
	aluminium oxide					0.6	1.0	0.5					0.12 0.68
Petrophysics													
Average porosity (%)		42	5	15	1.8–18.1	19–29	12.00	10.00	26.1	24.7	11.60	0.14–0.18	19.66
Horiz. permeability (m²)		3E−12	E−14	E−14	6E−23–3E−17	4–9.6E−14	1.65E−20		2.1E−12	2.39E−12	3.4E−21	1–100E−21	2.4E−13
Vert. permeability (m²)					1.1E−21–5.85E−18							0.6–1E−21	
Specific surface area (m²/g)						0.8–1.9			0.96		39.0		
Median pore radius (nm)					4.9–2292	6000–11,500	10–36		40,000	60,000	8.5		

[a]sst, sandstone; car, carbonate; I/S, illite/smectite. Compositions in wt%.
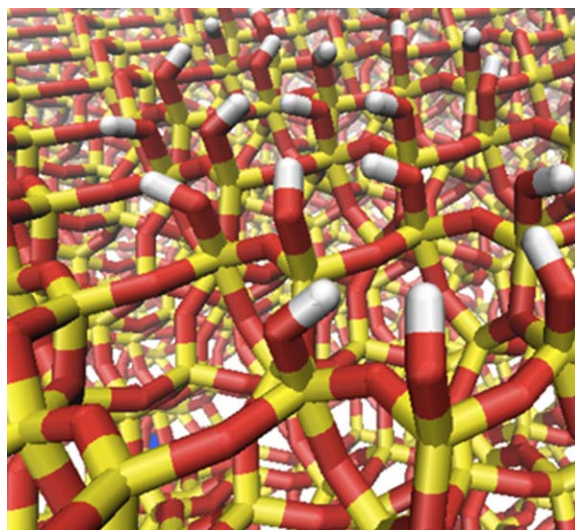
Figure 5. Schematic of an α-quartz surface and adjacent interior used in molecular dynamics simulations [*Iglauer et al.*, 2012b; *McCaughan et al.*, 2013]; hydrogen atoms are represented in white, oxygen atoms in red, and silicon atoms in yellow. The lateral length scale of this image is approximately 10 nm. The image shows the surface from a bird's perspective with the white-red hydroxyl groups covering the surface, particularly on the right upper side; the interior of the crystal can be seen at greater depths. (Image: Courtesy Fernando Bresme).

In order to tackle this complexity systematically, we briefly describe the chemistry for each mineral and then summarize the CO_2-wettability literature data. The Cassie-Baxter equation (equation (8)) can then be used to predict the contact angle on composite substrates [*Whyman et al.*, 2008] assuming that chemical heterogeneity is much smaller than the fluid droplets. In case the fluid droplets are of similar size as the chemical heterogeneity, the drop will move to the most lyophilic surface (i.e., the surface with the highest chemical affinity for the drop) as to minimize the system's Gibbs energy [*Berthier and Brakke*, 2012].

$$\gamma_{i,LF}\cos\theta^* = \sum_{n=1}^{N} f_i\left(\gamma_{i,SF} - \gamma_{i,SL}\right) \qquad (8)$$

i = number of surface component;
θ^* = contact angle on inhomogeneous surface, Cassie-Baxter apparent contact angle;
f = fraction of material on the substrate surface; γ = interfacial tension (S = solid; L = fluid 1, e.g., water; F = fluid 2, e.g., CO_2).

2.1. Quartz

Silicon dioxide (SiO_2) can exist as several polymorphs including α-quartz, β-quartz, β-tridymite, or β-cristobalite or simply as an amorphous phase (= glass, having no defined crystal structure). Here we discuss only α-quartz (also called "quartz" in this article) as this material is the most common constituent of mudrocks and sandstone storage rocks (cp. Table 3); in addition, we discuss glass as several researchers used glass as test substrates.

Quartz has a trigonal crystal structure (Figure 5), all Si atoms are tetrahedrically bonded to O atoms in a 3-D network. This crystal structure forms helices, so that the material is in fact chiral. The electronic charge distribution (which leads to the Coulombic and van der Waals forces) on the oxygen and silicon atoms can be considered to be $-1.2e$ and $2.4e$ [*Iglauer et al.*, 2012b]. The surface chemistry of amorphous silica has been reviewed by *Zhuralev* [2000], and depending on the history of the surface, hydroxyl (–OH) group surface concentrations varying between 0 and 4.6 OH/nm^2 (average maximum) have been measured with a range of techniques. In reservoir environments where quartz was exposed over geological time scales to water, the maximum degree of hydroxylation is expected (i.e., 4.6. OH/nm^2, which is the cited average maximum – OH group surface concentration by *Zhuravlev* [2000]). Quartz surfaces in mudrocks or sandstones may also be covered with organic material (e.g., kerogen), or secondary cement phases such as clays (e.g., illite, kaolinite) or carbonate. Cases of organic coating, which are probably most common in oil reservoirs [*Cuiec*, 1991], are discussed in section 2.7 in more detail. In case of inorganic cement coating, the type of mineral and its surface texture need to be considered (sections 2.2–2.5). As shown in molecular dynamics simulations [*Liu et al.*, 2010; *McCaughan et al.*, 2013], the concentration of OH groups strongly influences the surface's wettability: higher OH surface group concentration leads to higher hydrophilicity (i.e., lower water contact angles, more water-wet material) because of the highly polar character of the OH group.

2.1.1. CO_2-Wettability of Quartz and Glass
2.1.1.1. Contact Angle Measurements: Young's Contact Angles
Several researchers measured sessile (pendant) or captive drop CO_2/brine contact angles on quartz substrates at reservoir conditions, however a significant uncertainty remains. Figure 6 shows a compilation of these water contact angles [*Wesch et al.*, 1997; *Sutjadi-Sia et al.*, 2008; *Bikkina*, 2011; *Espinoza and*
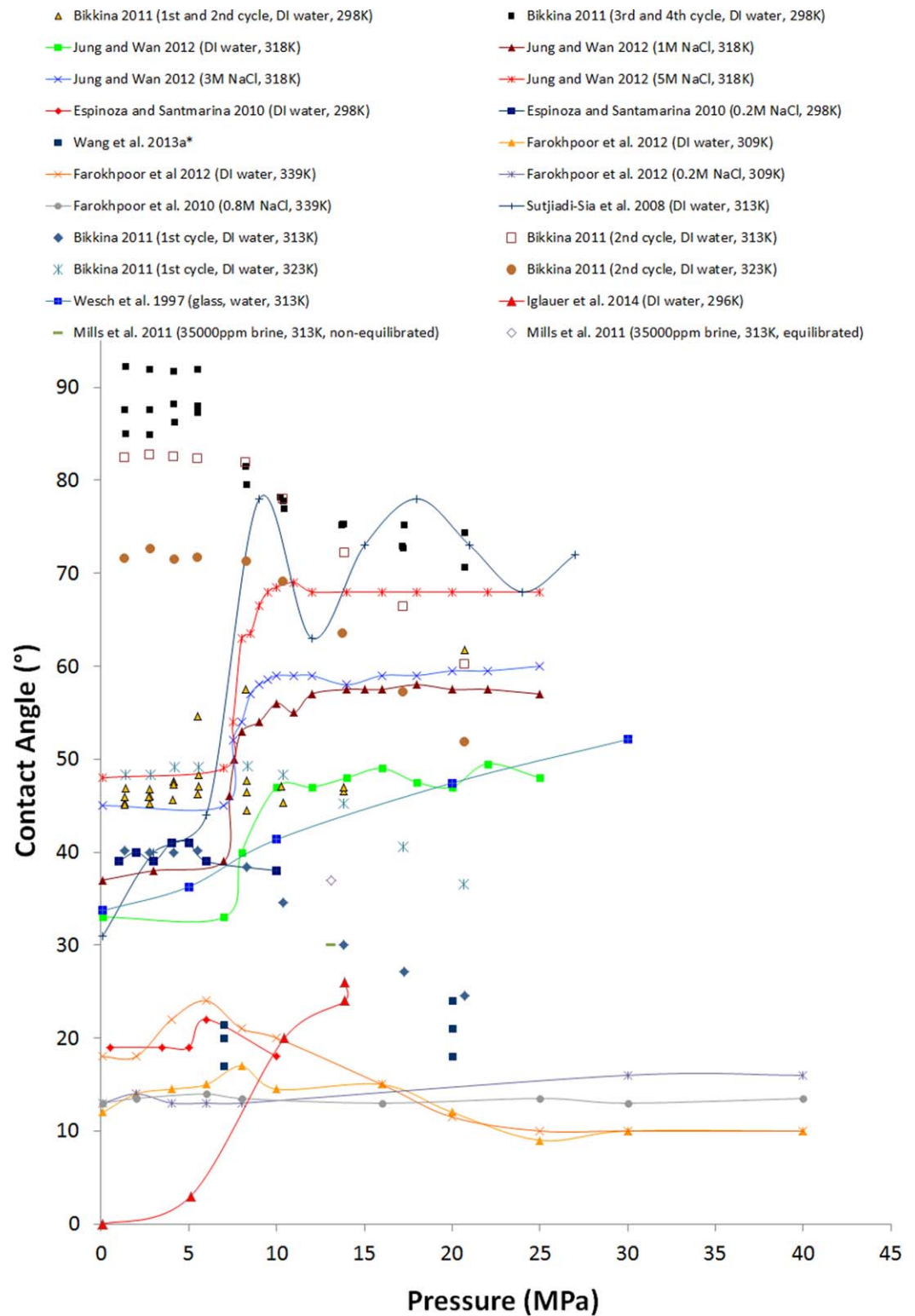
Figure 6. Experimental sessile drop Young's contact angles: compilation of water contact angles measured for the quartz/CO_2/water (or brine) system. DI water = deionized or distilled water. *Wang et al.* [2013a]: (1) The points at 7 MPa were measured at 303 K for three different salinities ((a) DI water, (b) brine: I = 1.1–1.2 mol/L; contains: Na^+, Cl^-, Ca^{2+}, SO_4^{2-}, Mg^{2+}; pH = 3.0–5.0; pH = 7.8 at ambient conditions; and (c). buffered brine: 0.74–0.75 mol/L; contains: Na^+, Cl^-, Ca^{2+}, SO_4^{2-}, Mg^{2+}, CO_3^{2-}, HCO_3^-, $B_4O_7^{2-}$; pH = 5.8–5.9; pH = 10.0 at ambient conditions.) (2) The points at 20 MPa were measured at 323 K for the same three salinities.

Table 4. "Reality Check": Sessile Drop Water Contact Angles θ Measured on an α-Quartz Single Crystal in CO_2 Atmosphere at Varying Cleanliness States and Ambient Conditions[a]

Surface Cleanliness State	Cleaned With Piranha Solution	Cleaned With Piranha Solution, Then a "Clean" Paper Towel	Cleaned With Piranha Solution Then Exposed to Laboratory Atmosphere for ~8 Weeks
θ	0°	25°	70°

[a]Piranha solution comprises 5vol:1vol H_2SO_4:H_2O_2.

Santamarina, 2010; *Mills et al.*, 2011; *Chiquet et al.*, 2007; *Wang et al.*, 2013a; *Broseta et al.*, 2012; *Jung and Wan*, 2012; *Saraji et al.*, 2013; *Farokhpoor et al.*, 2013; *Iglauer et al.*, 2014].

The large variation of θ (7–92°) is probably due to (a) surface roughness effects which induce a difference in advancing and receding contact angles—this is discussed in more detail in section 2.1.1.2, and (b) surface contamination [*Mahadevan*, 2012; *Bikkina*, 2012; *Iglauer et al.*, 2014. Such a contamination has been clearly identified as a major and highly significant problem [*Iglauer et al.*, 2014]: a quartz single crystal was cleaned with piranha solution (5vol:1vol H_2SO_4:H_2O_2) and a water contact angle of approximately 0° was measured at ambient conditions in CO_2 atmosphere in line with reported literature data [*Grate et al.*, 2012]. After this crystal was wiped with a "clean" paper towel and the test repeated (at identical conditions) the measured angle was approximately 25°; θ ($= 70°$) was then measured, again at identical conditions, on a crystal which was exposed to laboratory air for several weeks (Table 4). This and a more detailed discussion on how contamination affects θ measurements is provided by *Iglauer et al.* [2014]. This illustrates that such measurements need to be undertaken with great care and cleanliness.

Surface cleanliness of the substrate surface is therefore paramount (indeed even a partial monomolecular surface layer of contaminant can significantly change the contact angle [*Adamson and Gast*, 1997]). After reading carefully through the published literature, we conclude that a significant number of studies have used cleaning procedures which are not appropriate in our opinion [*Iglauer et al.*, 2014]. Ethanol or acetone have been used although these cleaning agents are insufficient to remove all organic contamination from a substrate's surface [*Love et al.*, 2005]; we conclude that this leads to significant uncertainty in the data. However, we note that it is unlikely that a clean surface represents subsurface conditions, this is further discussed in section 2.9.

2.1.1.2. Contact Angle Measurements: Receding and Advancing Contact Angles
It is well known that advancing and receding contact angles can differ significantly: this difference is controlled by surface roughness and/or chemical heterogeneity [*Berthier and Brakke*, 2012; *Adamson and Gast*, 1997; *Butt et al.*, 2006]. These effects were investigated by *Chiquet et al.* [2007], *Mills et al.* [2011], *Broseta et al.* [2012], *Wang et al.* [2013b], *Saraji et al.* [2013], and *Iglauer et al.* [2014] for water-quartz-CO_2 systems, and differences between receding and advancing contact angles up to 40° were reported (Figure 7). Although the above mentioned data set is probably again convoluted by surface contamination problems, it appears that overall θ increases with pressure as a general trendline, but this trend has a high standard deviation at this moment.

In summary, some researchers measured an increase in θ with pressure [*Wesch et al.*, 1997; *Chiquet et al.*, 2007; *Broseta et al.*, 2012; *Jung and Wan*, 2012; *Saraji et al.*, 2013; *Iglauer et al.*, 2014], while others did not measure such an increase [*Espinoza and Santamarina*, 2010; *Farokhpoor et al.*, 2013; *Wang et al.*, 2013a]. Furthermore, while some authors identified an increase in θ with salinity [*Jung and Wan*, 2012; *Espinoza and Santamarina*, 2010] others only measure a small change [*Chiquet et al.*, 2007; *Broseta et al.*, 2012]. *Saraji et al.* [2013] and *Farokhpoor et al.* [2013] investigated the dependency of θ on temperature, but they did not observe a clear trend. The likely cause for the large data spread is again surface contamination, although the distinction between receding and advancing θ reduces uncertainty significantly. Overall we think that *Saraji et al.* [2013], *Farokhpoor et al.* [2013], and *Iglauer et al.* [2014] used the most controlled cleaning methods and they found rather low θ, between 0° and 30°, which suggests that quartz and glass are completely wetted by water or are strongly water-wet. We also hypothesize that quantification of surface roughness will further reduce uncertainty. However, we note that under subsurface conditions, contaminants will be present in the pore fluids and they will quite likely affect the surface chemistry of the quartz surfaces, e.g., through adsorption. This is an important area for future study as this may strongly influence θ values.

2.1.1.3. Adhesion Tests and Surface Roughness
Wang et al. [2013b] also conducted adhesion tests (a tensile force was applied to detach a CO_2 bubble from a quartz surface in water), and found that silica was strongly or weakly water-wet at 0 MPa and 20 MPa/323K in
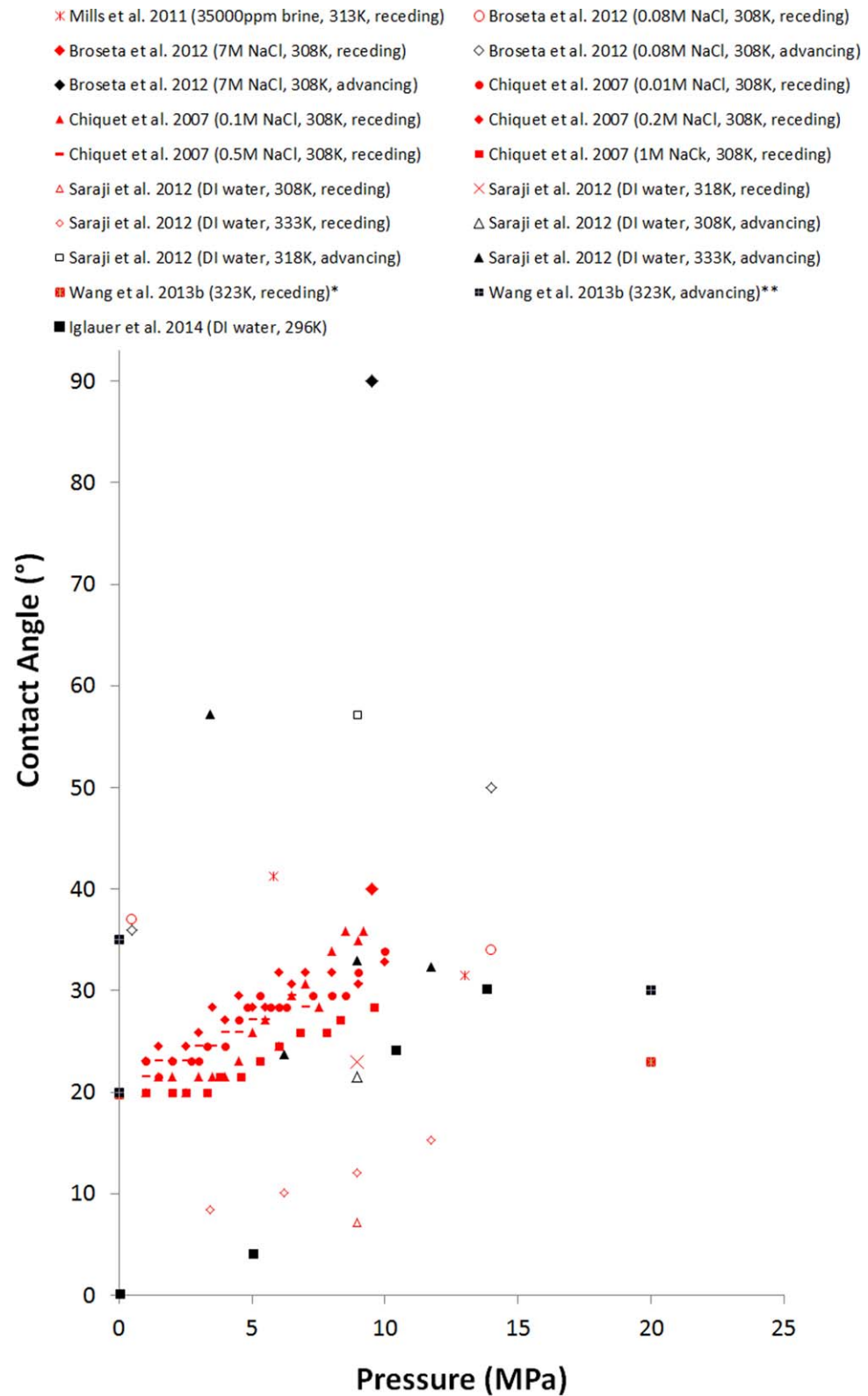
Figure 7. Receding (red) and advancing (black) water contact angles measured for the quartz/water/CO_2 system. *Mills et al.* [2011] used the following brine composition: 18,200 ppm Cl^-, 11,700 ppm Na^+, 3180 ppm SO_4^{2-}, 1170 ppm Ca^{2+}, 326 ppm Mg^{2+}, and 123 ppm K^+. *Wang et al.* [2013b] measured $\theta = 20°$ for all following conditions: (a) DI water, pressure = Mpa, (b) I (ionic strength) = 10^{-3} M, pressure = 20 MPa, (c) I = 1.5 M NaCl, pressure = 0 MPa, and (d) I = 1.5 M NaCl, pressure = 20 MPa. **Wang et al.* [2013b] measured a variation in the advancing water contact angle with the normalized contact length in brine systems. θ varied between ~20° and 55°, and as a trend dropped with increased normalized contact length. Only the average advancing θ is shown in the graph.
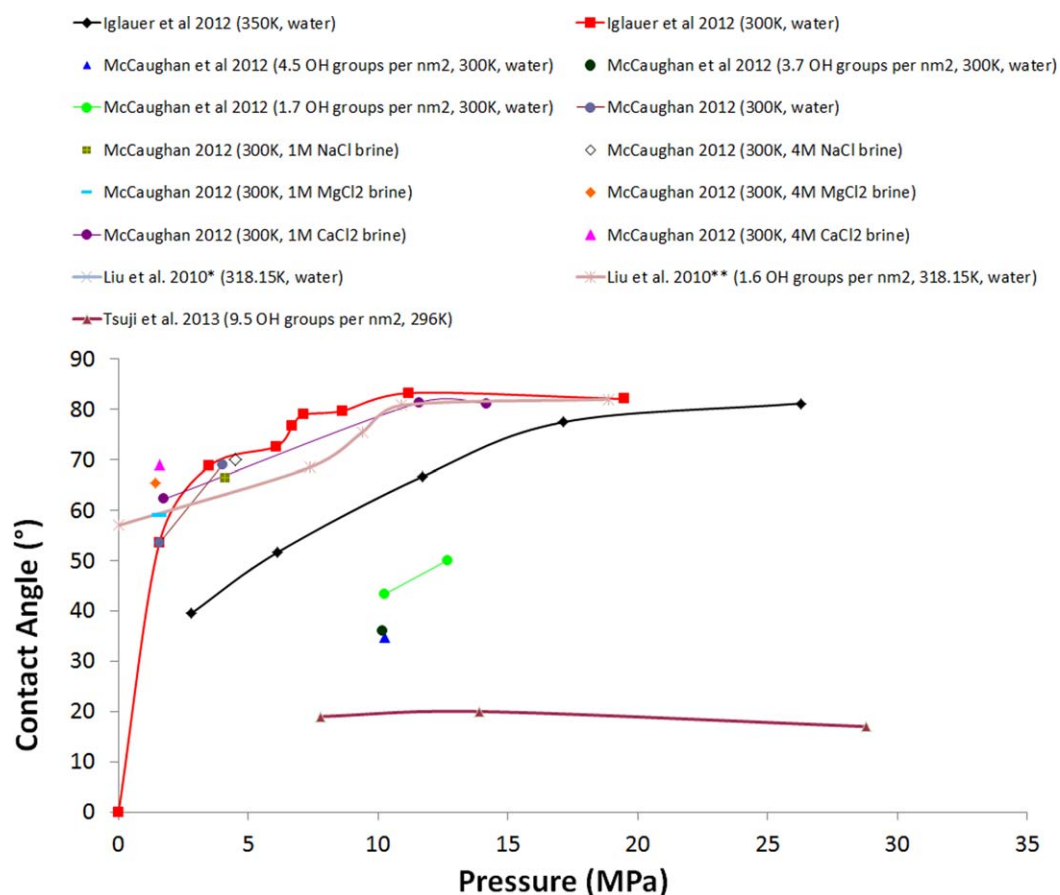
Figure 8. Water contact angles on quartz and β-cristobalite surfaces predicted with molecular dynamics simulations [*Liu et al.*, 2010; *Iglauer et al.*, 2012b; *McCaughan et al.*, 2013; *Tsuji et al.*, 2013]*on β-cristobalite; $\theta = 180°$ at 57.5 MPa. ** on β-cristobalite; $\theta = 88°$ at 57.5 MPa.

deionized water or 1.5 M NaCl brine. Increased surface roughness rendered the silica surface from weakly water-wet ($\theta = 31–38°$; surface roughness = 5.8 nm) to strongly water-wet ($\theta = 1°$; surface roughness = 2300 nm).

2.1.1.4. Contact Angle Predictions: Molecular Dynamics Simulations

Liu et al.'s [2010], *Iglauer et al.*'s [2012b], and *McCaughan et al.*'s [2013] molecular dynamics (MD) simulations predict that pressure and temperature strongly influence θ by changing CO_2 density: θ increases with pressure, but decreases with temperature; ρ_{CO2} increases with pressure, and decreases with temperature. The theoretical explanation for this phenomenon is that a higher CO_2 density leads to higher CO_2-quartz intermolecular interactions and thus a lower interfacial tension between CO_2 and quartz $\gamma_{quartz-CO2}$ directly impacting on θ, Figure 8 [cp. also Young's equation (1) and *Iglauer et al.*, 2012b]. *Tsuji et al.* [2013], however, predicted an approximately constant contact angle versus pressure for a hydrophilic quartz surface with their MD simulation. The discrepancy between these models is highly significant and may be due to the surface hydroxyl group concentration or distribution, which was significantly higher in Tsuji's model (9.5 OH groups per nm^2, Y. Liang, private communication, 2013)—which is higher than the maximum average OH group concentration reported for amorphous silica [*Zhuravlev*, 2000]. This difference could also be due to the difference in the used water and/or CO_2 models and their associated force field parameters.

A general further complication of such simulations is quantum mechanical effects (which are not considered in MD simulations; e.g., dissociation of OH surface groups), which are well known to occur (point of zero charge of quartz is at pH = 3.0) [*Bourikas et al.*, 2003], but have not yet been implemented in the MD models. In order to fully understand the θ behavior, this needs to be done. Moreover, an experimental study investigating OH-surface group concentrations on quartz is required as this may be different to what is occurring on amorphous silica.

Table 5. Trends for Measured and Simulated Water Contact Angles θ of CO_2/Water/SiO_2 Systems[a]

Reference	θ Change With Increasing Pressure	θ Change With Increasing Temperature	θ Change With Increasing Salinity
Wesch et al. [1997]	Increase		
Chiquet et al. [2007]	Slight increase		Small change with maximum
Sutjiadi-Sia et al. [2008]	Increase		
Espinoza and Santamarina [2010]	Constant		Slight increase
Bikkina [2011]	Decrease (third and fourth cycle)[b]	Minimum at 313 K	
	Increase (first and second cycle)[b]		
Mills et al. [2011]	Slight increase		
Jung and Wan [2012]	Increase		Increase
Wang et al. [2013a]	Slight increase	Constant	Constant
Broseta et al. [2012]	Receding: constant;		Receding: constant
	Advancing: slight increase		Advancing: strong increase
Saraji et al. [2013]	Advancing: slight increase;	Small increase	
	Receding: slight increase		
Farokhpoor et al. [2013]	Slight increase or constant	Slight increase or constant	Mixed small response
Iglauer et al. [2014]	Slight increase		
Kaveh et al. [2014]	Increase below the CO_2 critical pressure (for the smallest bubbles only)		
Iglauer et al. [2012b]*	Strong increase	Decrease	
McCaughan et al. [2013]*	Strong increase		Slight increase
Liu et al. [2010]*	Increase		
Tsuji et al. [2013]*	Constant		

[a]References marked with * are molecular dynamics predictions.
[b]This behavior is likely a surface contamination effect [*Mahadevan*, 2012].

2.1.2. Summary of CO_2-Water-Silica Contact Angle Data

In summary, it can be said that a substantial effort has now gone into CO_2-brine-quartz contact angle measurements (cp. Figures 6 and 7). The uncertainty associated with these data is mainly due to surface roughness effects (which lead to differences in advancing and receding θ), section 2.1.1.2, and surface contamination [*Mahadevan*, 2012; *Bikkina*, 2012; *Iglauer et al.*, 2014]. Table 5 summarizes approximate qualitative trends found for θ. Overall it only appears that θ slightly increases or is constant as a function of pressure. We suggest that these relationships are reinvestigated using representative silica surfaces with a known and quantified surface roughness. In addition, as was identified by *Wang et al.* [2013a] and *Kaveh et al.* [2014], contact angle measurements depend on equilibration time between the fluids and the solid and on bubble size. They found that contact angle increases with progressing equilibration time but decreases with bubble radius if placed underneath the solid surface. *Mills et al.* [2011], however, found an opposite result: their water contact angle was lower for an equilibrated system. Furthermore surface cleanliness must be considered carefully. We see value in the measurement of contact angles on perfectly cleaned surfaces as well as surfaces contaminated in such a way as to be representative of subsurface conditions, this is an important area for future study.

2.1.3. Bentheimer Sandstone

Kaveh et al. [2013, 2014] measured captive drop contact angles for the Bentheimer sandstone-CO_2-water system. The sandstone consisted of 96% quartz, ~2% feldspars, and ~2% kaolinite, and the kaolinite was homogeneously distributed throughout the rock matrix. The Bentheimer sample had a porosity of 20% and a permeability of 1.48×10^{-12} m^2 (1.5 Darcy). The sandstone substrate was polished and its surface roughness was measured prior to the θ measurements. The reported P_a factor (arithmetic mean of the height of the primary profile within a sampling length) for their substrate was 0.03 mm. The measurements were conducted at 318 K and a range of pressures (2.35, 5.54, 9.4, 12.95 MPa). Considering all bubble sizes, they found that pressure had no influence on θ; however, the CO_2 droplet radius had a significant impact: θ decreased from ~40° at a radius of 0.4 mm to ~5° at a bubble radius of 1.4 mm. When larger captive CO_2 bubbles were excluded and only bubbles with an apex radius of approximately 1 mm were considered then there was a slight increase in θ below the CO_2 critical pressure (from ~15° at 1 MPa to ~18° at ~7.3 MPa), above the critical pressure this trend was less clear. The influence of droplet radius may have to do with the composite character of the substrate (multimineral system, pores of different dimensions) and/or its significant surface roughness. *Kaveh et al.* [2014] also tested Bentheimer substrates having two different surface
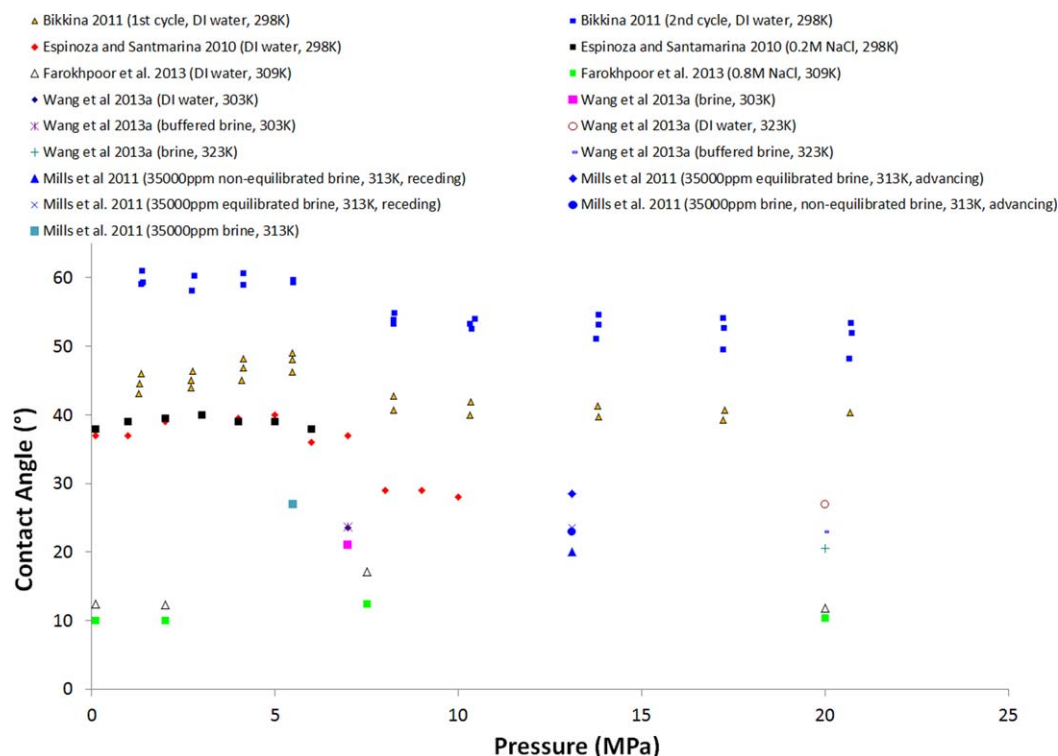
Figure 9. Young's water contact angles measured on calcite [*Bikkina*, 2011; *Jung and Wan*; 2012; *Espinoza and Santamarina*, 2010; *Farokh-poor et al.*, 2013; *Wang et al.*, 2013a; *Mills et al.*, 2011]. *Mills et al.* [2011] used following brine composition: 18,200 ppm Cl^-, 117,00 ppm Na^+, 3180 ppm SO_4^{2-}, 1170 ppm Ca^{2+}, 326 ppm Mg^{2+}, and 123 ppm K^+.

roughnesses (P_a values 0.032 and 0.059 mm were reported), and found a larger scatter for θ on the rougher substrate (θ varied from $\sim$7 to 38° with an approximately constant average value of $\sim$20° over the range $\sim$0.5–13.5 MPa) than on the smoother substrate (θ varied from $\sim$2° to 23° with an approximately constant value of $\sim$15° over the range $\sim$0.5–13.5 MPa). The fact that θ on average increased with surface roughness may have to do with the composite character of the sandstone surface or possibly experimental error.

2.2. Calcite

Calcium carbonate ($CaCO_3$) can exist as three different polymorphs: calcite, aragonite, and vaterite. While aragonite and vaterite mainly form in carbonate-rich and/or hydrothermal springs or through biochemical processes [e.g., *Bjørlykke*, 2010, exceptions apply], calcite is the most stable $CaCO_3$ polymorph at typical reservoir conditions, and consequently most limestone reservoirs mainly consist of this mineral. In addition, calcite is typically the main component of cement in sandstone. We here only report water/calcite/CO_2 contact angles; no such values were found for aragonite or vaterite in the literature (Figure 9).

Again there is significant uncertainty associated with these contact angles ranging from approximately 2–40°; but the available data indicate that the calcite system is strongly or at least weakly water wet.

Most researchers measured Young's contact angles; specifically *Espinoza and Santamarina* [2010] measured θ at room temperature (296.5 K) as a function of pressure, and they found that θ is constant ($\approx$ 40°) up to the critical CO_2 pressure (7.38 MPa), but drops above this pressure to approximately 28° at higher pressures. Small amounts of salt (0.2 M NaCl versus DI water) had no significant effect.

Mills et al. [2011] observed that θ depends on the base diameter of the drop; they measured $\theta = 9°$ at 0.2 mm base diameter and $\theta = 29°$ at 1.4 mm base diameter for the water advancing contact angle and $\theta = 9°$ at 0.22 mm base diameter and $\theta = 27°$ at 1.15 mm base diameter for the water receding contact angle. They did not find a difference in θ between equilibrated and nonequilibrated brine. Our interpretation of these results is that theoretically the drop size should not influence θ on an ideal surface (= no surface roughness, no chemical heterogeneity) unless the drop is too large and gravitational effects reach a

Table 6. Trends of Measured Water/CO$_2$/Calcite Contact Angles θ

Reference	θ Change With Increasing Pressure	θ Change With Increasing Temperature	θ Change With Increasing Salinity
Bikkina [2011]	Slight decrease		
Espinoza and Santamarina [2010]	Decrease above critical CO$_2$ pressure		Constant
Wang et al. [2013a]	Constant	Constant	Slight decrease
Farokhpoor et al. [2013]	Small maximum at $\approx$7 MPa		Slight decrease
Mills et al. [2011]	$\sim$ constant		

significant strength [*DeGennes et al.*, 2004; *Kaveh et al.*, 2014], so we conclude that these differences are likely caused by surface roughness and possibly sample contamination (surface cleanliness). However, the drop size effect should be studied further as there currently seems to be no clear answer to what is causing this effect.

Table 6 summarizes approximate qualitative trends found for θ. No clear trend can be identified, and the data may again be biased because of inappropriate substrate surface cleaning—the authors used the same cleaning methods as for silica (cf. Table 6).

Bikkina [2011] measured rather high θ, which is probably caused by surface contamination [*Mahadevan*, 2012], while *Farokhpoor et al.* [2013], who used a more stringent surface cleaning technique, measured much lower θ (θ ranged between $\sim$10° and 17° and was almost constant versus pressure up to 20 MPa in deionized water and 0.8 M NaCl brine at 309 K. *Wang et al.* [2013a] measured a small influence of salinity and pressure at 303 and 323 K and 7–20 MPa.

We conclude that *Farokhpoor et al.*'s [2013] data are most reliable because of the rigorous surface cleaning method used (cp. discussion in the quartz section 2.1.2), although $\theta = 10$–12° at ambient pressure indicates surface contamination [*Grate et al.*, 2012]. Again we highlight the difference between clean surfaces and contaminated surfaces representative of subsurface conditions.
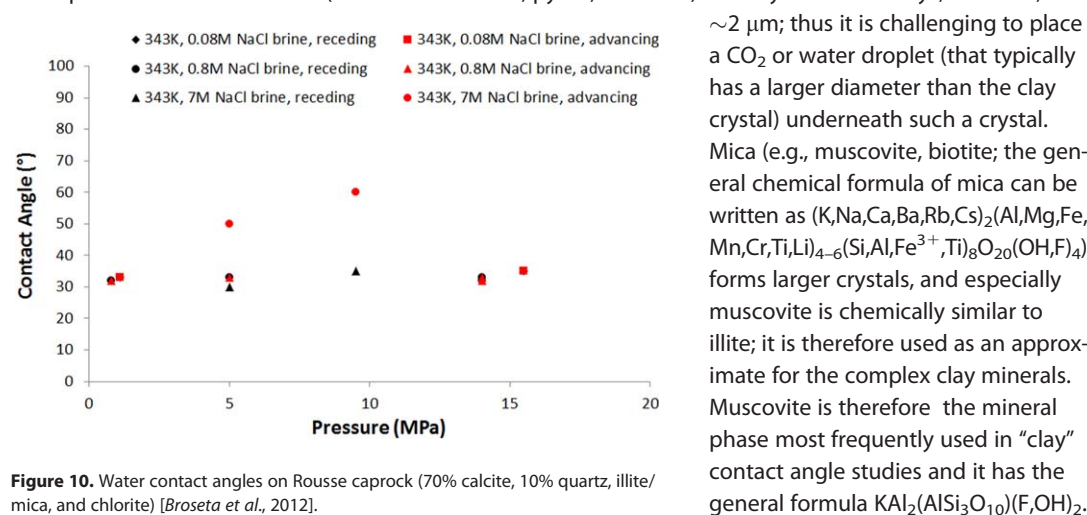
2.2.1. Rousse Caprock

Broseta et al. [2012] appear to be the only group who have measured CO$_2$-brine θ on actual caprock, Figure 10. Specifically they tested caprock from the Rousse depleted gas field in South France used in the Lacq CGS pilot project. The caprock consisted of approximately 70% calcite, 10% quartz, and a few percent chlorite and illite/mica. Its porosity was below 5% and its permeability in the nanodarcy range. The contact angle was almost constant, independent of pressure and salinity or whether θ was advancing or receding, except the advancing θ at 343 K and high salinity at 7 M NaCl concentration was higher and increased with pressure from 30 to 60° when pressure was increased from $\sim$1 to $\sim$10 MPa. This caprock was thus clearly strongly to weakly water-wet.

2.3. Clay Materials
2.3.1. Mica/Muscovite Mica/Biotite Mica

Several researchers have investigated the CO$_2$-wettability of mica, which was considered representative of clays. Clays (e.g., illite, smectite, kaolinite) act as rock-forming minerals in most siliciclastic caprocks together with quartz and other minerals (such as carbonates, pyrite, hematite). The crystal size of clays, however, is $\sim$2 µm; thus it is challenging to place a CO$_2$ or water droplet (that typically has a larger diameter than the clay crystal) underneath such a crystal. Mica (e.g., muscovite, biotite; the general chemical formula of mica can be written as (K,Na,Ca,Ba,Rb,Cs)$_2$(Al,Mg,Fe,Mn,Cr,Ti,Li)$_{4-6}$(Si,Al,Fe^{3+},Ti)$_8$O$_{20}$(OH,F)$_4$) forms larger crystals, and especially muscovite is chemically similar to illite; it is therefore used as an approximate for the complex clay minerals. Muscovite is therefore the mineral phase most frequently used in "clay" contact angle studies and it has the general formula KAl$_2$(AlSi$_3$O$_{10}$)(F,OH)$_2$.

● 343K, 0.08M NaCl brine, receding ■ 343K, 0.08M NaCl brine, advancing
● 343K, 0.8M NaCl brine, receding ▲ 343K, 0.8M NaCl brine, advancing
▲ 343K, 7M NaCl brine, receding ● 343K, 7M NaCl brine, advancing

Figure 10. Water contact angles on Rousse caprock (70% calcite, 10% quartz, illite/mica, and chlorite) [*Broseta et al.*, 2012].
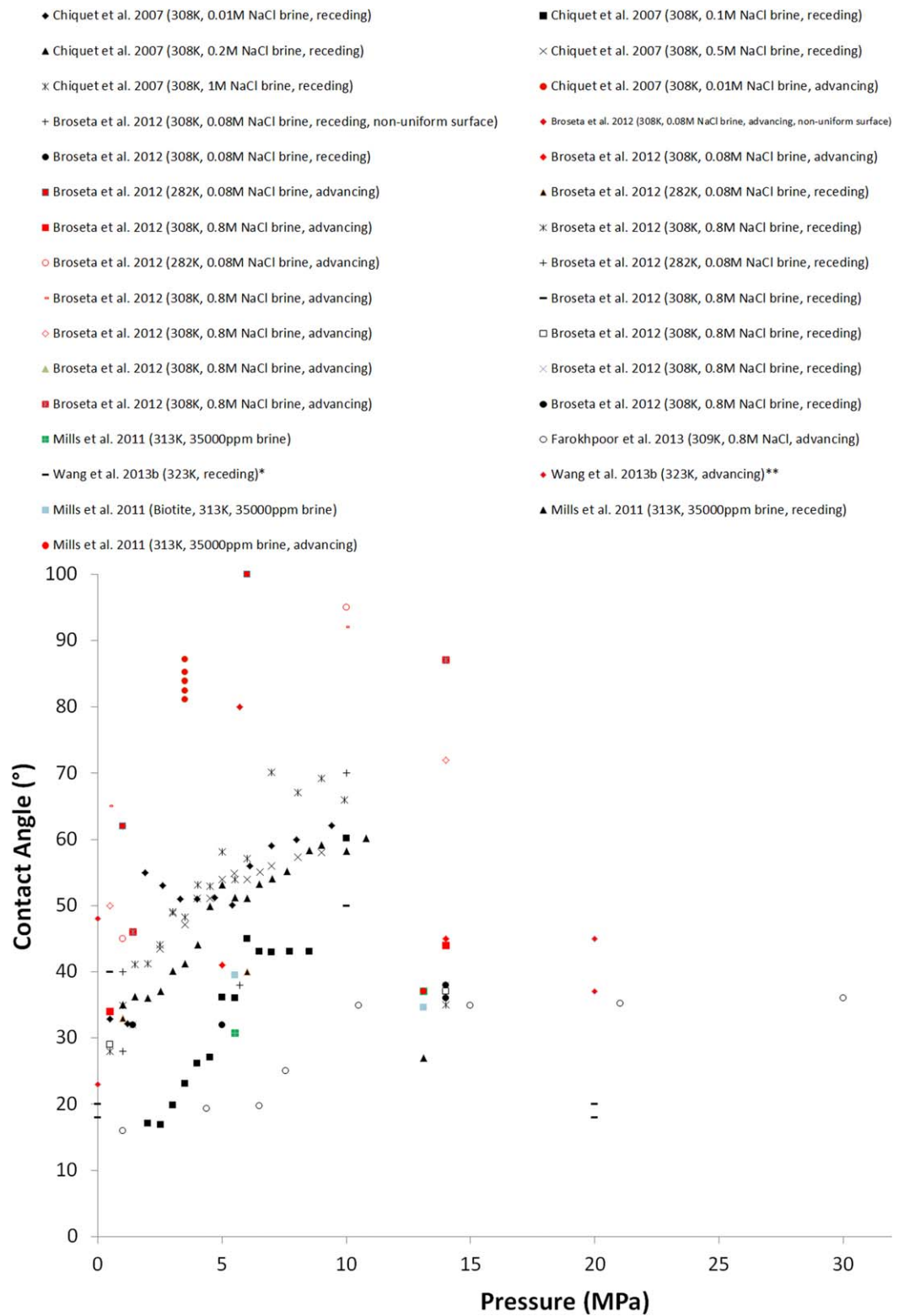
Figure 11. Water contact angles on mica surfaces. *Wang et al. measured $\theta = 20°$ for following conditions: (a) DI water, at reported $p = 0$, (b) I (ionic strength) $= 10^{-3}$ M, $p = 20$ MPa, (c) I $= 1.5$ M NaCl, reported $p = 0$ MPa, and (d) I $= 1.5$ M NaCl, $p = 20$ MPa. **Wang et al. (2013b) measured a variation in the advancing water contact angle with the normalized contact length in brine systems at 323K. θ varied between ~15° and 75°, and as a trend dropped with increased normalized contact length. Only the average advancing θ is shown in the graph.
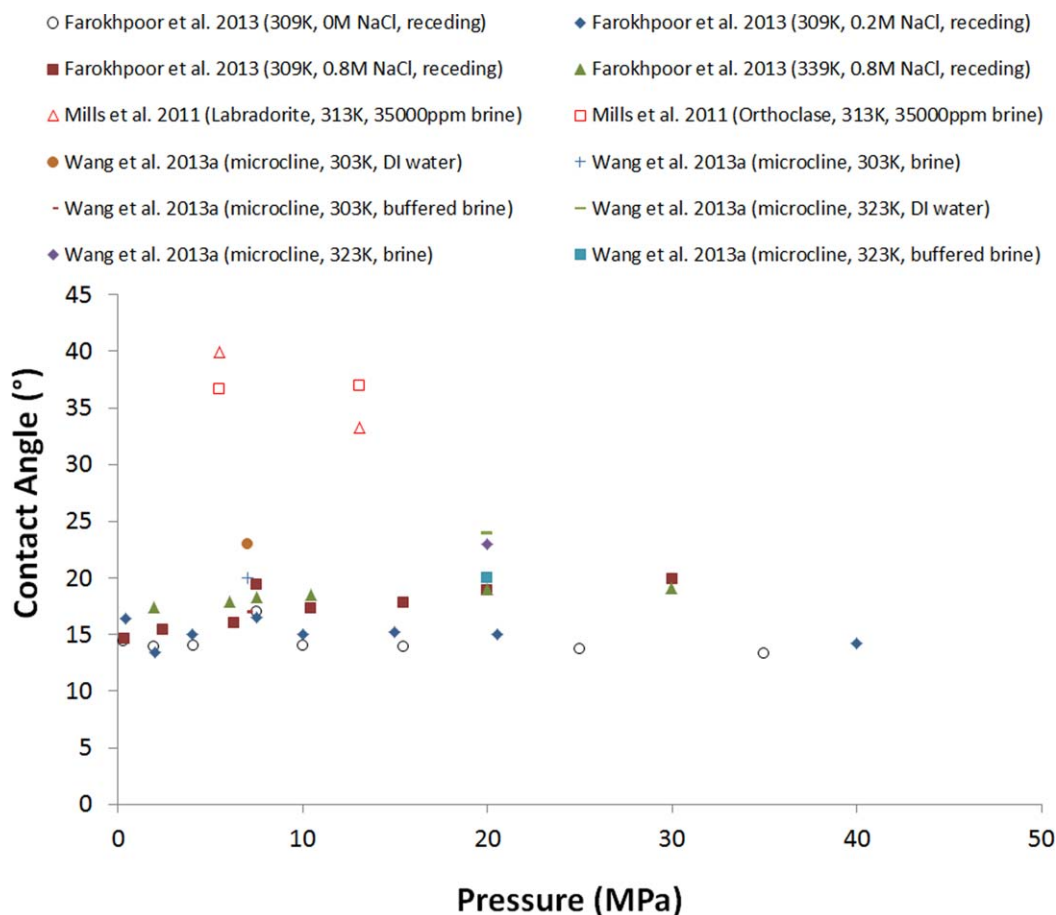
Figure 12. Water contact angles on feldspar surfaces.

Biotite has the general chemical formula $K(Mg,Fe)_3AlSi_3O_{10}(F,OH)_2$ with its Mg-end-member phlogopite $KMg_3(AlSi_3O_{10})(F,OH)_2$. Both biotite and phlogopite are usually metamorphic or igneous in origin and therefore uncommon in reservoir rocks, however, they are important metamorphic or igneous minerals. Sessile, receding, and advancing contact angle measurements on mica found in the literature are summarized in Figure 11 [*Chiquet et al.*, 2007; *Mills et al.*, 2011; *Broseta et al.*, 2012; *Farokhpoor et al.*, 2013]. In the studies conducted by *Chiquet et al.* [2007] and *Broseta et al.* [2012], the muscovite was fully cleaved along a crystal unit surface so that an ultrasmooth surface was obtained. They then measured advancing and receding contact angles as a function of pressure and salinity, Figure 11. In Chiquet et al.'s and Broseta et al.'s studies, the advancing contact angles were generally higher (θ between 35° and 100°) than the receding θ (between 18° and 70°), as expected. They did not find a clear influence of salinity on θ. *Farokhpoor et al.* [2013] measured significantly lower advancing contact angles than Chiquet et al. and Broseta et al., probably because of the surface cleaning procedures employed; as previously outlined the surface cleaning method has a profound impact on θ measurements [*Iglauer et al.*, 2014]. *Mills et al.* [2011] measured θ on biotite ($\sim$35–40°) at 313 K in 35,000 ppm brine, which is consequently strongly water-wet. *Wang et al.* [2013b] measured a low and constant receding θ ($\sim$20°) on magnesium mica; while the advancing θ was higher and increased with pressure (from $\sim$20° at a reported pressure of 0 MPa to 43° at a pressure of 20 MPa/323K). *Wang et al.* [2013b] also evaluated the influence of surface roughness on θ for magnesium mica, and θ decreased at 20 MPa and 323K from 79° at low surface roughness ($=$ 6.4 nm) to 11° at high surface roughness ($=$ 1600 nm). A general trendline through all data shows that θ increases with increasing pressure, however, data spread is large.

2.4. Feldspar

Farokhpoor et al. [2013] measured θ on feldspar ((K, Ca, Na)Al$_{1,2}$Si$_{2,3}$O$_8$), Figure 12. θ ranged between 10° and 20° and was quasi-independent of salinity or pressure. Feldspar thus seems to be strongly water-wet under storage conditions, although higher salinities also need to be tested. $\theta = 15°$ at ambient pressure is, however, an indication of surface contamination, cp. discussion section 2.1.1. Consistent with Farokhpoor et al., *Wang et al.* [2013a] measured θ between ∼15° and 25° for microcline (KAlSi$_3$O$_8$)) at 303–323 K and water with different salinities. *Mills et al.* [2011] measured slightly elevated θ (between 30° and 40°) on labradorite ((Ca, Na)(Al, Si)$_4$O$_8$) and orthoclase (KAlSi$_3$O$_8$) at 313 K using 35,000 ppm brine so these feldspar minerals are also strongly water-wet.

2.5. Na-Montmorillonite and Ca-Montmorillonite

No experimental data were found for montmorillonite (smectite) for the CO$_2$/water system. As mentioned earlier, this is mainly attributed to mineral crystal sizes being smaller than the expected droplet in conventional sessile or pendant drop measurements. However, *Myshakin et al.* [2013] conducted molecular dynamics simulations and found that at CGS conditions exposure of CO$_2$ to Na-montmorillonite or Ca-montmorillonite ((Na,Ca)$_{0.33}$(Al,Mg)$_2$(Si$_4$O$_{10}$)(OH)$_2$·nH$_2$O) can cause an increase of hydrophobicity of the clay surface. They attributed this effect to the mobilization of positively charged sodium ions, which then formed surface complexes and added to charge shielding of the electrical (surface) layer.

2.6. Kaolinite, Illite, and Smectite Mudrocks

Again no data were found for the CO$_2$-water system in kaolinite, illite, or smectite mudrocks. *Borysenko et al.* [2009], however, conducted a comprehensive study to evaluate the relative water-oil wettability of a range of shale samples. They concluded that shales with a higher surface charge density, specific area, and higher cation exchange capacity (illite (K,H$_3$O)(Al,Mg,Fe)$_2$(Si,Al)$_4$O$_{10}$[(OH)$_2$,(H$_2$O)]), and smectite mudrocks) are hydrophilic, whereas kaolinite (Al$_2$Si$_2$O$_5$(OH)$_4$) mudrocks are hydrophobic (note that this was measured for oil-water systems, not for CO$_2$-water systems). These conclusions were supported by a wide range of experimental results, including SEM, NMR, optical and fluorescence microscopy, contact angle measurements, imbibition floods, and liquid-liquid extraction studies.

2.7. Hydrophobic Rock Surfaces
2.7.1. Background: Crude Oil and Kerogen

Depleted oil and gas reservoirs are often considered suitable for CO$_2$ injection as it has been proven that the local geology traps buoyant hydrocarbons and because of preexisting infrastructure. Some of the first operating and planned CO$_2$ storage projects inject into hydrocarbon formations for these reasons or to produce additional oil reserves (e.g., Weyburn oil field, Canada [*Riding*, 2006], Goldeneye gas field, United Kingdom [*Tucker et al.*, 2013]). Overall these reservoirs provide relatively small storage capacities: 675–900 Gt/CO$_2$ total storage capacity versus 10,000 Gt/CO$_2$ total storage capacity for deep saline aquifers [*IPCC*, 2005].

The mineral surfaces in these reservoirs have in some cases changed wettability states due to their exposure to crude oils [cp. for instance *Iglauer et al.*, 2012a; *Buckley et al.*, 1997, 1998]. In this context, *Cuiec* [1991] measured oil-wettability of 35 plugs recovered from 33 different oil reservoirs and found that approximately 1/3 was water-wet, 1/3 intermediate-wet, and 1/3 oil-wet (carbonate reservoirs were typically more oil-wet).

Mechanistically, it is believed that surface active compounds in the crude oil (e.g., asphaltenes which are large organic molecules, Figure 13) adsorb and adhere to the mineral surface. This adsorption is thought to be caused by polar interactions, surface precipitation, acid-base interactions, ion binding, or any combination thereof [*Buckley et al.*, 1998].

Considering the chemical complexity of crude oil, two consequences follow: (a) a quartz surface (or indeed any mineral surface) exposed to crude oil over a long time period is very likely to show rendered wettability characteristics, with a shift toward increased oil-wettability, cp. *Cuiec*'s [1991] study discussed above, and (b) the exact wetting behavior of a quartz or glass surface depends on the crude oil itself and the sample preparation [*Buckley et al.*, 1997]. Significantly different wettabilities may be created by different crude oil and/or wettability alteration conditions as shown by oil-brine contact angle measurements performed by *Buckley et al.* [1997] and reproduced here in Table 7 (note: ageing is the process where wettability changes with time). It therefore seems necessary to evaluate individual crude oil/formation brine/reservoir rock systems case by case to acquire results representative of the true specific reservoir conditions. No doubt it is of key
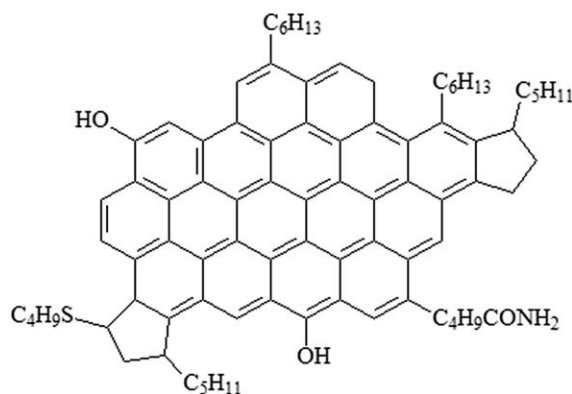
Figure 13. Example of an asphaltene molecule [*Aguilera-Mercado et al.*, 2006].

importance to replicate the reservoir rock surface at true reservoir conditions in the laboratory adequately which is certainly a very difficult task; this is discussed further in section 2.9.

Furthermore, it should be noted that CO_2 will mix to some degree with kerogen and it might displace it from the pores and/or surfaces. In fact CO_2 is used in enhanced oil recovery operations to recovery more hydrocarbons from reservoirs [*Blunt et al.*, 1993; *Manrique et al.*, 2007] and it is an excellent cleaning agent used for instance in dry cleaning [*Dutschk et al.*, 2013] or semiconductor manufacturing [*Liu et al.*, 2010]. An analogue situation, which, however, is based on a different physical phenomenon, is true for clays or cements: the acidic brine can react with these rock components and thus remove them from the surface [*Canal et al.*, 2012]. In this review, we ignore these dynamic effects (ageing and/or reactive transport), which, if they occur, would modify CO_2-wettability of the rock.

Now back to the discussion of the CO_2-water-hydrophobic rock system:

We compiled all literature data about contact angles measured on hydrophobic surfaces for the CO_2-water system we could find and plotted them again as a function of pressure (Figure 14). It is clear that the water contact angles on such hydrophobic surfaces are substantially higher than on hydrophilic surfaces, and θ is typically >90°, so these surfaces are CO_2-wet.

2.7.2. Methylated Glass Surface

Dickson et al. [2006] have partially methylated glass slides with dimethylchlorosilane. This surface corresponds approximately to an oil-wet surface with aliphatic hydrocarbons as surface functional groups, and which is more likely found in a light oil [*Pedersen and Christensen*, 2007]. They created two methylated glass surfaces, one with a 88 mol % methyl group (–CH_3 group) concentration and the other one with a 63 mol % methyl group concentration. On these partially methylated surfaces, they conducted contact angle measurements with scCO_2 (and water) at 296 K, and they found that both surfaces are CO_2-wet with water contact angles ranging between 90° and 160°. The surface with the higher degree of methylation had the higher water contact angle, Figure 14.

2.7.3. Coal Surface

Chi et al. [1988] measured θ on clean, feed, and refuse coal (Upper Freeport coal from Indiana, Pennsylvania), Figure 14. Feed coal is directly retrieved from the coal mine, not processed, and of most interest to our review. Clean and refuse coal were obtained after the water-liquid CO_2 separation process, where the clean coal floated in the CO_2 phase while the refuse remained in the aqueous phase. As expected, the clean coal sample data showed CO_2-wet characteristics (103–154°), while the refuse samples showed a wider range of

Table 7. Influence of Crude Oil and Ageing Procedure on Receding and Advancing Oil-Brine Contact Angles Measured on Quartz Plates (Adopted From *Buckley et al.* [1997])

Organic Fluid	Aging Time (Days)	Aging Temperature (K)	Advancing θ (°)	Receding θ (°)
Crude oil[a]	5	298	56	38
	14	298	43	28
Crude oil[a]	4	361	180	93
	14	361	163	93
Asphaltene[b]	1	298	24	9
Asphaltene[b]	10	298	41	26
Asphaltene[b]	14	298	57	27
Asphaltene[b]	14	353	62	25

[a]Asphaltic crude oil from Prudhoe Bay (density = 894.2 kg/m³, refractive index = 1.51, viscosity = 21.2 mPa s, small amounts of sulphur, nitrogen, oxygen detected).
[b]400 mg/L asphaltene dissolved in toluene. These physical crude oil properties are given to categorize the crude oil used.
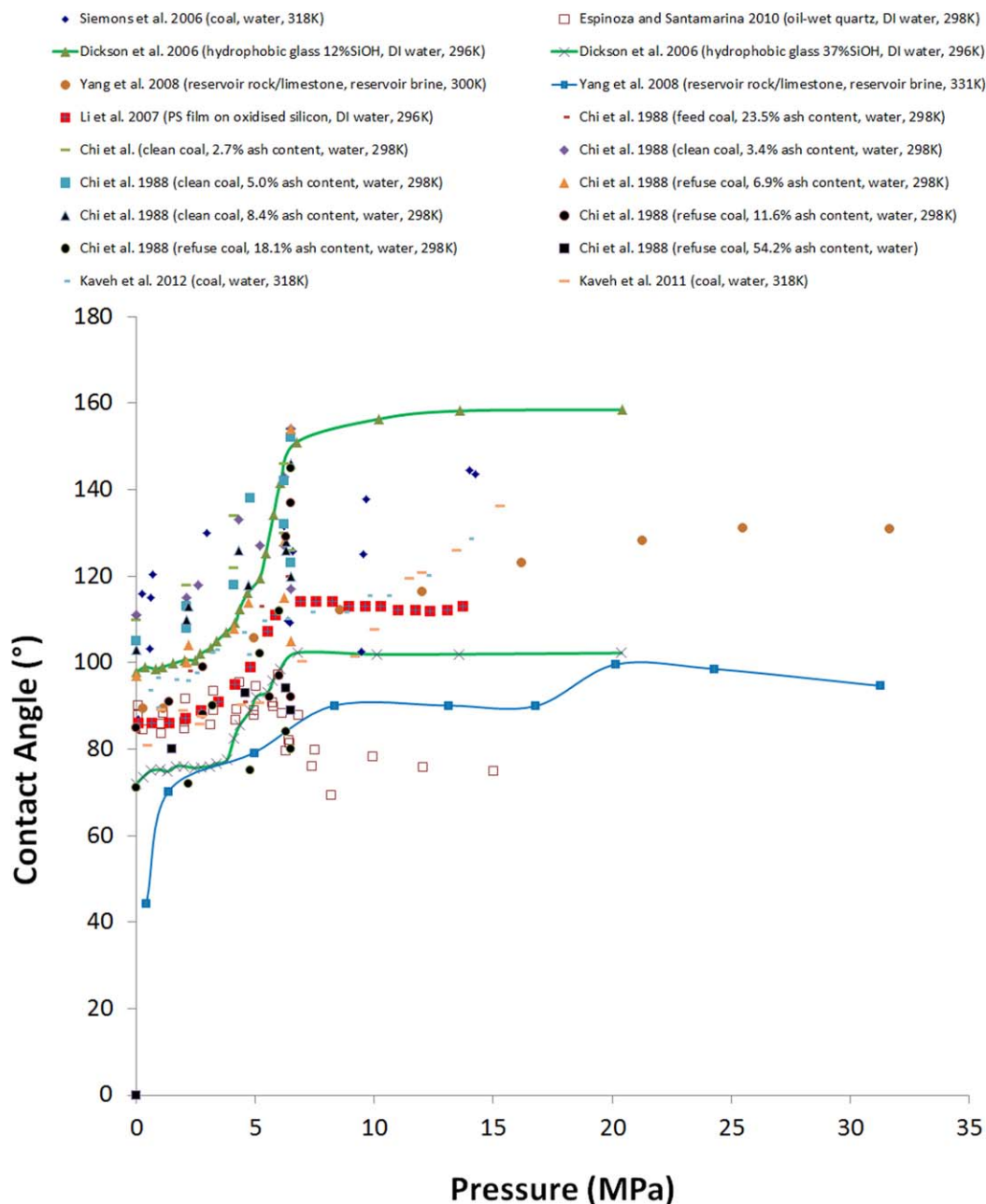
Figure 14. Water contact angles for CO_2-water systems on hydrophobic rock surfaces, including coal, oil-wet quartz/glass, and oil reservoir limestone rock.

wettability from strongly water-wet to CO_2-wet (0–154°). The feed coal was intermediate-wet at atmospheric pressures and turned to CO_2-wet at elevated pressures (84–145°).

Siemons et al. [2006] measured Young's contact angles with the captive bubble method for a coal-water-CO_2 system. The coal sample used was an anthracite mined in England (vitrinite reflectance R_{max} of 2.41%) with a maceral composition of 73.6% vitrinite and 24.6% inertinite and a chemical composition of 85.68 % carbon, 3.36% hydrogen, 1.56% nitrogen, 0.68% sulphur, and 5.58% oxygen. They conducted their experiments at 318 K, and they showed that the coal was intermediate-wet at ambient pressure ($\theta = 85°$) but CO_2-wet at higher pressures. The contact angle increased with pressure approximately following a statistically fitted linear curve ($\theta = 111° + 0.17° \times$ pressure in bar), and it reached approximately 140° at 14.1 MPa (highest investigated pressure), Figure 14.

Kaveh et al. [2011, 2012] measured θ on two coal samples: the high rank, semianthracite Selar Cornish coal (Selar colliery, South Wales, United Kingdom); and the high volatile bituminous medium ranked Warndt Luisenthal coal (Saar basin, Germany). The Warndt Luisenthal coal was polished with abrasive papers, alumina powders, and a fibrous cloth, before being rinsed with water and cleaned ultrasonically [*Kaveh et al.*, 2011], we assume the same preparation procedure was used for the Selar Cornish coal [*Kaveh et al.*, 2012]. Surface roughness was investigated with 2-D and 3-D microscopic images. Petrological properties of the Warndt Luisenthal coal were 74.4% vitrinite, 15.6% liptinite, and 9% inertinite. The volatile matter weight fraction was 40.5% and the vitrinite reflectance R_{max} was 0.71%. Petrological properties of the Selar Cornish coal were 73.6% vitrinite, 0.0% liptinite, and 24.6% inertinite. The volatile matter weight fraction was 10.4% and the vitrinite reflectance R_{max} was 2.41%. Measurements were performed at a constant temperature of 318 K and at pressures from atmospheric to 16 MPa. Measured contact angles increased approximately linearly with pressure for both coals with wettability ranging from $80° < \theta < 90°$ at approximately 0.5 MPa to $\theta \approx$ 130° at 15 MPa. Analysis of the CO_2 density, solubility in water and sorption on wet coal showed that all of these properties change within the pressure range investigated.

2.7.4. Oil-Wet Quartz Surface

Espinoza and Santamarina [2010] aged quartz minerals in medium viscosity Maracaibo Lake crude oil. They then measured the sessile drop water contact angle and found (a) an approximately intermediate-wet surface (θ varied from $\sim 70°$ to 95°), and (b) a small increase in θ with increasing pressure with a maximum around the critical CO_2 pressure, followed by a small drop. This decrease in θ may be due to the cleaning effect of scCO_2, which might remove some of the oil-layer, i.e., the oil-layer introduced by aging could have been instable. This effect needs to be analyzed further.

2.7.5. Polystyrene Surface Layer on Oxidized Silicon

Li et al. [2007] measured water contact angles on an oxidized silicon wafer which was coated with a thin polystyrene (molecular weight = 30 kg/mol) layer. The thickness of the polystyrene layer was varied between 21 and 625 nm. This surface corresponds approximately to an oil-wet surface with aromatic hydrocarbons as surface functional groups; such aromatics are more likely found in heavy oil [*Pedersen and Christensen*, 2007]. The behavior of these surfaces was intermediate-wet ($\theta = 86–114°$), and θ increased with increasing pressure. A relatively high increase was observed at approximately the critical CO_2 pressure, and a thicker polystyrene layer slightly increased θ (by an additional $\sim 5–7°$).

2.7.6. Oil-Wet Reservoir Limestone Rock

Yang et al. [2008] measured water contact angles on an oil-wet reservoir limestone sample from the Weyburn oilfield in Saskatchewan, Canada, Figure 14. This rock was found to be intermediate-wet by multiphase porous media flow experiments [*Potocki et al.*, 2003]. Yang et al. measured (a) a quite wide range of contact angles from $\sim 40°$ to 130°, depending on pressure and temperature, (b) an increase in θ with increasing pressure, and (c) a drop in θ with increasing temperature. At typical storage conditions, this rock would be intermediate-wet toward CO_2 ($\theta \sim 90–100°$).

2.8. Miscellaneous Surfaces

In addition, various other mineral, metal, and polymer surfaces have been tested in terms of CO_2-wettability. Sapphire (Al_2O_3) had a θ between $\sim 45°$ (at a reported pressure of 0 MPa) and $\sim 60°$ (at 30 MPa) [*Wesch et al.*, 1997]; sapphire is thus weakly water-wet. This data set may again be biased because of the surface cleaning method used (cp. section 2.1.2) [*Iglauer et al.*, 2014].

Polytetrafluoroethylene is weakly CO_2-wet (lower pressures) or strongly CO_2-wet (higher pressures), ($\sim 100–150°$) [*Wesch et al.*, 1997; *Espinoza and Santamarina*, 2010; *Sutjiadi-Sia et al.*, 2008]; however, it is not a good representation of an oil-wet rock surface because it is halogenated, i.e., artificially produced and not naturally found. Polyvinylchloride, again an artificial substance, is intermediate-wet to CO_2-wet ($\sim 85–140°$) [*Wesch et al.*, 1997]. We are not discussing CO_2-wettability of metal surfaces here as they are not relevant in a subsurface CCS context.

2.9. Subsurface Conditions

It is recognized that most of the subsurface exists under suboxic or even reducing conditions; consequently, it is highly probable that mineral surfaces in the subsurface are not clean, but instead doped with a variety of molecules which adsorb on the mineral surface. Such adsorbed molecules, however, can be expected to

significantly alter the wettability of the surface [*Adamson and Gast*, 1997]. We thus believe that the effect of adsorption of different molecules onto the relevant mineral surfaces and their impact on θ should be examined, including the influence of their concentration, molecular structure, and distribution on the surface. One challenge in this context is to recover representative cores with representative wettability from the subsurface as drilling mud may have contaminated the samples [*Wunderlich*, 1991] and the change in pressure and temperature conditions may have affected the wettability. Thus possible measures to restore subsurface wettability in the laboratory should be investigated. It may ultimately be required to conduct in situ field tests to measure the true wettability character of a formation, although the outlined laboratory experiments will add substantial confidence to the analysis.

2.10. Conclusions on CO$_2$ Wettability of Mineral and Rock Surfaces

The minerals that form the bulk of storage rock, i.e., quartz and calcite, appear to be strongly or weakly water-wet with fairly low water contact angles (measured in CO$_2$/water/mineral systems). The large uncertainty in the data (cp. Figures 6, 7, and 9) is probably due to surface contamination [*Iglauer et al.*, 2014] and surface roughness effects. It can also be seen from general trendlines that water advancing contact angles are generally higher (between 0° and 60° higher) than the corresponding receding θ as expected. This effect is caused by surface roughness as substantiated by some measurements conducted by *Wang et al.* [2013b], but it is again clouded by possible surface contamination effects; consequently this effect needs to be further analyzed in a more systematic way. However, distinguishing advancing and receding contact angles clearly reduces uncertainty.

Kaveh et al. [2014] measured strongly water-wet conditions for Bentheimer sandstone, which mainly (~96%) consisted of quartz. They found that θ strongly drops with increasing CO$_2$ bubble size, which the authors explain in terms of the interplay of interfacial and buoyancy forces.

Generally similar results as for quartz and calcite were found for mica/muscovite/phlogopite, which are assumed to be representative of caprock forming minerals. Mica appears to be more CO$_2$-wet than quartz or calcite, but it is still weakly or strongly water-wet (Figure 11), especially when considering surface contamination is again likely to be responsible for a shift toward higher measured θ. Feldspar, which is another mineral found in caprocks, has similar wetting properties with regard to CO$_2$ as quartz or calcite, and it is strongly to weakly water-wet. The Rousse caprock (70% calcite, 10% quartz, illite, and chlorite) investigated by *Broseta et al.* [2012] also showed similar CO$_2$-wettability characteristics. In terms of clay materials, it appears that montmorillonite and kaolinite could be CO$_2$-wet, while illite and smectite are likely to be water-wet; however, more data are required to make a conclusion with high confidence about this. It is also not clear—because of the large data spread—whether θ increases with increased pressure or not. Although this increase has been observed in many cases and has been theoretically predicted by molecular dynamics simulations, it has not been observed in other studies or an independent molecular dynamics model. The effects of temperature and salinity could also not be clearly identified because of the large data spread. It is, however, clear that these parameters are important in a CGS context, and new studies should be conducted where (a) controlled surfaces are investigated (e.g., the characteristics of contaminations are well understood or all contaminants are completely removed), and (b) the influence of surface roughness is quantified experimentally. One clear conclusion is that θ on hydrophobic surfaces (including oil-wet quartz and limestone, and coal) are intermediate-wet or CO$_2$-wet, and that θ increases with increasing pressure on such surfaces. Theoretically an increase in θ with a pressure increase can be explained by higher molecular interactions between CO$_2$ and quartz at increased pressure (because CO$_2$ is then denser) [*Iglauer et al.*, 2012b] but it is unclear why some experiments did not confirm this prediction and why *Tsuji et al.*'s [2013] model does not predict that.

Overall it is clear that condensed scCO$_2$ behaves significantly different than gaseous CO$_2$ in terms of wettability, and it is important that these effects are considered in field scale predictions for CGS. We highlight this with examples in the discussion section of this review. We can generally say that none of the CO$_2$ systems is completely water-wet (i.e., $\theta = 0°$) at reservoir conditions as sometimes assumed. Furthermore, we think that—because of the complex geology and caprock formation process and exposure of the caprock to reservoir fluids over very long time periods—caprock surfaces could in theory be either hydrophilic or hydrophobic, which would mainly depend on the organic molecules present in the reservoir fluids, but also to some extent on the mineral surfaces and thermophysical conditions. The hydrophobicity could have been attained by exposure to organic molecules which adhere to the rock surface (molecular monolayer concentrations of such organic

molecules would be sufficient), or precipitation of organic molecules onto the rock surface. This area requires more study.

We also note that information about a few important rock-forming minerals are missing, including dolomite, anhydrite, siderite, and halite.

Furthermore, conducting θ measurements directly on small clay crystals (size $\sim$2 μm) using the standard sessile or captive drop technique (with a fluid drop length $\sim$1 mm) is not possible and an improved technique needs to be developed to dispense smaller droplets on these small crystals, or altogether different techniques need to be employed (see discussion in the following sections).

3. Capillary Pressure Measurements on Tight Rocks

Generally, CO_2 migration through the water-saturated pore network of a caprock may occur when the CO_2 fluid pressure in the reservoir exceeds the capillary entry pressure p_e (i.e., nonwetting fluid is entering the capillary pore space of a sealing formation). This is valid for the intergranular pore space but also for water-filled (micro-)fractures, for which p_e would be much lower because of their much larger idealized radii (cp. equation (5)). At pressures above the capillary breakthrough pressure p_{br}, at which a continuous flow path of the nonwetting fluid forms across the pore system, CO_2 can escape from the upper top of the caprock sequence [e.g., *Al-Basali et al.*, 2005; *Busch and Amann-Hildenbrand*, 2013; *Hildenbrand et al.*, 2002; *Li et al.*, 2005] through convective flow.

Measurements of capillary pressure p_c of low permeability rocks have initially been performed for the characterization of hydrocarbon reservoirs or nuclear waste disposals [*Gallé*, 2000; *Pusch et al.*, 1985; *Schlömer and Krooss*, 1997; *Schowalter*, 1979]. In recent years, the focus of research shifted more to the characterization of CO_2 storage reservoirs and their sealing lithologies [*Bennion and Bachu*, 2007; *Hildenbrand et al.*, 2002, 2004; *Li et al.*, 2005, 2006; *Wollenweber et al.*, 2009, 2010], an overview is provided by *Busch and Amann-Hildenbrand* [2013].

Thus the capillary entry pressure p_e determines the maximum gas column height which can be permanently stored by structural trapping. p_c is also the pressure difference at the reservoir/caprock interface that evolves after CO_2 injection into a reservoir. Consequently, the precise determination of p_c, p_e, and p_{br} is crucial for leakage risk assessments and the associated public and legal acceptance of geological CO_2 storage.

3.1. Definitions of Capillary Pressures of Caprocks

By definition, the drainage process refers to a nonwetting phase displacing the wetting phase, and the scale of this displacement process can exceed the percolation threshold so that continuous flow paths of the nonwetting phase form across the pore system. Especially with respect to low-permeability rocks, the literature terminology describing this process includes "threshold displacement pressure" [*Ibrahim et al.*, 1970], "threshold pressure" [*Thomas et al.*, 1967], "pore entry pressure" [*Gallé*, 2000], "critical pressure" [*Gallé*, 2000], or "breakthrough pressure" [*Horseman et al.*, 1999]. If the excess pressure of the nonwetting phase increases further, additional fluid flow pathways will develop across the porous medium, thus increasing the effective permeability to the nonwetting phase and the nonwetting phase saturation. For low-permeability rocks, several authors determine p_{br} from drainage experiments [*Egermann et al.*, 2006a; *Gallé*, 2000; *Horseman et al.*, 1999; *Li et al.*, 2005]. A detailed list of terms is provided in *Hildenbrand et al.* [2002]. A reduction of the excess pressure in the nonwetting phase after gas breakthrough will lead to the reimbibition of the wetting phase, starting with the smallest pores and proceeding successively to larger pores. This process results in a continuous decrease in permeability for the nonwetting phase. Ultimately, when the last interconnected flow-path is blocked with the reimbibing phase (e.g., water if the rock is water-wet), the permeability for the nonwetting phase will drop to zero and a pressure difference will persist between the gas phases below and above the seal. This residual pressure difference or "snap-off" pressure p_{sn} (pressure at which the largest interconnecting capillary is blocked with the wetting phase) is assumed to be lower than p_{br} of the drainage path [e.g., *Busch and Amann-Hildenbrand*, 2013; *Zweigel et al.*, 2004]. Drainage and imbibition processes are characterized by different pressure/saturation and relative permeability/saturation curves. In general, the wetting fluid permeability is lower during imbibition than during drainage. For low-permeability rocks, this phenomenon has so far only been marginally investigated experimentally [e.g., *Bennion and Bachu*, 2007; *Hildenbrand et al.*, 2002; *Busch and Amann-Hildenbrand*, 2013].

Table 8. Breakthrough Pressures (p_{br}) Determined With Different Gases on Weyburn Anhydrite Seal Formation Rock [*Li et al.*, 2005][a]

| Sample | ϕ (%) | k (10^{-21} m^2) | p_{br} (MPa) | | | p_{br} Ratio | | γ Ratio | | |
			N$_2$	CO$_2$	CH$_4$	N$_2$/CO$_2$	CH$_4$/CO$_2$	N$_2$/CO$_2$	CH$_4$/CO$_2$	$\theta_{CO2\text{-}brine}$ (°)[b]
A15	0.3	6.41	27.9	9.2		3.0		2.7		27
A5	0.3	25.6	29.7	11.2		2.7		2.8		0
A8	0.7			5	12.8		2.6		2.3	

[a]Interfacial tension data from *Li et al.* [2005].
[b]Assumed circular capillary tube and θ (N$_2$-brine-rock) = 0°.

Methods to determine capillary breakthrough and snap-off pressures p_{br} and p_{sn} have been described and compared in detail by *Egermann et al.* [2006a].

In the following the term "breakthrough" (for primary drainage) and "snap-off" (for secondary imbibition) will consistently be used in the context of the characterization of low-permeability rocks serving as seals above CO$_2$ storage reservoirs. Experimental methods have been summarized comprehensively in *Egermann et al.* [2006a] and *Busch and Amann-Hildenbrand* [2013]. These include the direct methods of measuring "snap-off" and "breakthrough" pressures on sample plugs as well as mercury porosimetry conventionally performed on sample fragments.

3.2. Capillary Pressure Data for Caprocks
3.2.1. Breakthrough Pressure on Drainage Path
Boulin et al. [2011] used four different methods (all described in *Egermann et al.* [2006a]) to obtain breakthrough and snap-off nitrogen-brine p_c values for two different seal formations at 298 K: a carbonatitic sandstone (Tavel), characterized by a mean pore diameter r' of 250 nm, permeability k of 1.48×10^{-18} m^2 (1.5 μD), and porosity ϕ of 14%; and the sealing formation overlying the Stuttgart formation used as storage horizon in the CO$_2$SINK project near Ketzin, Germany. This is an anhydrite-rich mudrock with $r' = 10$ nm, $k = 1.63 \times 10^{-20}$ m^2 (16.5 nD), and $\phi = 15\%$. It was shown that the standard, continuous, and dynamic methods provide approximately the same breakthrough p_c value, in this case ranging between 1.1 and 1.3 MPa (depending on confining pressure) for the Tavel sample. The difference is rather related to the confining pressure than to the method used. The authors also performed a residual pressure experiment (imbibition path) and found that p_c decreased by ~50% to a value of ~0.5 MPa. As mentioned previously, a lower value is expected given the differences in advancing and receding contact angles. A similar attempt was made for the Ketzin sample while only the standard and dynamic methods provided suitable values which, however, gave a consistent result, $p_c \sim 12$ MPa.

Li et al. [2005] examined the seal formation of the Weyburn project at 332 K; there CO$_2$ is injected to enhance oil recovery and at the same time the project is used as a test site to verify carbon storage options. The sealing formation is the Midale evaporite, consisting of anhydrite and anhydritic dolomite with permeabilities as low as $6.9 \times 10^{-21} - 2.56 \times 10^{-20}$ m^2 (7–26 nD) and porosities of 0.3–0.7% (for the samples used for the CO$_2$ tests). The authors used the standard (step-by-step) approach [*Egermann et al.*, 2006a] to measure breakthrough pressures, and they used CO$_2$, N$_2$, and CH$_4$ as test gases. Results are summarized in Table 8 showing that the ratio in p_{br} values determined with different gases approximately corresponds to the ratio of their respective fluid-fluid interfacial tension values. Li et al., therefore, concluded that CO$_2$/brine/anhydrite is water wetting (when assuming that the corresponding N$_2$ and CH$_4$ systems are also water-wet). Table 8 also includes an estimate of the CO$_2$-brine-rock contact angle. We base our estimate on the assumption that the largest pore can be modeled by a cylindrical capillary tube. We thus equate equation (5) for the CO$_2$-brine and N$_2$-brine cases assuming the N$_2$-brine-rock contact angle is zero. We then insert interfacial tensions and breakthrough pressure ratios for the N$_2$-brine and CO$_2$-brine systems listed in Table 8 (from *Li et al.* [2005]); and we solve for the unknown CO$_2$-brine-rock contact angle. The resulting estimates indicate that the systems are completely or strongly water-wet. As pointed out in section 1.2, our estimate is only rough and it is biased because p_c is also a strong function of the pore morphology [cp. for instance *Purcell*, 1950].

3.2.2. Snap-Off Pressure During Imbibition
The snap-off pressure, on the imbibition path, is typically lower than the corresponding entry or breakthrough pressure on the drainage path. While this parameter is less relevant for caprock sealing assessment

Table 9. CO_2/Brine and N_2/Brine Snap-Off Capillary Pressures Determined on Identical Boom Clay Plug Samples From the Nuclear Waste Storage Research Site at Bure, Belgium at 323 K and Related Hg/Air Capillary Pressures Determined on Associated Cuttings[a]

| Sample | ϕ (%) | k ($\times 10^{-21}$) | p_{sn} (MPa) | | | p_c Ratio | | | γ Ratio[b] | | | $\theta_{CO2\text{-}Brine}$ (°)[c] |
			N_2/Brine	CO_2/ Brine	Hg/Air	N_2-Brine/ CO_2-Brine	Hg-Air/ CO_2-Brine	Hg-Air/ N_2-Brine	N_2-Brine/ CO_2-Brine	Hg-Air/ CO_2-Brine	Hg-Air/ N_2-Brine	
2000254	24	40.4	0.5	0.3	15.5	1.7	51.7	31.0	1.9	11.8	5.9	0
2000251	23.5	23.7	1.3	0.1	0.8	13.0	8.0	0.6	1.9	11.8	5.9	82
2000253	23.4	64.1	0.8	0.3	0.7	2.7	2.3	0.9	1.9	11.8	5.9	45
2000253	23.4	16.7	1.4	0.5	0.7	2.8	1.4	0.5	1.9	11.8	5.9	47

[a]All data by *Hildenbrand et al.* [2002, 2004]. CO_2 contact angles $\theta_{CO2\text{-}brine}$ have been estimated, scaling the N_2 and CO_2 p_{sn} pressures and assuming perfect water-wet conditions for the N_2 measurements.
[b]Note that Hg/air contact angle is included, based on a value of 141°.
[c]Assumed circular capillary tube and θ (N_2-brine) = 0°.

it is easier and more time-efficient to determine and therefore used as a conservative value for the more relevant capillary entry pressure. In addition, knowing the snap-off pressure gives an estimate of the reduction in reservoir pressure needed to stop capillary leakage in case the breakthrough pressure was exceeded. There are few studies reporting snap-off capillary pressures using CO_2 on plug samples of different lithotypes, including mudrocks, sandstones, and carbonate-rich rocks that all originate from the same research group [*Alles*, 2008; *Amann-Hildenbrand et al.*, 2013a, 2013b; *Hildenbrand et al.*, 2002, 2004; *Wollenweber et al.*, 2010]. A summary of these studies is provided in *Busch and Amann-Hildenbrand* [2013]. For the purpose of this review, we focus on measurements using the same rock sample, and discuss different reference fluids with known wettability and interfacial tensions [*Hildenbrand et al.*, 2002, 2004]. These experiments were conducted on four different Boom Clay samples, and are summarized in Table 9, while permeability and porosity of these four samples were similar with 23–24% and 1.67–6.41 $\times 10^{-20}$ m^2 (17–65 nD), respectively, N_2/brine and CO_2/brine snap-off pressures varied quite notably. The ratio of these two parameters ranges between 1.5 and 2.7 with one exception (ratio of 13). This is in line with the interfacial tension ratio of 1.9 for these two fluid pairs. We also compared the gas/brine p_c data with measured Hg/air values (to determine capillary entry pressures) in the same table. It is obvious that there is a mismatch between the p_{sn} and the corresponding interfacial tension ratios that is significant. Reasons are unclear, interfacial tension, and contact angle data for Hg/air are well established and we assume that this is related to the usage of the Hg porosimetry method in general, in the interpretation of the data, or to the effect that θ values below 22° can be ignored for imbibition (cp. section 1.2) [*Anderson*, 1987b; *Morrow*, 1976]. Table 9 also includes our estimates for the CO_2-brine-rock contact angle, we apply the same methodology as for the breakthrough pressure data in Table 8 as described above. The estimated contact angles indicate that the samples were completely ($\theta = 0°$) or still strongly water-wet ($\theta = 45°$, 47°), with the exception of sample 2000251 which was intermediate-wet ($\theta = 82°$).

As attempted previously by *Busch and Amann-Hildenbrand* [2013], we tried to infer some relationships from the CO_2/brine snap-off data by plotting p_{su} (snap-off capillary
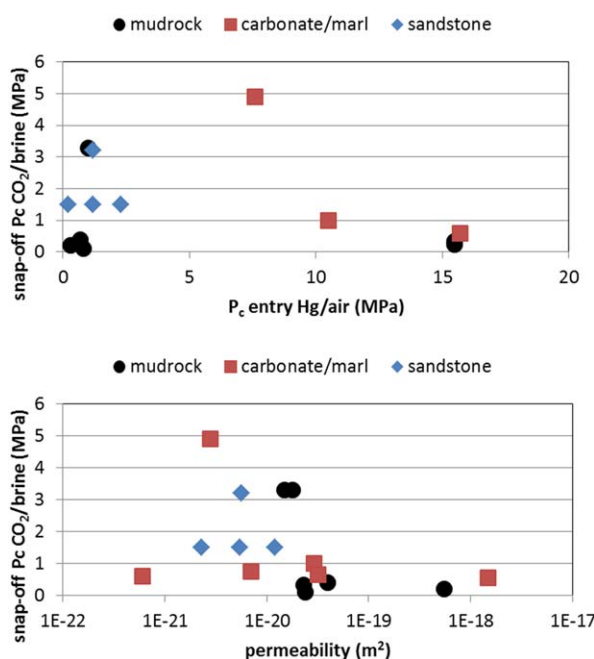

Figure 15. CO_2/brine snap-off capillary pressures as a function of (top) Hg/air entry pressures and (bottom) brine permeability for available data sets on mudrocks, sandstones, and carbonates. Data from *Alles* [2008], *Amann-Hildenbrand et al.* [2013a, 2013b], *Hildenbrand et al.* [2002, 2004], and *Wollenweber et al.* [2010].

Table 10. A Summary of the Flow Sequences, and Their Definitions, Considered in This Work[a]

Flow Sequence	Description
Primary imbibition	The initial filling of the dry pore space with brine. Usually occurs significantly earlier than the subsequent flow sequences
Primary drainage	Brine is displaced from a fraction of the pore space by the introduction of a nonwetting phase (assuming water-wet conditions)
Secondary imbibition	Brine reimbibes into the pore space, displacing a fraction of the nonwetting phase
Secondary drainage	The nonwetting phase reenters the pore space, displacing a fraction of the wetting phase

[a]Tertiary flow sequences are not summarized although they simply represent the third sequence of displacements, following the same pattern described. Water-wet conditions are assumed—in case of CO_2-wet rock drainage and imbibition are interchanged.

pressure) against permeability and Hg/air capillary entry pressures (Figure 15). The expectation would be that within a certain error range CO_2/brine and Hg/air capillary pressures correlate and that a relationship between CO_2/brine capillary pressure and permeability can be identified. In both cases, this was not possible. There is only a tendency of increasing CO_2/brine p_c values with decreasing permeability (Pearson correlation coefficient $R^2 = 0.07$) which is however not dominant. This leaves us with a range of speculations: (a) different CO_2/brine/rock contact angles could impact results. This might be the case especially when comparing rocks of different mineralogy (quartz-rich, clay-rich, and carbonate-rich). Another reason might be (b) errors induced by sample preconditioning for Hg/air data, especially for rocks rich in swelling clays such as some of the mudrocks used in Figure 15. Interpretation of Hg porosimetry curves is also not straightforward as discussed by *Amann-Hildenbrand et al.* [2013a, 2013b]. Furthermore, (c) the general alteration state of the samples is certainly an important factor and it is known that especially clay-rich rocks tend toward dehydration-cracking, while such cracks can completely determine capillarity in such rocks. Microfractures during plug drilling or sample mounting might also play a role and p_c values would be dramatically underestimated.

Assuming the correctness of the data (no error bars were given in the article), these and probably some more factors can cause the inconsistency of the results and it is not possible to rank these reasons. In conclusion, no general statements on wettability can be drawn from the given CO_2/brine snap-off pressures, and more experiments of this kind should be conducted.

4. Wettability of Reservoir Rocks

4.1. Capillary Pressure

We now extend our discussion of capillary pressures to include reservoir formation rock types. There are two saturation change processes of interest as mentioned above: drainage and imbibition. The order in which displacements take place is denoted by the terms primary, secondary, tertiary, and so on. Table 10 summarizes the flow sequences of interest in our discussion. It is important to note that the capillary pressure can be negative when the wetting phase pressure exceeds the nonwetting phase pressure (cf. equation (2)) during both drainage and imbibition. We refer to imbibition at positive capillary pressure as spontaneous imbibition and imbibition at negative capillary pressure as forced imbibition. As previously discussed, drainage and imbibition capillary pressure curves are typically not identical due to capillary pressure hysteresis which is caused by the difference between advancing and receding contact angles (i.e., surface roughness and chemical heterogeneity), impact of pore morphology (e.g., compare discussion in section 1.2 and, for instance, *Purcell* [1950]), and residual trapping (caused by nonwetting fluid snap-off [*Roof*, 1970]).

An analysis of the form of the drainage and imbibition $p_c(S_w)$ curves with respect to the $p_c = 0$ axis can give a clear indication of wettability. This approach is favored in the petroleum industry where a range of wettability indices have been proposed as a means to quantify wettability behavior [*Amott*, 1959; *Donaldson et al.*, 1969; *Longeron et al.*, 1995]. These wettability indices consider the relative shape of the secondary imbibition and secondary drainage curves in relation to the $p_c = 0$ axis.

We do not provide a detailed description of wettability indices here; rather we describe how to qualitatively interpret $p_c(S_w)$ curves with regard to the system's wettability. For this thought experiment, we consider the primary drainage and secondary imbibition $p_c(S_w)$ curves of a CO_2-brine-rock system: these are the relevant flow sequences when CO_2 is injected into a brine filled aquifer, and is subsequently displaced by inflowing water.
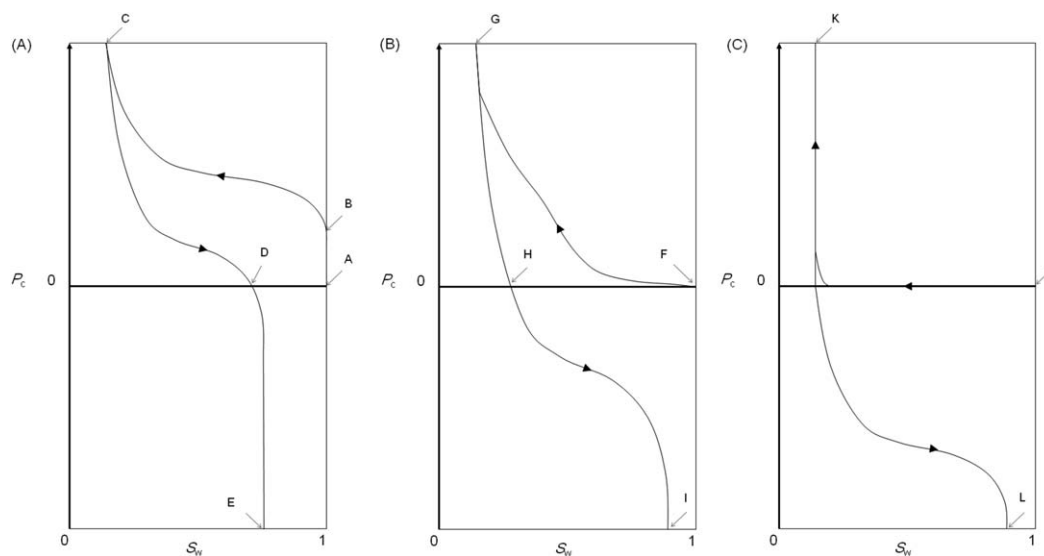
Figure 16. $p_c(S_w)$ relationships for (a) a strongly water-wet system, (b) an intermediate-wet system, (c) and a CO_2-wet system.

4.1.1. Water-Wet Rock

First, imagine a strongly hydrophilic system where there is a preference for the rock surface to be covered by water. Initially the pore space is filled with water and CO_2 will not enter ($p_c = 0$; point A, Figure 16a); for this to occur a capillary entry pressure (p_e) constraint or threshold must be overcome (point B, Figure 16a). This is because water-wet rock has a higher affinity to water and it requires energy to displace the water with CO_2 (which has a lower affinity to the rock). As p_c is increased more CO_2 enters the system displacing water until an irreducible water saturation is attained, we define an irreducible saturation as one where an increase in p_c (within typical laboratory and reservoir ranges) will not result in further saturation changes (point C, Figure 16a). p_c is subsequently decreased causing water to spontaneously imbibe into the system: the secondary imbibition flow sequence has begun. During imbibition virtually all saturation change occurs spontaneously and no water imbibes at negative p_c (between points D and E, Figure 16a). In this example, work is required during primary drainage due to the unfavorable surface free energy change when CO_2 displaces water; the work required being related to the area under the capillary pressure curve [*Leverett*, 1941; *Morrow*, 1970]. Conversely no—or very little—work is performed to change the saturation during imbibition due to the favorable surface free energy change [*Schwartz*, 1969]. This is a clear indication that the system is strongly water-wet.

4.1.2. Intermediate-Wet Rock

We can also consider an alternative state where the rock is less hydrophilic and hence termed intermediate-wet. CO_2 now enters the rock at a lower p_e in the range $0 < p_e < p_{e\_water-wet}$ (where $p_{e\_water-wet}$ is the capillary entry pressure in the water-wet scenario) (point F, Figure 16b). As p_c is increased water is displaced until an irreducible water saturation is reached (point G, Figure 16b). Note that the area under the primary drainage curve is smaller than in the water-wet scenario: less work is required to achieve a comparable displacement of water by CO_2. During secondary imbibition, the water saturation increases and importantly this occurs at both positive (points G to H, Figure 16b) and negative (points H to I, Figure 16b) p_c, in contrast to the water-wet case (Figure 16a). In this example, we see that both CO_2 saturation and water saturation can increase with only limited work being performed. This indicates that the system is not strongly wetting to either phase. It is important to note that positive or negative p_c does not in itself describe wettability. Saturation changes occurring when the CO_2 pressure exceeds the water pressure is not a measure of CO_2-wetting in a particular saturation range. If the pore space were an idealized capillary tube this would be true but in reality the complex interplay of pore morphology and wettability allows for both spontaneous and forced saturation changes even for strongly water-wet systems (excluding $\theta = 0°$) [*Purcell*, 1950].

4.1.3. CO_2-Wet Rock

Finally, we consider a strongly CO_2-wet system. While our discussion of the strongly water-wet and intermediate-wet cases is informed by experimental studies from the petroleum industry [notably *Killins*

Table 11. CO_2 Capillary Entry Pressure (p_e) Measurements on a Limestone [*Egermann et al.*, 2006b] and Quartz Sand Systems [*Plug and Bruining*, 2007; *Tokunaga et al.*, 2013][a]

Reference	S_w (–)	p_e (Pa)	T (K)	$p_{\_water}$ (MPa)
Egermann et al. [2006b]	1.00	20,500	333	14.0
		19,500	353	10.0
		18,000		18.0
Plug and Bruining [2007]	1.00	−35	313	8.5
Tokunaga et al. [2013]	1.00	105	318	8.5
	0.97	252		
	0.96	90		12.0
	0.94	127		

[a]Measurements in the limestone match closely to an (γ-scaled) Hg-air p_e of 24,000 Pa reported in the same study.

et al., 1953], there are few measurements of the shape of the $p_c(S_w)$ curve when a strongly wetting phase displaces a nonwetting phase from a porous medium initially entirely saturated with the nonwetting phase. The only example we are aware of is that measured on preferentially oil-wet sandstone from the Elk Basin reservoir (Wyoming, USA) using formation brine and stripped (degassed) reservoir oil [*Welge*, 1949]; where oil was observed to spontaneously enter the rock, without the application of force. With this data as a reference, we envisage that the $p_c(S_w)$ curves for a strongly CO_2-wet system are of the form illustrated in Figure 16c. CO_2 enters the rock at $p_c = 0$ (points J to K, Figure 16c) displacing water until an irreducible saturation is achieved. Most of this saturation change is achieved at $p_c = 0$ with only a minimal amount of work required to expel additional water from the system (i.e., upon increasing p_c). As p_c is decreased water will only enter the system upon the application of force (i.e., at negative p_c: points K to L, Figure 16c). We refrain from using the terms drainage and imbibition in the CO_2-wet context due to the change in their definitions compared to the water-wet case (drainage would indicate the water saturation is increasing in the CO_2-wet system).

In summary, studying the relative saturation changes at positive and negative capillary pressures during primary drainage and secondary imbibition can aid our understanding of wettability in CO_2-brine-rock systems.

Primary drainage capillary pressure curves have been measured for scCO$_2$-brine-sand [*Plug and Bruining*, 2007; *Tokunaga et al.*, 2013], scCO$_2$-brine-sandstone [*Pentland et al.*, 2011; *Pini et al.*, 2012; *Akbarabadi and Piri*, 2013; *Sarmadivaleh and Iglauer*, 2014] and scCO$_2$-brine-carbonate systems [*El-Maghraby and Blunt*, 2013]. Furthermore imbibition capillary pressure curves have been measured for scCO$_2$-brine-sand systems [*Plug and Bruining*, 2007; *Tokunaga et al.*, 2013]. Only one study has reported both spontaneous and forced imbibition data [*Plug and Bruining*, 2007]. No scCO$_2$-brine secondary drainage data have been reported to date. We now consider three aspects of capillary-pressure measurements: capillary entry pressure (p_e); the relative shapes of the drainage and imbibition $p_c(S_w)$ curves with respect to the $p_c = 0$ axis; and the scaling of $p_c(S_w)$ curves for different fluid pairs. The lack of secondary drainage data means wettability index analysis is not possible.

4.1.4. Capillary Entry Pressure of CO_2 Entering Reservoir Rocks During Primary Drainage

At the start of primary drainage, a capillary entry pressure (p_e) (the maximum p_c reported at $S_w = 1$) must be applied to force a nonwetting phase into a sample saturated with the wetting phase. Table 11 summarizes reported p_e measurements for scCO$_2$-brine fluid systems [*Egermann et al.*, 2006b; *Plug and Bruining*, 2007; *Tokunaga et al.*, 2013]. For quartz sands, *Plug and Bruining* [2007] measured a small negative p_e and *Tokunaga et al.* [2013] measured small positive p_e values at or close to $S_w = 1$; while for a quarry limestone, *Egermann et al.* [2006b] measured positive p_e at the start of unsteady-state coreflood experiments. S_w values below unity in the results of Tokunaga et al. indicate spontaneous scCO$_2$ invasion at $p_c = 0$. This may be due to system wettability, large open pores at the outer edges of the sample, or measurement accuracy (uncertainty in p_c and S_w was 20 Pa and 0.03, respectively). Entry pressures scaled with γ (using the Young-Laplace relationship) show that scCO$_2$-brine p_e/γ was lower than air-brine p_e/γ [*Tokunaga et al.*, 2013], slightly lower than liquidCO$_2$-brine p_e/γ [*Plug and Bruining*, 2007] and comparable to Hg-air p_e/γ [*Egermann et al.*, 2006b], when measured for the same porous media. Overall most p_e data [*Egermann et al.*, 2006b; *Tokunaga et al.*, 2013] are positive; work must be performed to force CO_2 into a water-filled sample indicative of the sample being water-wet. However, *Plug and Bruining* [2007] reported a small negative p_e and as such further data are required to reach a firm conclusion.

Further studies reporting primary drainage capillary pressure curves on sandstones [*Pentland et al.*, 2011; *Pini et al.*, 2012; *Pini and Benson*, 2013; *Sarmadivaleh and Iglauer*, 2014] and a limestone [*El-Maghraby and Blunt*, 2013] lack data close to $S_w = 1$, making it difficult to draw conclusions regarding p_e for the sandstones and limestone investigated.
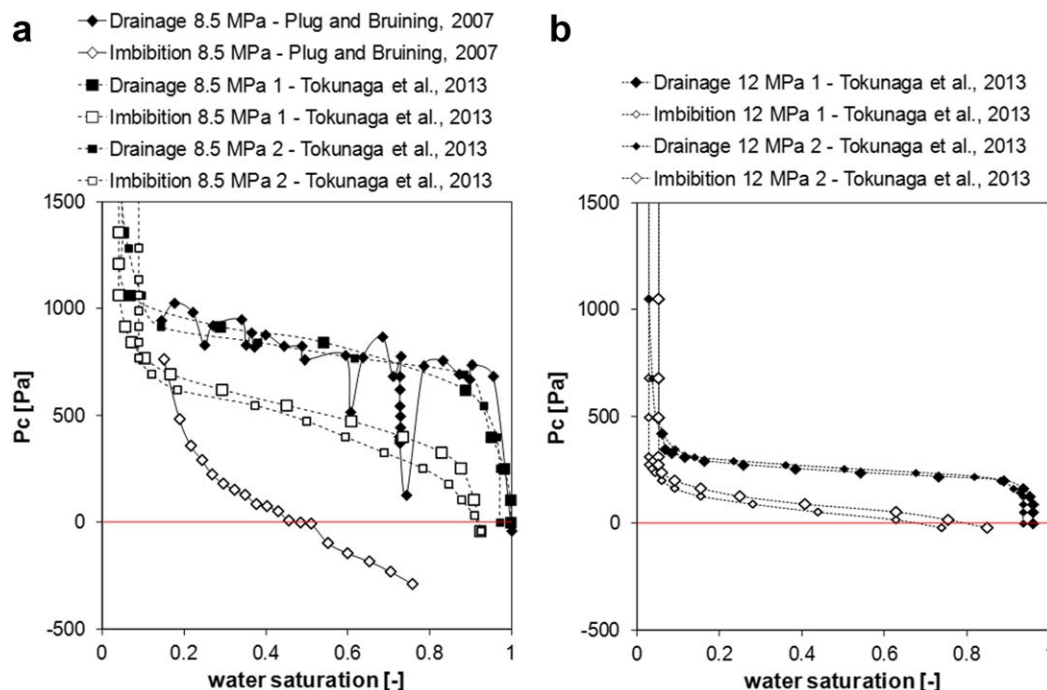
Figure 17. Primary drainage (solid markers) and secondary imbibition (open markers) capillary pressure curves for scCO$_2$-brine-sand systems measured at (left) p_{water} = 8.5 MPa and (right) p_{water} = 12 MPa. Measurements were made at 8.5 MPa and 313 K [*Plug and Bruining*, 2007], 8.5 MPa and 318 K [*Tokunaga et al.*, 2013], and 12 MPa and 318 K [*Tokunaga et al.*, 2013]. The p_c = 0 axis is highlighted in red.

4.1.5. Form of the $p_c(S_w)$ Relationship

To the best of our knowledge, only two studies have reported primary drainage and secondary imbibition $p_c(S_w)$ data for scCO$_2$-brine systems [*Plug and Bruining*, 2007; *Tokunaga et al.*, 2013], both for quartz sands (Figure 17).

From the data, we see that most of the saturation changes occur at positive capillary pressure; with the exception of the first drainage point (S_w = 1) and part of the secondary imbibition curve ($S_w > \sim 0.5$) in the data of *Plug and Bruining* [2007]. This indicates that the scCO$_2$-brine-quartz sand system is water-wet: work must be performed to force CO$_2$ into the pore space during drainage and most of the water imbibition occured spontaneously. The presence of saturation change at negative p_c discounts the system being perfectly water wet ($\theta = 0°$); cf. wettability definitions in Table 2. It is interesting to note that for the measurements performed at p_{water} = 8.5 MPa, the primary drainage curves match closely whereas the imbibition curves differ significantly between these studies.

4.1.6. Capillary Scaling Relationships

A number of studies have compared the $p_c(S_w)$ relationship for different fluid pairs, and also different rock types, through scaling analyses (Table 12). *Plug and Bruining* [2007] showed that primary drainage curves for gaseous and supercritical CO$_2$ coincided when capillary pressure was scaled by interfacial tension (p_c/γ) using the Young-Laplace relationship; while for secondary imbibition this was not possible. The authors concluded that if the CO$_2$ is in a supercritical state, then quartz sand could be altered to an intermediate wetting state. *Pentland et al.* [2011] showed that mercury-air, decane-brine, and scCO$_2$-brine primary drainage curves in Berea sandstone coincided within experimental error after scaling with γ and contact angle, although measurement uncertainty was higher than in other studies. The scCO$_2$-brine drainage contact angle was assumed to be 0°. Consistent with Pentland et al., *Pini et al.* [2012] found close agreement between scCO$_2$-brine and mercury-air primary drainage curves in Arqov and Berea sandstone by scaling using the Leverett-*J* function [*Leverett*, 1941] that considered both contact angle and γ [after *Rose and Bruce*, 1949]. Mercury-air and scCO$_2$-brine primary drainage measurements were shown to match after scaling for γ (contact angles were assumed equal) in Berea, Paaratte, and Mt. Simon sandstones [*Krevor et al.*, 2012]. *Pini and Benson* [2013] used θ as a fitting parameter to achieve coalescene of mercury-air, nitrogen-brine, and scCO$_2$-brine primary drainage curves in Berea sandstone after scaling for γ. Fitted contact angles were

Table 12. A Summary of the CO_2-Brine-Mineral Studies That Have Investigated $p_c(S_w)$ Scaling

Reference	Rock Type	T (K)	P (MPa)	K (m^2)	ϕ (–)	Scaling Method
Plug and Bruining [2007]	Unconsolidated quartz sand	313	8.5	2×10^{-10}	0.32	γ
Pentland et al. [2011]	Berea sandstone	343	9.0	4.6×10^{-13}	0.22	$\gamma\cos\theta$
Krevor et al. [2012]	Berea sandstone	323	9.0	9.0×10^{-13}	0.22	$\gamma\cos\theta$
	Paaratte sandstone			1.1×10^{-12}	0.28	
	Mt. Simon sandstone			7.4×10^{-15}	0.24	
Pini et al. [2012]	Arqov sandstone	298 and 323	9.0	2.8×10^{-14}	0.11 and 0.10	$\gamma\cos\theta$
	Berea sandstone			2.7×10^{-13}	0.20	
Pini and Benson [2013]	Berea sandstone	323	9.0	3.0×10^{-13}	0.19	$\gamma\cos\theta$[a]
Sarmadivaleh and Iglauer [2014]	Berea sandstone	323	10.0	4.4×10^{-13}	0.20	$\gamma\cos\theta$
Tokunaga et al. [2013]	Unconsolidated quartz sand	318	8.5 and 12.0	3.9×10^{-11}	0.38	Both γ and $\gamma\cos\theta$

[a]Variations in fitted θ were found to be small and were subsequently ignored.

found to be very similar ($\sim$40°) and were hence ignored in further scaling analysis. A result consistent with *Pentland et al.* [2011] and *Pini et al.* [2012] was obtained by *Sarmadivaleh and Iglauer* [2014] when using the Leverett-*J* scaling function on a Berea plug, measurement conditions were 323 K and 10 MPa water pressure. *Tokunaga et al.* [2013] showed that by scaling γ it was not possible to coalesce air-brine and scCO$_2$-brine (p_{water} = 8.5 and 12 MPa) curves for either primary drainage or secondary imbibition, but by scaling for contact angle (drainage imbibition angles of 77° and 85°, respectively) coalescence was achieved. The authors concluded that scCO$_2$ exposure time may be an important factor in altering the wettability of silica surfaces.

It should be noted that the basis for contact angle scaling has been questioned (as summarized by *Anderson* [1987b]) due to the inherent assumption of a bundle of tubes (cylindrical) pore geometry. By considering more complex pore geometries such as a toroid, *Purcell* [1950] has shown that there is a different capillary entry pressure behavior for contact angles above 90° where entry depends not only on geometry and contact angle, but also the position of the interface within the pore. Simplistic scaling relationships for contact angles greater than 90° would thus appear questionable. This finding is consistent with a previous experimental study that showed that air-liquid drainage curves in teflon cores, scaled for γ only, coalesced if the equilibrium contact angle was less than 50°, whereas the imbibition curves coalesced for contact angles <22° [*Morrow*, 1976]. This difference in behavior between drainage and imbibition may go some way to explain the inability of *Plug and Bruining* [2007] and *Tokunaga et al.* [2013] to coalesce their imbibition measurements through γ scaling alone.

It is nevertheless clear that θ has an influence, which, however, is clouded by the complicated pore morphology; advanced pore space models (e.g., network models) [*Dong and Blunt*, 2009], or direct microcomputed tomography images [*Iglauer et al.*, 2010; *Jettestuen et al.*, 2013] may improve θ scaling and associated $p_c(S_w)$ curve predictions in the future.

4.2. Relative Permeability

The concept of relative permeability arises when more than one fluid phase resides within a porous medium. The relative permeability of a fluid is defined as its effective permeability divided by the absolute (single-phase) permeability of the medium. In case of multiple fluids in the rock, the flow of each fluid phase is typically impeded by the presence of the other phase(s), and relative permeability (k_r) is hence a function of saturation, $k_r(S_w)$. In addition, relative permeability is a function of rock properties, fluid properties, and thermophysical conditions, including wettability [*Bear*, 1988; *McCaffery and Bennion*, 1974]. These relationships are difficult to predict and hence relative permeabilities of wetting and nonwetting phases are traditionally measured experimentally [e.g., *Honarpour and Mahmood*, 1988; *Oak et al.*, 1990]. With regard to wettability, it has been reported for oil/water and air/water systems that the wetting phase relative permeability will increase as the system becomes less wetting to that phase; while the nonwetting phase relative permeability will decrease for the same wettability shift [*Craig*, 1971; *McCaffery and Bennion*, 1974]. Consequently, k_r can be used as a qualitative indicator to assess the wettability of a rock-fluid-fluid system.

A number of studies have investigated scCO$_2$-brine relative permeability relationships in a range of reservoir and outcrop rocks [*Bennion and Bachu*, 2008; *Perrin and Benson*, 2010; *Shi et al.*, 2011; *Krevor et al.*, 2012; *Akbarabadi and Piri*, 2013; *Berg et al.*, 2013a; *Kogure et al.*, 2013; *Pini and Benson*, 2013]. For the Berea outcrop
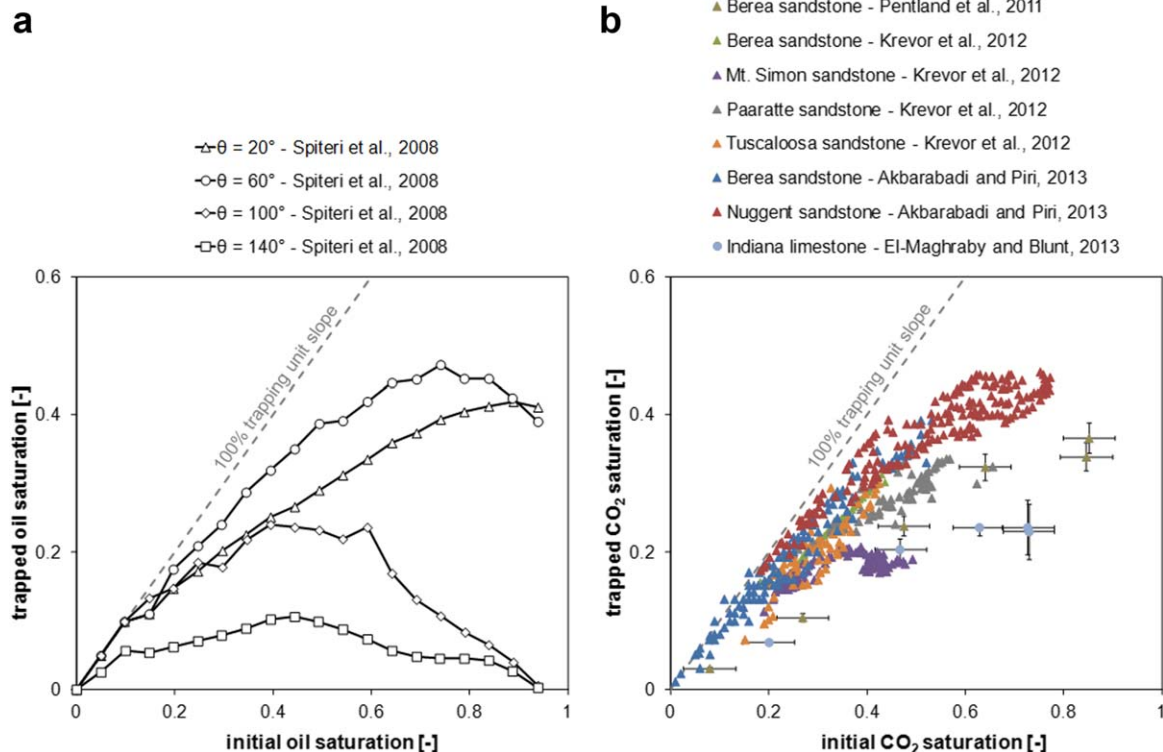
Figure 18. Initial-residual saturation relationships from (a) pore-network modeling and (b) laboratory measurements. In the pore network modeling study [*Spiteri et al.*, 2008], the initial-residual saturation relationship of oil is shown for a range of contact angles. We believe this relation would be an analogue for the scCO$_2$-brine fluid system. Data for a range of sandstones and one limestone has been measured for the scCO$_2$-brine system [*Krevor et al.*, 2011, 2012; *Pentland et al.*, 2011; *Akbarabadi and Piri*, 2013; *El-Maghraby and Blunt*, 2013]. Most data exhibit water-wet behavior with the exception of the illite-rich Mt. Simon sandstone and possibly Indiana limestone.

sandstone, a number of fluid systems have been investigated, making a comparison of results with regard to wettability enlightening. Relative permeabilites have been measured for helium-oil [*Richardson et al.*, 1952], air-oil (The oil used was listed as Soltrol "C" core test fluid. Phillips Petroleum Company, Special Products Division, Bartlesville, Oklahoma.) [*Brooks and Corey*, 1964], N$_2$-brine [*Oak et al.*, 1990], gaseous CO$_2$-water [*Botset*, 1940], as well as scCO$_2$-brine [*Perrin and Benson*, 2010; *Krevor et al.*, 2012; *Akbarabadi and Piri*, 2013; *Pini and Benson*, 2013] systems. A detailed comparison and discussion of these works are provided by *Krevor et al.* [2012] and *Pini and Benson* [2013] who both conclude that there is little wettability change between the scCO$_2$-brine system and these other systems which are strongly wetted by one phase (the aqueous phase in gas-water and gas-brine systems; or the liquid phase in gas-hydrocarbon liquid systems); this indicates that the scCO$_2$-brine-Berea system is strongly water-wet.

4.2.1. Residual Trapping

Residual saturations of nonaqueous phase liquids have been measured extensively in the groundwater [e.g., *Hoag and Marley*, 1986; *Lenhard et al.*, 1993] and hydrocarbon [e.g., *Land*, 1968; *Gittins et al.*, 2010] literature. More recently measurements have been made in the context of CGS [e.g., *Pentland et al.*, 2011; *Krevor et al.*, 2012; *Akbarabadi and Piri*, 2013]. The magnitude of residual trapping and the relationship between initial saturation (S_i) and residual saturation (S_r) was shown to be wettability dependent for oil-water systems, based on laboratory measurements [*Iglauer et al.*, 2012a; *Tanino and Blunt*, 2013] and numerical modeling [*Spiteri et al.*, 2008]; with stongly water-wet conditions generally resulting in more trapping and a monotonic $S_i - S_r$ relationship, while intermediate-wet conditions resulted in less trapping and a nonmonotonic $S_i - S_r$ relationship.

For the scCO$_2$-brine fluid system, a number of studies have measured the relationship between initial and residual scCO$_2$ saturation for outcrop sandstones [*Pentland et al.*, 2011; *Krevor et al.*, 2012; *Akbarabadi and Piri*, 2013], reservoir sandstones [*Krevor et al.*, 2011, 2012], and outcrop limestone [*El-Maghraby and Blunt*, 2013]. With the exception of one illite-rich reservoir sample (Mt. Simon sandstone) [*Krevor et al.*, 2011, 2012],

all scCO$_2$ measured data show a monotonic trend with significant maximum residual saturation ($S_r > 0.18$), indicative of water-wet conditions. It is notable that the maximum residual saturation in limestone is lower than that for the range of sandstones studied. The $S_i - S_r$ saturation relationship for the illite-rich Mt. Simon reservoir sandstone is concave; an indication of intermediate-wet behavior (cf. Figure 18a). Some of these studies also measured—in the same rocks as the scCO$_2$ measurements—the initial-residual saturation relationship for the analogue decane-brine [*Pentland et al.*, 2011] and gaseous CO$_2$-brine systems [*Akbarabadi and Piri*, 2013; *El-Maghraby and Blunt*, 2013], which are considered to be strongly water-wet. The form of the $S_i - S_r$ relationships is similar although the magnitude of the residual analogue saturations was slightly higher in sandstones and slightly lower in limestone when compared to the scCO$_2$ data. These relatively small differences could be due to changes in wettability within the water-wet range (cf. the $\theta = 20°$ and $\theta = 60°$ curves in Figure 18a).

It is also worth highlighting that the characteristics of the porous medium itself can also affect residual trapping. In unconsolidated media such as sands, there is typically a smaller difference between pore-throat diameter and pore-body diameter than there is in consolidated media such as sandstones; the result being that snap-off is suppressed in unconsolidated media as there is insufficient water locally to cause the instability that bridges the pore-throat opening [*Iglauer et al.*, 2011b; *Pentland et al.*, 2012]. For similar fluid pairs in water-wet siliciclastic material, lower maximum residual oil saturations were reported in sands ($0.11 < S_r < 0.13$, *n*-octane-brine) [*Gittins et al.*, 2010; *Pentland et al.*, 2010] than in sandstones ($S_r \sim 0.48$, *n*-decane-brine) [*Pentland et al.*, 2011]. The convolution of porous media geometry and wettability effects makes data interpretation more challenging but we propose that it is the geometry effects which suppress snap-off and cause the lower maximum residual saturations measured for unconsolidated scCO$_2$-brine systems [*Plug and Bruining*, 2007; *Tokunaga et al.*, 2013], and not wettability effects such as scCO$_2$ being neutrally wetting in these systems.

4.2.2. 2-D Micromodels

Chalbaud et al. [2009] imaged the pore-scale fluid distribution of CO$_2$/water in a 2-D glass micromodel with an optical microscope at different thermophysical conditions: (a) for gaseous CO$_2$ ($p = 6$ MPa, $T = 292$ to 298 K), (b) liquid CO$_2$ ($p = 10$ MPa, $T = 296$ to 298 K), and (c) scCO$_2$ ($p = 10$–10.5 MPa, $T = 333$ K) and different wettability states: water-wet, intermediate-wet, and oil-wet. They altered the wettability of the glass surfaces through a treatment with silane or asphaltic crude oil and wettability alteration was confirmed by air-brine contact angle measurements (water wet $\sim 0°$; intermediate-wet $\sim 55°$; oil-wet $\sim 85°$). They found that in case of a water-wet surface, CO$_2$ was nonwetting for all thermophysical conditions, although no water surface films were identified at high pressures. However, at high pressures CO$_2$ was the wetting phase for intermediate and oil-wet surfaces. They also observed that CO$_2$-wettability was stronger at lower temperatures.

Kim et al. [2012] extended this work by studying the effect of brine salinity on water fluid distributions in their scCO$_2$/brine/silica micromodel systems. They conducted their experiments at 318 K and 8.5 MPa and measured the water contact angle directly on the images. They found that θ increases with increasing salinity (measured θ ranged from 37° to 87°; specifically an average θ of 54° was measured for 0.01 M NaCl brine, 66° for 1 M NaCl brine, 65° for 3 M NaCl brine, and 75° for 5 M NaCl brine).

Other studies used micromodels to investigate CO$_2$-brine dissolution kinetics [*Buchgraber et al.*, 2012] and CO$_2$ exosolution [*Zuo et al.*, 2013]. While the focus of these studies was not wettability characterization their data give a qualitative understanding of wettability for the systems studied. Both Buchgraber et al. and Zuo et al. used silicon micromodel's whose structure were based on a sandstone thin section image (Berea and Mt. Simon, respectively). The micromodels were etched using deep reactive ion etching prior to bonding to a glass plate. Buchgraber et al. reported that this process resulted in the oxidation of the micromodel surface. Buchgraber et al. performed flooding experiments at low and at elevated pressure and temperature conditions (low: $p_{water} = 75.8$ kPa, $T = 295$ K; high: $p_{waterd} = 7.9$ MPa, $T = 318$ K) while Zuo et al., equilibrated their system at $p_{water} = 9$ MPa and $T = 318$ K prior to depressurization. Contact angles were not reported but a visual analysis of Figures 12–14 in Buchgraber et al. and Figure 8 in Zuo et al. indicate that the systems were either intermediate-wet or water-wet with the CO$_2$ bubbles occupying the centre of the pore space.

Some authors did not report how they cleaned the surfaces in their micromodels, and it is possible that surface contamination shifted measured θ to unrealistically high values [cp. section 2.1, *Iglauer et al.*, 2014].

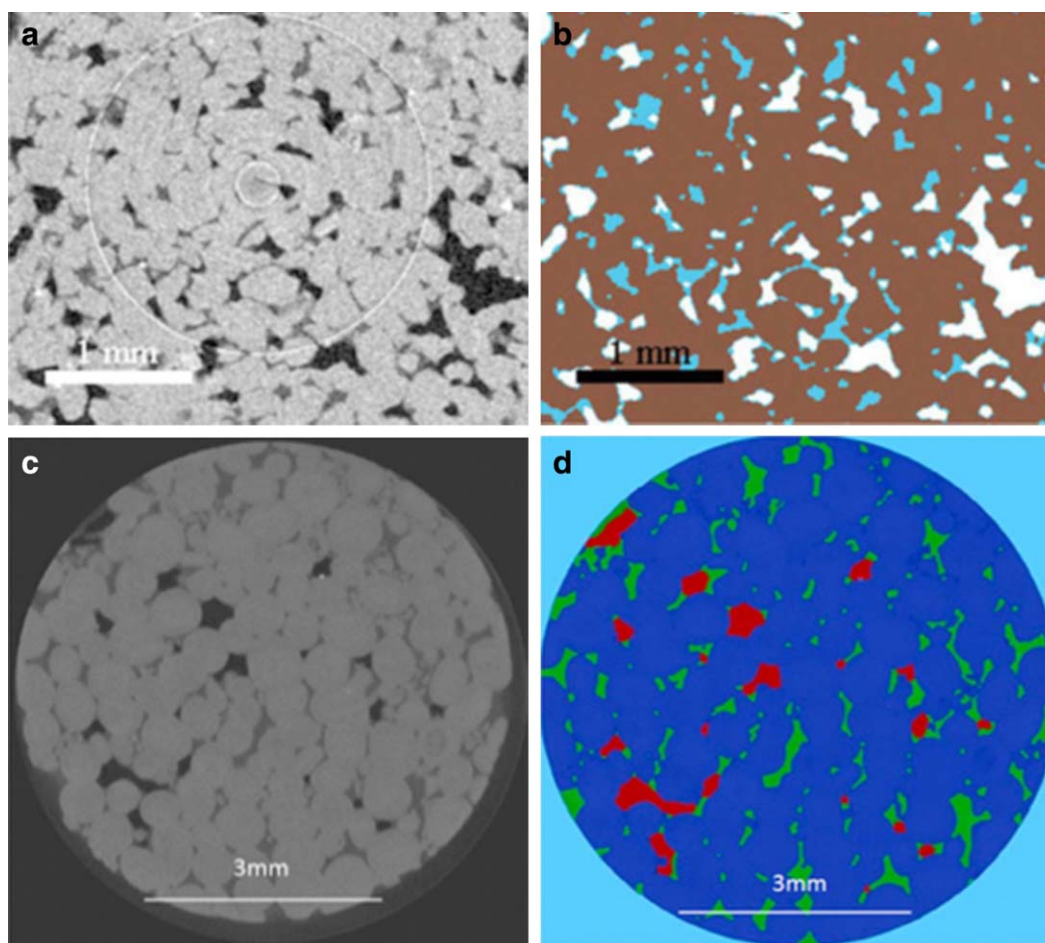IGLAUER ET AL.   762

Figure 19. (left) Selected original image slices, measured by μCT, and (right) same image slices after image processing. The scCO$_2$-brine-Doddington sandstone system is shown in the top row [*Iglauer et al.*, 2011a]. In the processed image scCO$_2$ is white, brine blue, and rock brown. The scCO$_2$-brine-Ketton Oolite limestone system is shown in the bottom row [*Andrew et al.*, 2013]. In the processed image scCO$_2$ is red, brine green, and rock dark blue. As the CO$_2$ resides mainly in the large pores, we conclude that Doddington sandstone and Ketton limestone are water-wet.

Moreover, it should be kept in mind that such 2-D models are not necessarily representative of storage rock or caprock as the models' surfaces are smoother and chemically almost homogeneous, however, they contribute important basic data to the overall analysis.

4.2.3. 3-D X-ray Microcomputed Tomography Imaging

With recent advances in 3-D X-ray microcomputed tomography (herein referred to as μCT), it is now possible to study systems contained at pressures and temperatures representative of storage formations [*Iglauer et al.*, 2011a; *Andrew et al.*, 2013; *Chaudhary et al.*, 2013]. The resulting images of pore space fluids (Figure 19) provide an enlightening insight into many pore-scale processes, including wettability influence [cp. e.g., *Iglauer et al.*, 2012a]. As with 2-D micromodels, qualitative analysis of μCT images informs our understanding of scCO$_2$-brine wettability.

Iglauer et al. [2011a] imaged a Doddington sandstone (composition = 98 wt % quartz, 2 wt % K-feldspar, traces of kaolinite, measured by X-ray diffraction analysis (XRD)) at initial and residual scCO$_2$ saturation at reservoir conditions (p_{water} = 10 MPa and T = 323 K in 13 wt % potassium iodide brine); and from the phase distribution in the pore space, the observed cluster size distributions and scCO$_2$ saturations, it was qualitatively concluded that the system was somewhere between water-wet and possibly intermediate-wet. *Suekane et al.* [2011] imaged scCO$_2$ residual saturations in a range of glass bead packs and quartz sand packs (p_{water} = 8.5 MPa, T = 313 K, 10 wt % sodium iodide brine), and again similar fluid pore configurations were observed [*Pentland et al.*, 2012]. *Andrew et al.* [2013] imaged the oolitic Ketton limestone (composition = 99.1% calcite

Table 13. Range of Impurities in Dry CO_2 Streams After CO_2 Capture[a]

	Coal-Fired Plants			Gas-Fired Plants		
	Postcombustion	Precombustion	Oxy-Fuel	Postcombustion	Precombustion	Oxy-Fuel
SO_2	<0.01	0	0.5	<0.01	0	<0.01
NO	<0.01	0	0.01	<0.01	0	<0.01
H_2S	0	0.01–0.6	0	0	<0.01	0
H_2	0	0.8–2.0	0	0	1	0
CO	0	0.03–0.4	0	0	0.04	0
CH_4	0	0.01	0	0	2	0
$N_2/Ar/O_2$	0.01	0.03–0.6	3.7	0.01	1.3	4.1
Total	0.01	2.1–2.7	4.2	0.01	4.4	4.1

[a]Summary taken from *IPCC* [2005]. Numbers are in vol %.

and 0.9% quartz measured by XRD) at residual $scCO_2$ saturation (p_{water} = 10 MPa and T = 336 K in 5 wt % KI brine) while maintaining conditions of chemical equilibrium between phases, they suggest in conclusion that $scCO_2$ acts as the nonwetting phase in the system. A recent study illustrated the importance of wettability for $scCO_2$ capillary trapping [*Chaudhary et al.*, 2013]. The residual saturation after water imbibition was shown to vary between 2% and 20% in unconsolidated bead packs depending on bead shape and wettability. Angular water-wet glass beads trapped the most CO_2 while CO_2-wet rounded polytetrafluoroethylene (Teflon) beads trapped the least amount [*Chaudhary et al.*, 2013]. Finally *Silin et al.* [2011] imaged the subcritical CO_2-brine (p_{water} = 6.5 MPa, temperature was not specified, so we assume that the experiment was performed at laboratory conditions; approximately 298 K, so that the CO_2 was in the liquid phase) distribution in Frio sandstone. CO_2 appears to be the nonwetting phase in this system [see Figure 11 in *Silin et al.*, 2011]. To conclude, a qualitative analysis of μCT images indicates that CO_2 behaves as the nonwetting phase in the systems studied to date (with the exception of a Teflon bead system). CO_2 tends to occupy the center of the pores with water preferentially being in contact with the solid surfaces. Recently $scCO_2$-brine contact angles have been measured in situ within a porous medium at representative subsurface conditions (10 MPa and 323 K) for the first time [*Andrew et al.*, 2014]. The Ketton quarry limestone studied was 99.1% calcite and 0.9% quartz and a distribution of contact angles ranging from 35° to 55° was measured, thus this system can be classified as strongly or weakly water-wet. The authors proposed that the range in contact angles was caused by contact angle hysteresis and surface heterogeneity effects.

5. Influence of Contaminants

Until now, we have only discussed how pure CO_2 wets the various mineral and rock surfaces; however, in an industrial project, CO_2 purity will only reach a certain, comparatively low, degree, as further purification would be uneconomical. As a consequence, the injected CO_2 stream will contain several impurities, of which H_2S, N_2, SO_2, and CH_4 are the most prominent ones (Table 13) [*IPCC*, 2005].

And it is clear from a theoretical perspective that these contaminants have the potential to significantly change wettability. Such wettability change can in principle be induced via two ways: (1) directly, through a change in fluid composition, which results in a change in the intermolecular forces. On a macroscopic level, this can be expressed as a change in the three interfacial tensions and the resulting contact angle (equation (1)); and (2) the contaminants can change the surface chemistry in a subtle way, e.g., increase or reduce the number of hydroxyl groups, change the dissociation equilibria of the hydroxyl groups or oxidize or reduce surface functional groups. Particularly point (2) is not easily assessed by "back of the envelope" analysis, and it should thus be measured. As usual we expect that reservoir conditions (i.e., high pressure, elevated temperature) render the CO_2-wettability substantially, cp. the discussion above. In this context, a few groups have experimentally and theoretically analyzed the effect of contaminants in the CO_2 stream, and we will discuss each contaminant examined below.

5.1. Nitrogen (N_2)
Kaveh et al. [2014] measured sessile contact angles on Bentheimer sandstone at 318 K for a 20 mol %CO_2/ 80 mol % N_2 mixture. They found that pressure had a slight influence on θ: θ increased from 1–5° at ~1.8 MPa pressure to 4–13° at 14 MPa pressure. Furthermore, they found a decrease in θ with increasing gas bubble radius; this could be caused by mass transfer (the fluids might not have been completely equilibrated) or possibly gravity effects—which, however, should be negligible according to a first approximation

based on the assessment of the capillary length [*DeGennes et al.*, 2004]. Consistent with *Kaveh et al.* [2014], *McCaughan et al.* [2013] predict 0° contact angles for a N_2/H_2O/fully coordinated (= no surface hydroxyl groups present) quartz surface system.

5.2. Hydrogen Sulphide (H_2S)

Shah et al. [2008] and *Broseta et al.* [2012] measured receding and advancing θ for the systems H_2S/ 0.08 M NaCl brine/quartz, mica, and Rousse caprock (the Rousse caprock consisted of ~70% calcite, 10% quartz, a few percent chlorite, and illite/mica). On mica, the receding θ increased from 62° to 110° when pressure was increased from 1.5 to 13 MPa (at 323 K), while advancing θ increased from 82° to 150° (for the same pressure increase). Thus mica is mixed-wet for the H_2S system at reservoir conditions. Considering the high toxicity of H_2S (the IDLH—immediately dangerous to life or health concentration—is 100 ppm [*US National Institute for Occupational Safety and Health (NIOSH)*, 2014]), this finding should be taken seriously as it follows that H_2S leakage is more likely than that of CO_2. However, θ on quartz (42–45° for both, receding and advancing θ at 323 K and a pressure range of 0.6–12.5 MPa) and the Rousse caprock (θ was 35–40° for both, receding and advancing θ at 343 K and a pressure range of 1.5–14.2 MPa) was significantly lower, and these minerals were still weakly water-wet. *McCaughan et al.* [2013] conducted molecular dynamics studies for the H_2S/H_2O/quartz (fully coordinated) system at 350 K, and they predicted a θ of 65° (at ~2.5 MPa), which increased to ~80° at 6 MPa; θ remained constant with further pressure increase. The fact that a fully coordinated quartz surface was investigated implies that θ at real reservoir conditions is lower as surface silanol groups will be present (cp. section 2.1.1.4). However, the MD simulations are consistent with *Shah et al.*'s [2008] and *Broseta et al.*'s [2012] measurements. We conclude that H_2S is more wetting than CO_2 at storage conditions.

5.3. Sulphur Dioxide (SO_2)

Saraji et al. [2014] measured the advancing and receding θ on an ultrasmooth quartz substrate (surface roughness below 0.5 nm) for $SO_2 + CO_2$/1 M brine fluid pairs as a function of SO_2 concentration (which varied from 0 to 6 wt %). Both θ were approximately constant (the advancing θ was ~28° and the receding θ ~14°), thus SO_2 had no significant influence on the wettability. We note that *Saraji et al.* [2014] measured a significant decrease in interfacial tension γ with increasing SO_2 concentration: γ decreased from 28 mN/m (at 0% SO_2, 100% CO_2) to ~17 mN/m at 6 wt % SO_2 (94 wt % CO_2) concentration.

6. Discussion

While considerable effort has been made in the past decade to determine the wettability of subsurface minerals with respect to CO_2 and brine the reported data are characterized by marked variability (e.g., Figure 6 for quartz). This variability can lead to uncertainty in our understanding in terms of how injected CO_2 moves and is trapped in the subsurface; impacting our predictive capability and the planning associated with CGS projects. While variability does exist the data indicate that most subsurface minerals and porous media studied are water-wet, or in some limited cases possibly intermediate-wet. However, hydrophobic surfaces such as coal or oil-wet mineral surfaces appear to be intermediate-wet or CO_2-wet (Figure 14). While this in itself is an important conclusion there are a number of topics (discussed below) where further study may lead to reduced experimental variability and an improved general understanding of CO_2-brine-mineral wettability.

During our review, we did not find (scCO_2-brine subsurface condition) data for a number of important rocks or minerals, including: dolomite; anhydrite; halite; mudrocks; clays. Experimental data for all of these rocks and minerals would be desirable if CGS were considered in such lithologies. Based on the data given in this review, we hypothesize that mudrocks could possibly take any wettability classification depending upon the exact rock composition: water-wet, intermediate-wet, or CO_2-wet.

Performing wettability measurements on mineral surfaces that are chemically representative of subsurface storage conditions is highly desirable. Achieving such representative conditions is, however, very challenging and little discussed in the context of CGS. Further research on preparing such mineral surfaces in the laboratory would be highly desirable. This has been investigated in the petroleum literature where surface cleaning is followed by an ageing process using representative formation fluids so that
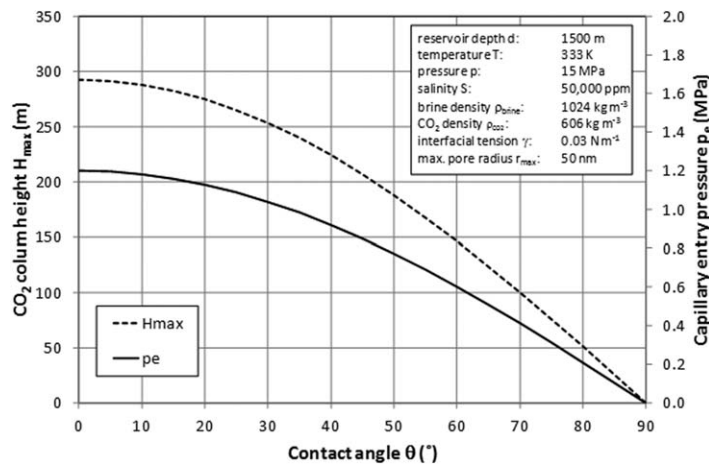
Figure 20. Capillary entry pressures p_e and maximum CO_2 column heights H_{max} for a reservoir/caprock interface at 1500 m depth calculated from equations (5) and (7). Average interfacial tension γ data from *Hebach et al.* [2002]; *Li et al.* [2012a, 2012b], CO_2 density calculated from *Span and Wagner* [1996].

subsurface wettability conditions are restored within a sample prior to measurements being made [e.g., *Wunderlich*, 1991]. We propose that such an approach may also be necessary in the context of CGS. For sensitive clay-rich samples, special attention is required to minimize dehydration and to ensure brine composition and experimental stress conditions are closely aligned with those in the subsurface. Finally, we acknowledge that the long-term wettability of mineral systems exposed to CO_2 and brine has not been investigated experimentally (i.e., wettability changes over time). However, some natural subsurface CO_2 accumulations have demonstrated containment below tight sealing rocks which strongly indicates that these clay or evaporate-rich rocks are and remain rather water-wet [e.g., *Lombardi et al.*, 2006; *Lu et al.*, 2009].

It should be mentioned that most data summarized here refer to contact angle measurements on single mineral surfaces, neglecting the influence pore systems could have on wettability. It seems sensible that this point needs to be addressed by alternative or indirect measurement techniques to obtain a more realistic picture of the subsurface, reflecting the complexity of multimineral porous systems. Recently advances in X-ray microcomputed tomography techniques have allowed contact angles to be measured within a porous media at subsurface conditions for the first time [*Andrew et al.*, 2014]; providing an exciting additional avenue for wettability research.

We now illustrate the implications of mineral wettability for CO_2 movement and trapping in the subsurface. Water contact angles deviating from completely water-wet conditions will have significant implications in terms of the maximum CO_2 column height a caprock can sustain before capillary leakage initiates (cf. Figure 3). For a reservoir scenario where we set the caprock/reservoir rock interface to 1500 m depth, corresponding to 15 MPa reservoir pressure, and 333 K reservoir temperature, we calculate capillary entry pressures according to equation (5) as well as maximum CO_2 column heights according to equation (7). Figure 20 shows that CO_2 column heights are close to 300 m for completely water-wet conditions (contact angle of 0°). This value decreases to 150 m at a contact angle of 45° and 0 m at 90°. For values higher than 90°, spontaneous CO_2 imbibition (suction of CO_2 into the water-filled caprock pore space) would be observed.
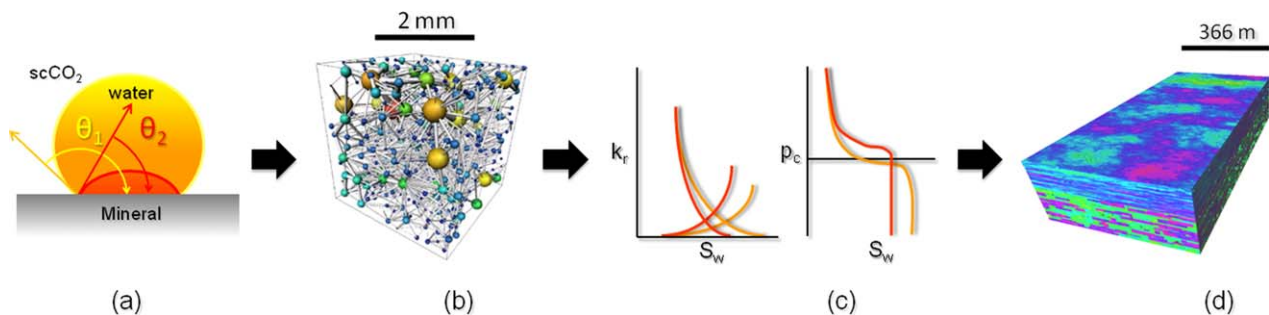

Figure 21. An example workflow leading from (a) millimeter scale contact angle measurements to (d) hectometer scale pilot-project simulation via (b) millimeter scale pore-network modeling and (c) the predicted macroscale saturation functions for relative permeability and capillary pressure. The image of a pore network model is reproduced from *Blunt et al.* [2013]. The permeability array is displayed per grid-block on a logarithmic scale in the pilot-scale model (d): the permeability scale is from 0.001 mD (green) to 10,000 mD (red) ($9.87 \times 10^{-19} - 9.87 \times 10^{-12}$ m²).
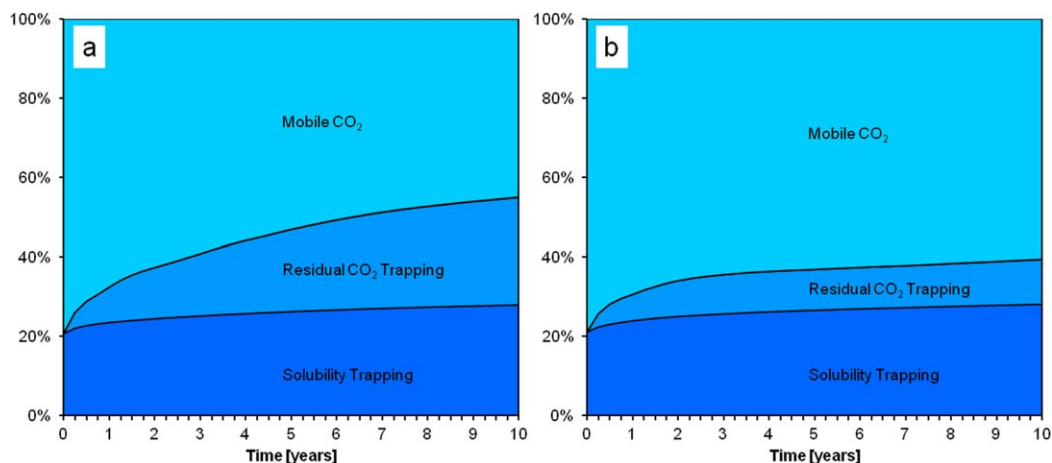
Figure 22. CO$_2$ fate simulation results from the modified tenth SPE Comparative Solution Project model using saturation functions derived from the contact angle to simulation workflow illustrated in Figure 21. (a) In the water-wet scenario significantly more CO$_2$ is immobilized as a residually trapped phase than (b) in the CO$_2$-wet scenario, leading to significantly reduced CO$_2$ leakage risk.

Predicting the fate of CO$_2$ injected into the subsurface typically involves numerical modeling of the storage formation, requiring an understanding of the relationship between capillary pressure, relative permeability, and the phase saturations ($k_r(S_w)$ and $p_c(S_w)$, respectively). In many cases $k_r(S_w)$ and $p_c(S_w)$ may not be known a priori and must be estimated. In such scenarios, $k_r(S_w)$ and $p_c(S_w)$ can be predicted by numerical simulation on pore network models. These simulations typically require a contact angle (or range of contact angles) as a direct input [e.g., *Gharbi and Blunt*, 2012]. We undertook the workflow described above to illustrate the impact contact angles can have on subsurface CO$_2$ trapping. We used the $k_r(S_w)$ and $p_c(S_w)$ data of *Jackson et al.* [2003] which were generated using a Berea sandstone pore network model. Two scenarios were considered: weakly water-wet to intermediate-wet (based on a contact angle assumption of $50° < \theta < 80°$) and CO$_2$-wet (we assumed this to be analogues to the oil-wet data presented, which assumed a contact angle range of $110° < \theta < 180°$). We assumed that the overlying caprock is completely impervious to CO$_2$. The $k_r(S_w)$ and $p_c(S_w)$ data were used as input for field-scale simulation using the publically available tenth SPE Comparative Solution Project reservoir simulation model [*Christie and Blunt*, 2001]. A limited number of modifications were made to the 1.12 million cell model to render it representative of a pilot-scale CGS project. The depth of the model top was 1500 m (initial pressure 15 MPa; initial temperature 333 K), numerical infinite aquifers were attached to the lateral model boundaries, the *Killough* [1976] relative permeability hysteresis model was used, and 10,000 t/yr (0.317 kg/s) of CO$_2$ were injected for 1 year into the central injection well (the four production wells were deactivated). The model was simulated using Shell's proprietary reservoir simulator MoReS [*Por et al.*, 1989]. The components of this workflow are illustrated in Figure 21 and the fate of the injected CO$_2$ over a 10 year period following the end of injection is illustrated in Figure 22. We see that the wettability has a significant impact on the ratio of mobile to residually trapped CO$_2$; the water-wet scenario traps approximately 240% more CO$_2$ as a residual phase after 10 years compared to the CO$_2$-wet scenario. The increased storage security of residually trapped CO$_2$ compared to mobile CO$_2$ has clear implications for CGS project site selection and planning.

7. Conclusions

The wettability of various subsurface minerals and rocks with respect to CO$_2$ and water are considered in this review paper. While variability in measured data is acknowledged inorganic minerals or rocks are not shown to be preferentially wetted by CO$_2$. However, hydrophobic surfaces, e.g., oil-wet carbonate, or coal are CO$_2$-wet. This has important implications for the flow of CO$_2$ and its entrapment in the subsurface as part of carbon geo-sequestration, particularly with respect to capillary entrapment of CO$_2$ on the pore-scale and retention below low permeability structural seals. Moreover, there are important minerals and

rock types that have not yet been investigated in terms of CO_2-wettability (including dolomite, anhydrite, halite, mudrocks, clays). Furthermore, the restoration of mineral surface chemistry to conditions representative of the subsurface is an important topic for future study. Coring, core handling, and core preservation procedures, in addition to the laboratory preparation of the samples, will then play a vital but challenging role.

Notation

θ	water contact angle (°).
γ	interfacial tension (N/m).
r	pore radius (m).
$CaCO_3$	calcium carbonate.
SiO_2	silicon dioxide (e.g., alpha-quartz).
CGS	carbon geo-sequestration (of carbon dioxide).
CO_2	carbon dioxide.
Hg	mercury.
H_2SO_4	sulphuric acid.
H_2O_2	hydrogenperoxide.
NaCl	sodium chloride.
–OH	hydroxyl group (on the surface).
DI water	deionized water.
CH_4	methane.
N_2	dinitrogen.
e	elementary charge (C).
sc	supercritical.
Gt	gigatons $= 10^9$ tons.
Mt	megatons $= 10^6$ tons.
ϕ	porosity.
k	permeability (m^2).
k_r	relative permeability.
M	molar mass (g/mol).
p	pressure (Pa).
T	temperature (K).
μ	viscosity (Pa s).
μ_{CO_2}	viscosity of CO_2 (Pa s).
μ_{H2O}	viscosity of water (Pa s).
ρ	density (kg/m^3).
ρ_{brine}	density of brine (kg/m^3).
ρ_{CO_2}	CO_2 density (kg/m^3).
$\rho_{CO_2,brine}$	density of CO_2-enriched brine (kg/m^3).
$\Delta\rho$	density difference (kg/m^3).
g	gravitational constant (m/s^2).
S_w	water saturation of the porous rock = volume fraction of water in the pore space.
S_{CO_2}	CO_2 saturation of the porous rock = volume fraction of CO_2 in the pore space.
S_i	initial saturation.
S_r	residual saturation.
p_b	buoyancy pressure (Pa).
p_c	capillary pressure = pressure between wetting and nonwetting phase (Pa).
p_w	pressure of the wetting phase (Pa).
p_{nw}	pressure of the nonwetting phase (Pa).
p_e	capillary entry pressure of the nonwetting phase into the rock saturated with the wetting phase (Pa) at $S_w = 1$.
p_{br}	capillary breakthrough pressure of the nonwetting phase: continuous nonwetting phase transport pathway through the rock sample/formation (Pa).

p_{sn}	capillary snap-off pressure ; lowest pressure where the continuous transport pathway across the rock sample/formation is blocked during imbibition (Pa).
α	contact angle measured through the lighter phase $= 180° - \theta$ (°).
γ_{SL}	interfacial tension between solid and liquid (water) (N/m).
γ_{SF}	interfacial tension between solid and fluid (CO_2) (N/m).
γ_{LF}	interfacial tension between fluid (CO_2) and liquid (water) (N/m).
MIP	mercury injection porosimetry.
r_1, r_2	principal radii of curvature (at any point on the surface) (m).
C	curvature of the surface ($= 1/r_1 + 1/r_2$) (1/m)
h	CO_2 plume height (m).
HP	high pressure.
f	surface fraction of material.
θ^*	contact angle on inhomogeneous surface (°).
MD	molecular dynamics.

References

Adamson, A. W., and A. P. Gast (1997), *Physical Chemistry of Surfaces*, 6th ed., Wiley-Interscience, N. Y.

Aguilera-Mercado, B., C. Herdes, J. Murgich, and E. A. Müller (2006), Mesoscopic simulation of aggregation of asphaltenes and resin molecules in crude oils, *Energy Fuels*, 20, 327–338.

Akbarabadi, M., and M. Piri (2013), Relative permeability hysteresis and capillary trapping characteristics of supercritical CO_2/brine systems: An experimental study at reservoir conditions, *Adv. Water Resour.*, 52, 190–206.

Alam, W., and E. C. Donaldson (2008), *Wettability*, 336 pp., Gulf, Houston, Tex.

Al-Basali, T. M., J. Zhang, and M. M. Sharma (2005), Measurement of the sealing capacity of shale caprocks, paper presented at the SPE Anual Technology Conference and Exhibition, Soc. of Pet. Eng., Dallas, Tex., 9–12 Oct.

Alles, S. B. (2008), Experimentelle Untersuchungen zu Fluidtransportprozessen in pelitischen Sedimentgesteinen [in German], MSc thesis, 118 pp., RWTH Aachen Univ., Aachen, Germany.

Amann-Hildenbrand, A., A. Busch, and B. Krooss (2013a), *N_2 and CO_2 Capillary Breakthrough Experiments on Opalinus Clay*, Eur. Geosci. Union Gen. Assem., Vienna.

Amann-Hildenbrand, A., P. Bertier, A. Busch, and B. M. Krooss (2013b), Experimental investigation of the sealing capacity of generic clay-rich caprocks, *Int. J. Greenhouse Gas Control*, 19, 620–641.

Amott, E. (1959), Observations relating to the wettability of porous rock, *Trans. AIME*, 216, 156–162.

Anderson, W. G. (1987a), Wettability literature survey—Part 6: The effects of wettability on waterflooding, *JPT J. Pet. Technol.*, 39(12), 1605–1622.

Anderson, W. G. (1987b), Wettability literature survey—Part 4: Effects of wettability on capillary pressure, *JPT J. Pet. Technol.*, 39(10), 1283–1300.

Andrew, M., B. Bijeljic, and M. J. Blunt (2013), Pore-scale imaging of geological carbon dioxide storage under in situ conditions, *Geophys. Res. Lett.*, 40, 3915–3918, doi:10.1002/grl.50771.

Andrew, M., B. Bijeljic, and M. J. Blunt (2014), Pore-scale contact angle measurements at reservoir conditions using X-ray microtomography, *Adv. Water Resour.*, 68, 24–31.

Armitage, P. J., R. H. Worden, D. R. Faulkner, A. C. Aplin, A. R. Butcher, and J. Iliffe (2010), Diagenetic and sedimentary controls on porosity in Lower Carboniferous fine-grained lithologies, Krechba field, Algeria: A petrological study of a caprock to a carbon capture site, *Mar. Pet. Geol.*, 27(7), 1395–1410.

Armitage, P. J., D. R. Faulkner, R. H. Worden, A. C. Aplin, A. R. Butcher, and J. Iliffe (2011), Experimental measurement of, and controls on, permeability and permeability anisotropy of caprocks from the CO_2 storage project at the Krechba Field, Algeria, *J. Geophys. Res.*, 116, B12208, doi:10.1029/2011JB008385.

Arts, R. J., A. Chadwick, O. Eiken, S. Thibeau, and S. Nooner (2008), Ten years' experience of monitoring CO_2 injection in the Utsira Sand at Sleipner, offshore Norway, *First Break*, 26(1), 65–72.

Atkins, P., and J. de Paula (2010), *Physical Chemistry*, Oxford Univ. Press, N. Y.

Audigane, P., I. Gaus, T. Xu, and K. Pruess (2005), Reactive transport modeling using TOUGHREACT for the long term CO_2 storage at Sleipner, North Sea, paper presented at the Fourth Annual Conference on Carbon Capture and Sequestration, Alexandria, Va.

Bando, S., F. Takemura, M. Nishio, E. Hihara, and M. Akai (2003), Solubility of CO_2 in aqueous solutions of NaCl at (30 to 60)°C and (10 to 20) MPa, *J. Chem. Eng. Data*, 48, 576–579.

Bear, J. (1988), *Dynamics of Fluids in Porous Media*, Dover, N. Y.

Bennion, D. B., and S. Bachu (2007), Permeability and relative permeability measurements at reservoir conditions for CO_2-water systems for ultralow permeability confining caprocks, paper SPE 106995 presented at the SPE Europec/EAGE Annual Conference and Exhibition, Soc. of Pet. Eng., London, U. K.

Bennion, D. B., and S. Bachu (2008), Drainage and imbibition relative permeability relationships for supercritical CO_2/brine and H_2S/brine systems in intergranular sandstone, carbonate, shale, and anhydrite rocks, *SPE Reservoir Eval. Eng.*, 11(3), 487–496.

Berg, R. R. (1975), Capillary pressure in stratigraphic traps, *AAPG Bull.*, 59(6), 939–956.

Berg, S., S. Oedai, and H. Ott (2013a), Displacement and mass transfer between saturated and unsaturated CO_2-brine systems in sandstone, *Int. J. Greenhouse Gas Control*, 12, 478–492.

Berg, S., et al. (2013b), Real-time 3D imaging of Haines jump in porous media flow, *Proc. Natl. Acad. Sci. U. S. A.*, 110(10), 3755–3759.

Berthier, J., and K. A. Brakke (2012), *The Physics of Microdroplets*, Scrivener Publ., Beverly, Mass.

Bigelow, W. C., D. L. Pickett, and W. A. Zisman (1946), Oleophobic monolayers: I. Films adsorbed from solution in non-polar liquids, *J. Colloid Sci.*, 1(6), 513–538.

Bikkina, P. K. (2011), Contact angle measurements of CO_2-water-quartz/calcite systems in the perspective of carbon sequestration, *Int. J. Greenhouse Gas Control*, *5*, 1259–1271.

Bikkina, P. K. (2012), Reply to the comments on "Contact angle measurements of CO_2-water-quartz/calcite systems in the perspective of carbon sequestration", *Int. J. Greenhouse Gas Control*, *7*, 263–264.

Birkholzer, J. T., and Q. Zhou (2009), Basin-scale hydrogeologic impacts of CO_2 storage: Capacity and regulatory implications, *Int. J. Greenhouse Gas Control*, *3*(6), 745–756.

Bjørlykke, K. (2010), *Petroleum Geoscience: From Sedimentary Environments to Rock Physics*, Springer, Heidelberg, Germany.

Blunt, M. J., F. J. Fayers, and F. M. Orr (1993), Carbon dioxide in enhanced oil recovery, *Energy Convers. Manage.*, *34*(9–11), 1197–1204.

Blunt, M. J., B. Bijeljic, H. Dong, O. Gharbi, S. Iglauer, P. Mostaghimi, A. Paluszny, and C. H. Pentland (2013), Pore-scale imaging and modelling, *Adv. Water Resour.*, *51*, 197–216.

Borysenko, A., B. Clennell, R. Sedev, I. Burgar, J. Ralston, M. Raven, D. Dewhurst, and K. Liu (2009), Experimental investigations of the wettability of clays and shales, *J. Geophys. Res.*, *114*, B07202, doi:10.1029/2008JB005928.

Botset, H. G. (1940), Flow of gas-liquid mixtures through consolidated sand, *Trans. AIME*, *136*(1), 91–105.

Boulin, P. F., P. Bretonnier, V. Vassil, A. Samouillet, M. Fleury, and J. M. Lombard (2011), *Entry Pressure Measurements Using Three Unconventional Experimental Methods*, pp. 12, Soc. of Core Anal., Austin, Tex.

Bourikas, K., J. Vakras, C. Kordulis, and A. Lycourghiotis (2003), Potentiometric mass titrations: Experimental and theoretical establishment of a new technique for determining the point of zero charge (pzc) of metal(hydr)oxides, *J. Phys. Chem. B*, *107*, 9441–9451.

Brooks, R. H., and A. T. Corey (1964), *Hydraulic Properties of Porous Media, Hydrology Pap.*, vol. 3, 27 p., Civil Eng. Dep., Colo. State Univ., Fort Collins.

Broseta, D., N. Tonnet, and V. Shah (2012), Are rocks still water-wet in the presence of dense CO_2 or H_2S? *Geofluids*, *12*(4), 280–294.

Brunsting, S., M.d. Best-Waldhober, C. F. J. Feenstra, and T. Mikunda (2011), Stakeholder participation practices and onshore CCS: Lessons from the dutch CCS case barendrecht, *Energy Procedia*, *4*, 6376–6383.

Buchgraber, M., A. R. Kovscek, and L. M. Castanier (2012), A study of microscale gas trapping using etched silicon micromodels, *Transp. Porous Media*, *95*(3), 647–668.

Buckley, J. S., Y. Liu, X. Xie, and N. Morrow (1997), Asphaltenes and crude oil wetting—The effect of oil composition, *SPE J.*, *2*, 107–119.

Buckley, J. S., Y. Liu, and S. Monsterleet (1998), Mechanisms of wetting alteration by crude oils, *SPE J.*, *54–61*.

Busch, A., and A. Amann-Hildenbrand (2013), Predicting capillarity of mudrocks, *Mar. Pet. Geol.*, *45*, 208–223.

Busch, A., S. Alles, Y. Gensterblum, D. Prinz, D. N. Dewhurst, M. D. Raven, H. Stanjek, and B. M. Krooss (2008), Carbon dioxide storage potential of shales, *Int. J. Greenhouse Gas Control*, *2*(3), 297–308.

Busch, A., A. Amann-Hildenbrand, P. Bertier, M. Waschbuesch, and B. M. Krooss (2010), The significance of caprock sealing integrity for CO_2 storage, paper presented at the SPE International Conference on CO_2 Capture, Storage, and Utilization, Soc. of Pet. Eng., New Orleans, La.

Butt, H.-J., K. Graf, and M. Kappl (2006), *Physics and Chemistry of Interfaces*, Wiley, Weinheim, Germany.

Canal, J., J. Delgado, I. Falcon, Q. Yang, R. Juncosa, and V. Barrientos (2012), Injection of CO_2-saturated water through a siliceous sandstone plug from Hontomin test site (Spain): Experiment and modelling, *Environ. Sci. Technol.*, *47*, 159–167.

Carroll, S., W. McNab, and S. Torres (2011), Experimental study of cement-sandstone/shale-brine-CO_2 interactions, *Geochem. Trans.*, *12*(1), 9.

Chalbaud, C., M. Robin, J. Lombard, F. Martin, P. Egermann, and H. Bertin (2009), Interfacial tension measurements and wettability evaluation for geological CO_2 storage, *Adv. Water Resour.*, *32*(1), 98–109.

Chang, J., J. Han, L. Yang, R. L. Jaffe, and D. Y. Yoon (2001), Structure and properties of polyethylene melt surfaces from molecular dynamics, *J. Chem. Phys.*, *115*(6), 2831–2840.

Chaudhary, K., M. Bayani Cardenas, W. W. Wolfe, J. A. Maisano, R. A. Ketcham, and P. C. Bennett (2013), Pore-scale trapping of supercritical CO_2 and the role of grain wettability and shape, *Geophys. Res. Lett.*, *40*, 3878–3882, doi:10.1002/grl.50658.

Chi, S.-M., B. I. Morsi, G. E. Klinzing, and S.-H. Chiang (1988), Study of interfacial properties in the liquid CO_2-water-coal system, *Energy Fuels*, *2*, 141–145.

Chiquet, P., D. Broseta, and S. Thibeau (2007), Wettability alteration of caprock minerals by carbon dioxide, *Geofluids*, *7*, 112–122.

Christie, M. A., and M. J. Blunt (2001), Tenth SPE comparative solution project: A comparison of upscaling techniques, *SPE Reservoir Eval. Eng.*, *4*(4), 308–317.

Craig, F. F. (1971), *The Reservoir Engineering Aspects of Waterflooding*, H. L. Doherty Mem. Fund of AIME, N. Y.

Cuiec, L. E. (1991), Evaluation of reservoir wettability and its effect on oil recovery, in *Interfacial Phenomena in Petroleum Recovery*, edited by N. R. Morrow, Marcel Dekker, N. Y.

Dake, L. P. (1978), *Fundamentals of Reservoir Engineering. Developments in Petroleum Science*, 8 pp., Elsevier, Amsterdam.

DeGennes, P.-G., F. Brochart-Wyart, and D. Quéré (2004), *Capillarity and Wetting Phenomena*, Springer, N. Y.

Dickson, J. L., G. Gupta, T. S. Horozov, B. P. Binks, and K. P. Johnston (2006), Wetting phenomena at the CO_2/water/glass interface, *Langmuir*, *22*(5), 2161–2170.

Donaldson, E., R. Thomas, and P. Lorenz (1969), Wettability determination and its effect on recovery efficiency, *Soc. Pet. Eng. J.*, *9*(1), 13–20.

Dong, H., and M. J. Blunt (2009), Pore-network extraction from micro-computerized-tomography images, *Phys. Rev. E*, *80*(3), 036307.

Dullien, F. A. L. (1991), *Porous Media: Fluid Transport and Pore Structure*, Academic, N. Y.

Dutschk, V., S. Sutanto, and A. Calvimontes (2013), Cleanability of textile materials in liquid CO_2, *Tenside Surf. Detergents*, *50*, 21–25.

Ebrahimi, A., S. Jamshidi, S. Iglauer, and R. B. Boozarjomehry (2013), Genetic algorithm-based pore network extraction from micro-computed tomography images, *Chem. Eng. Sci.*, *92*, 157–166.

Egermann, P., J.-M. Lombard, and P. Bretonnier (2006a), A fast and accurate method to measure threshold capillary pressure of caprocks under representative conditions, paper presented at the SCA International Symposium.

Egermann, P., C. Chalbaud, J. Duquerroix, and Y. Le Gallo (2006b), An integrated approach to parameterize reservoir models for CO_2 injection in aquifers, paper SPE 102308 presented at SPE Annual Technical Conference and Exhibition, Soc. of Pet. Eng., San Antonio, Tex.

Elliot, G. E. P., and A. C. Riddiford (1967), Dynamic contact angles I. The effect of impressed motion, *J. Colloid Interface Sci.*, *23*, 389–398.

El-Maghraby, R. M., and M. J. Blunt (2013), Residual CO_2 trapping in Indiana limestone, *Environ. Sci. Technol.*, *47*(1), 227–233.

Espinoza, D. N., and J. C. Santamarina (2010), Water-CO_2-mineral systems: Interfacial tension, contact angle, and diffusion—Implications to CO_2 geological storage, *Water Resour. Res.*, *46*, W07537, doi:10.1029/2009WR008634.

Farokhpoor, R., B. J. A. Bjørkvik, E. Lindeberg, and O. Torsæter (2013), Wettability behaviour of CO_2 at storage conditions, *Int. J. Greenhouse Gas Control*, *12*, 18–25.

Fatt, I. (1956), The network model of porous media, *Trans AIME*, *207*, 144–181.

Foerster, A., R. Giese, C. Juhlin, B. Norden, and N. Springer (2009), The geology of the CO2SINK site: From regional scale to laboratory scale, *Energy Procedia*, *1*(1), 2911–2918.

Folk, R. L. (1980), *Petrology of Sedimentary Rocks*, 190 pp., Hemphill Publ., Austin, Tex.

Gallé, C. (2000), Gas breakthrough pressure in compacted Fo-Ca clay and interfacial gas overpressure in waste disposal context, *Appl. Clay Sci.*, *17*(1–2), 85–97.

Gaus, I. (2010), Role and impact of CO_2/rock interactions during CO_2 storage in sedimentary rocks, *Int. J. Greenhouse Gas Control*, *4*(1), 73–89.

Gaus, I., M. Azaroual, and I. Czernichowski-Lauriol (2005), Reactive transport modelling of the impact of CO_2 injection on the clayey cap rock at Sleipner (North Sea), *Chem. Geol.*, *217*(3–4), 319–337.

Gharbi, O., and M. J. Blunt (2012), The impact of wettability and connectivity on relative permeability in carbonates: A pore network modeling analysis, *Water Resour. Res.*, *48*, W12513, doi:10.1029/2012WR011877.

Giesting, P., S. Guggenheim, A. F. Koster van Groos, and A. Busch (2012), Interaction of carbon dioxide with Na-exchanged montmorillonite at pressures to 640 bars: Implications for CO_2 sequestration, *Int. J. Greenhouse Gas Control*, *8*, 73–81.

Gittins, P., S. Iglauer, C. H. Pentland, S. Al-Mansoori, S. Al-Sayari, B. Bijeljic, and M. J. Blunt (2010), Nonwetting phase residual saturation in sandpacks, *J. Porous Media*, *13*(7), 591–599.

Golab, A., R. Romeyn, H. Averdunk, M. Knackstedt, and T. J. Senden (2012), 3D characterisation of potential CO_2 reservoir and seal rocks, *Aust. J. Earth Sci.*, *60*(1), 111–123, doi:10.1080/08120099.2012.675889.

Good, R. J., and L. A. Girifalco (1960), A theory for estimation of surface and interfacial energies. III Estimation of surface energies of solids from contact angle data, *J. Phys. Chem.*, *64*(5), 561–565.

Grate, J. W., K. J. Dehoff, M. G. Warner, J. W. Pittman, C. Zhang, and M. Oostrom (2012), Correlation of oil-water and air-water contact angles of diverse silanized surfaces and relationship to fluid interfacial tensions, *Langmuir*, *28*, 7182–7188.

Hardy, W. B. (1919), The spreading of fluids on glass, *Philos. Mag.*, *38*, 49–55.

Hebach, A., A. Oberhof, N. Dahmen, A. Kögel, H. Ederer, and E. Dinjus (2002), Interfacial tension at elevated pressure measurements and correlations in the water + carbon dioxide system, *J. Chem. Eng. Data*, *47*, 1540–1546.

Hesse, M. A., F. M Orr Jr., and H. A. Tchelepi (2008), Gravity currents with residual trapping, *J. Fluid Mech.*, *611*, 35–60.

Hildenbrand, A., S. Schlömer, and B. M. Kroos (2002), Gas breakthrough experiments on fine-grained sedimentary rocks, *Geofluids*, *2*, 3–23.

Hildenbrand, A., S. Schlömer, B. M. Krooss, and R. Littke (2004), Gas breakthrough experiments on pelitic rocks: Comparative study with N_2, CO_2 and CH_4, *Geofluids*, *4*, 61–80.

Hoag, G., and M. Marley (1986), Gasoline residual saturation in unsaturated uniform aquifer materials, *J. Environ. Eng.*, *112*(3), 586–604.

Honarpour, M., and S. M. Mahmood (1988), Relative-permeability measurements: An overview, *JPT J. Pet. Technol.*, *40*(8), 963–966.

Horseman, S. T., J. F. Harrington, and P. Sellin (1999), Gas migration in clay barriers, *Eng. Geol.*, *54*(1–2), 139–149.

Ibrahim, M. A., M. R. Tek, and D. L. Katz (1970), *Threshold Pressure in Gas Storage*, Pipeline Res. Comm., Am. Gas Assoc. at the Univ. of Mich., Ann Arbor.

Iglauer, S. (2011), *Dissolution Trapping of Carbon Dioxide in Reservoir Formation Brine—A Carbon Storage Mechanism. Mass Transfer*, InTech, Rijeka, Croatia.

Iglauer, S., S. Favretto, G. Spinelli, G. Schena, and M. J. Blunt (2010), X-ray tomography measurements of power-law cluster size distributions for the nonwetting phase in sandstones, *Phys. Rev. E*, *82*, 056315.

Iglauer, S., A. Paluszny, C. H. Pentland, and M. J. Blunt (2011a), Residual CO_2 imaged with X-ray micro-tomography, *Geophys. Res. Lett.*, *38*, L21403, doi:10.1029/2011GL049680.

Iglauer, S., W. Wuelling, C. H. Pentland, S. K. Al-Mansoori, and M. J. Blunt (2011b), Capillary-trapping capacity of sandstones and sandpacks, *SPE J.*, *16*(4), 778–783.

Iglauer, S., M. A. Fernø, P. Shearing, and M. J. Blunt (2012a), Comparison of residual oil cluster size distribution, morphology and saturation in oil-wet and water-wet sandstone, *J. Colloid Interface Sci.*, *375*(1), 187–192.

Iglauer, S., M. Mathew, and F. Bresme (2012b), Molecular dynamics computations of brine-CO_2 interfacial tensions and brine-CO_2-quartz contact angles and their effects on structural and residual trapping mechanisms in carbon geo-sequestration, *J. Colloid Interface Sci.*, *386*, 405–414.

Iglauer, S., A. Hassan, M. Sarmadivaleh, K. Liu, and C. Pham (2014), Contamination of silica surfaces: Impact on water-CO_2-quartz and glass contact angle measurements, *Int. J. Greenhouse Gas Control*, *22*, 325–328.

IPCC (2005), *Carbon Dioxide Capture and Storage, Working Group III of the Intergovernmental Panel on Climate Change*, 443 pp.

Jackson, M. D., P. H. Valvatne, and M. J. Blunt (2003), Prediction of wettability variation and its impact on flow using pore- to reservoir-scale simulations, *J. Pet. Sci. Eng.*, *39*(3–4), 231–246.

Jackson, M. D., P. H. Valvatne, and M. J. Blunt (2005), Prediction of wettability variation within an oil/water transition zone and its impact on production, *SPE J.*, *10*(2), 185–195.

Jadhunandan, P. P., and N. Morrow (1995), Effect of wettability on waterflood recovery for crude-oil/brine/rock systems, *SPE Reservoir Eng.*, *10*, 40–46.

Jettestuen, E., J. O. Helland, and M. Prodanovic (2013), A level set method for simulating capillary-controlled displacements at the pore scale with nonzero contact angles, *Water Resour. Res.*, *49*, 4645–4661.

Joanny, J. F., and P. G. de Gennes (1984), A model for contact angle hysteresis, *J. Chem. Phys.*, *81*(1), 552–562.

Juanes, R., E. J. Spiteri, F. M. Orr Jr., and M. J. Blunt (2006), Impact of relative permeability hysteresis on geological CO_2 storage, *Water Resour. Res.*, *42*, 1–13.

Jung, J.-W., and J. Wan (2012), Supercritical CO_2 and ionic strength effects on wettability of silica surfaces: Equilibrium contact angle measurements, *Energy Fuels*, *26*, 6053–6059.

Kaveh, N., E. S. J. Rudolph, K.-H. A. A. Wolf, and S. N. Ashrafizadeh (2011), Wettability determination by contact angle measurements: hvbB coal/water system with injection of synthetic flue gas and CO_2, *J. Colloid Interface Sci.*, *364*(1), 237–247.

Kaveh, N., K.-H. Wolf, S. N. Ashrafizadeh, and E. S. J. Rudolph (2012), Effect of coal petrology and pressure on wetting properties of wet coal for CO_2 and flue gas storage, *Int. J. Greenhouse Gas Control*, *115*, 91–101.

Kaveh, N., E. S. J. Rudolph, W. R. Rossen, P. van Hemert, and K.-H. Wolf (2013), Interfacial tension and contact angle determination in water-sandstone systems with injection of flue gas and carbon dioxide, in *IOR 2013—17th European Symposium on Improved Oil Recovery*, EAGE, St. Petersburg, Russia.

Kaveh, N. S., E. S. J. Rudolph, P. van Hemert, W. R. Rossen, and K. H. Wolf (2014), Wettability evaluation of a CO_2/water/bentheimer sandstone system: Contact angle, dissolution, and bubble size, *Energy Fuels 28*(6), 4002–4020.

Killins, C. R., R. F. Nielsen, and J. C. Calhoun (1953), Capillary desaturation and imbibition in porous rocks, *Prod. Mon.*, *18*(2), 30–39.

Killough, J. E. (1976), Reservoir simulation with history-dependent saturation functions, *Soc. Pet. Eng. J.*, *16*(1), 37–48.

Kim, Y., J. Wan, T. J. Kneafsey, and T. K. Tokunaga (2012), Dewetting of silica surfaces upon reactions with supercritical CO_2 and brine: Pore-scale studies in micromodels, *Environ. Sci. Technol.*, *46*(7), 4228–4235.

Kogure, T., O. Nishizawa, S. Chiyonobu, Y. Yazaki, S. Shibatani, and Z. Xue (2013), Effect of sub-core scale heterogeneity on relative permeability curves of porous sandstone in a water-supercritical CO_2 system, *Energy Procedia*, *37*, 4491–4498.

Krevor, S. C. M., R. Pini, B. Li, and S. M. Benson (2011), Capillary heterogeneity trapping of CO_2 in a sandstone rock at reservoir conditions, *Geophys. Res. Lett.*, *38*, L15401, doi:10.1029/2011GL048239.

Krevor, S. C. M., R. Pini, L. Zuo, and S. M. Benson (2012), Relative permeability and trapping of CO_2 and water in sandstone rocks at reservoir conditions, *Water Resour. Res.*, *48*, W02532, doi:10.1029/2011WR010859.

Kuehn, M., U. J. Gaerke, J. T. Birkholzer, and O. Kolditz (2012), The CLEAN project in the context of CO_2 storage and enhanced gas recovery, *Environ. Earth Sci.*, *67*(2), 307–310.

Kwok, D. Y., and A. W. Neumann (1999), Contact angle measurement and contact angle interpretation, *Adv. Colloid Interface Sci.*, *81*(3), 167–249.

Land, C. (1968), Calculation of imbibition relative permeability for two- and three-phase flow from rock properties, *Soc. Pet. Eng. J.*, *8*(2), 149–156.

Landrot, G., J. B. Ajo-Franklin, L. Yang, S. Cabrini, and C. I. Steefel (2012), Measurement of accessible reactive surface area in a sandstone, with application to CO_2 mineralization, *Chem. Geol.*, *318–319*, 113–125.

Laplace, P.-S. (1806), *Mécanique Céleste*, Supplement to 10th Book, Duprat, Paris.

Lenhard, R. J., T. G. Johnson, and J. C. Parker (1993), Experimental observations of nonaqueous-phase liquid subsurface movement, *J. Contam. Hydrol.*, *12*(1–2), 79–101.

Leverett, M. C. (1941), Capillary behavior in porous solids, *Pet. Trans. AIME*, *142*, 152–169.

Li, S., M. Dong, Z. Li, S. Huang, H. Qing, and E. Nickel (2005), Gas breakthrough pressure for hydrocarbon reservoir seal rocks: Implications for the security of long-term CO_2 storage in the Weyburn field, *Geofluids*, *5*, 326–334.

Li, X., E. Boek, G. C. Maitland, and J. P. M. Trusler (2012a), Interfacial tension of (brines + CO_2): (0.864 NaCl + 0.136 KCl) at temperatures between (298 and 448) K, pressures between (2 and 50) MPa, and total molalities of (1 to 5) mol·kg^{-1}, *J. Chem. Eng. Data*, *57*(4), 1078–1088.

Li, X., E. S. Boek, G. C. Maitland, and J. P. M. Trusler (2012b), Interfacial tension of (brines + CO_2): $CaCl_2$(aq), $MgCl_2$(aq), and Na_2SO_4(aq) at temperatures between (343 and 423) K, pressures between (2 and 50) MPa, and molalities of (0.5 to 5) mol·kg^{-1}, *J. Chem. Eng. Data*, *57*(5), 1369–1375.

Li, Y., J. Q. Pham, K. P. Johnston, and P. F. Green (2007), Contact angle of water on polystyrene thin films: Effects of CO_2 environment and film thickness, *Langmuir*, *23*, 9785–9793.

Li, Z., M. Dong, S. Li, and S. Huang (2006), CO_2 sequestration in depleted oil and gas reservoirs—Caprock characterization and storage capacity, *Energy Convers. Manage.*, *47*(11–12), 1372–1382.

Lindeberg, E., and D. Wessel-Berg (1997), Vertical convection in an aquifer column under a gas cap of CO_2, *Energy Convers. Manage*, *38*, 229–234.

Liu, S. Y., X. N. Yang, and Y. Qin (2010), Molecular dynamics simulation of wetting behaviour at CO_2/water/solid interfaces, *Chin. Sci. Bull.*, *55*, 2252–2257.

Lombardi, S., L. K. Altunina, S. E. Beaubien, and J. M. Pearce (2006), What can we learn from natural analogues?, in *Advances in the Geological Storage of Carbon Dioxide. Nato Science Series: IV: Earth and Environmental Sciences*, vol. 65, pp. 127–139, Springer, Netherlands.

Longeron, D., W. Hammervold, and S. Skjaeveland (1995), Water-oil capillary pressure and wettability measurements using micropore membrane technique, paper SPE 30006 presentend at the International Meeting on Petroleum Engineering, Soc. of Pet. Eng., Beijing.

Love, J. C., L. A. Estroff, J. K. Kriebel, R. G. Nuzzo, and G. M. Whitesides (2005), Self-assembled monolayers of thiolates on metals as a form of nanotechnology, *Chem. Rev.*, *105*, 1103–1169.

Lu, J., M. Wilkinson, R. S. Haszeldine, and A. E. Fallick (2009), Long-term performance of a mudrock seal in natural CO_2 storage, *Geology*, *37*(1), 35–38.

Mahadevan, J. (2012), Comments on the paper titled "Contact angle measurements of CO_2-water-quartz/calcite systems in the perspective of carbon sequestration: A case of contamination?" *Int. J. Greenhouse Gas Control*, *7*, 261–262.

Maloney, D. R., M. M. Honarpour, and A. D. Brinkmeyer (1990), The effects of rock characteristics on relative permeability, *Top. Rep. NIPER-441*, IIT Res. Inst., Natl. Inst. for Pet. and Energy Res., Batlesville, Okla.

Manrique, E. J., V. E. Muci, and M. E. Gurfinkel (2007), EOR field experiences in carbonate reservoirs in the United States, *SPE Reservoir Eval. Eng.*, *10*(6), 667–686.

McCaffery, F. G., and D. W. Bennion (1974), The effect of wettability on two phase relative permeabilities, *J. Can. Pet. Eng.*, *13*(4), 42–53.

McCaughan, J., S. Iglauer, and F. Bresme (2013), Molecular dynamics simulation of water/CO_2-quartz interfacial properties: Application to subsurface gas injection, *Energy Procedia*, *37*, 5387–5402.

Mills, J., M. Riazi, and M. Sohrabi (2011), Wettability of common rock-forming minerals in a CO2-brine system at reservoir conditions, paper SCA 2011-06 presented at the International Symposium of the Society of Core Analysts, Austin, Tex., 18–21 Sept.

Morrow, N. R. (1970), Physics and thermodynamics of capillary action in porous media, *Ind. Eng. Chem.*, *62*(6), 32–56.

Morrow, N. R. (1976), Capillary pressure correlations for uniformly wetted porous media, *J. Can. Pet. Technol.*, *15*(4), 49–69.

Morrow, N. R. (1990), Wettability and its effect on oil recovery, *JPT J. Pet. Technol.*, *42*(12), 1476–1484.

Myshakin, E. M., W. A. Saidid, V. N. Romanov, R. T. Cygan, and K. D. Jordan (2013), Molecular dynamics simulations of carbon dioxide inter-calaction in hydrated Na-montmorillonite, *J. Phys. Chem. C*, *117*, 11,028–11,039.

Norden, B., A. Föster, D. Vu-Huang, F. Marcelis, N. Springer, and I. Le Nir (2010), Lithological and petrophysical core-log interpretation in CO2SINK, the European CO_2 onshore research storage and verification project, *SPE Reservoir Eval. Eng.*, *13*(2), 172–192.

Oak, M. J., L. E. Baker, and D. C. Thomas (1990), Three-phase relative permeability of Berea sandstone, *JPT J. Pet. Technol.*, *42*(8), 1054–1061.

Pedersen, K. S., and P. L. Christensen (2007), *Phase Behaviour of Petroleum Reservoir Fluids*, Taylor and Francis, Boca Raton, Fla.

Pentland, C., S. Iglauer, O. Gharbi, K. Okada, and T. Suekane (2012), The influence of pore space geometry on the entrapment of carbon dioxide by capillary forces, paper SPE 158516 presented at the SPE Asia Pacific Oil and Gas Conference and Exhibition, Soc. of Pet. Eng., Perth, Australia.

Pentland, C. H., E. Itsekiri, S. Al-Mansoori, S. Iglauer, B. Bijeljic, and M. J. Blunt (2010), Measurement of nonwetting-phase trapping in sand-packs, *SPE J.*, *15*(2), 274–281.

Pentland, C. H., R. El-Maghraby, S. Iglauer, and M. J. Blunt (2011), Measurements of the capillary trapping of super-critical carbon dioxide in Berea sandstone, *Geophys. Res. Lett.*, *38*, L06401, doi:10.1029/2011GL046683.

Perrin, J.-C., and S. Benson (2010), An experimental study on the influence of sub-core scale heterogeneities on CO_2 distribution in reservoir rocks, *Trans. Porous Media*, *82*(1), 93–109.

Pini, R., and S. M. Benson (2013), Simultaneous determination of capillary pressure and relative permeability curves from core-flooding experiments with various fluid pairs, *Water Resour. Res.*, *49*, 3516–3530, doi:10.1002/wrcr.20274.

Pini, R., S. C. M. Krevor, and S. M. Benson (2012), Capillary pressure and heterogeneity for the CO_2/water system in sandstone rocks at reservoir conditions, *Adv. Water Resour.*, *38*, 48–59.

Plug, W., and J. Bruining (2007), Capillary pressure for the sand-CO_2-water system under various pressure conditions: Application to CO_2 sequestration, *Adv. Water Resour.*, *30*(11), 2339–2353.

Por, G. J., P. Boerrigter, J. G. Maas, and A. de A. Vries (1989), A fractured reservoir simulator capable of modeling block-block interaction, paper SPE 19807 presented at SPE Annual Technical Conference and Exhibition, Soc. of Pet. Eng., San Antonio, Tex., 8–11 Oct.

Potocki, D., M. Ding, and A. Kantzas (2003), Carbonate rock wettability interpreted from capillary pressure and imbibition resistivity index analysis, paper SCA 2003-03 presented at the International Symposium of the Society of Core Analysts, Pau, France, 21–24 Sept.

Pruess, K. (2008a), Leakage of CO_2 from geologic storage: Role of secondary accumulation at shallow depth, *Int. J. Greenhouse Gas Control*, *2*(1), 37–46.

Pruess, K. (2008b), On CO_2 fluid flow and heat transfer behavior in the subsurface, following leakage from a geologic storage reservoir, *Environ. Geol.*, *54*, 1677–1686.

Pruess, K., and N. Müller (2009), Formation dry-out from CO_2 injection into saline aquifers: 1. Effects of solids precipitation and their mitigation, *Water Resour. Res.*, *45*, W03402, doi:10.1029/2008WR007101.

Purcell, W. R. (1950), Interpretation of capillary pressure data, *J. Pet. Technol.*, *2*(8), 11–12.

Pusch, G., M. Hoffmann, R., Miehe, P. Schweitzer, and J. Siebert (1985), *Untersuchungen zur Permeabilität und Porosität von Steinkohlen und Stimulation der Kohlepermeabilität durch Elektroosmose und Extraktion mittels überkritischem CO_2-Stand der Forschung*, pp. 115–131, K2G—Status—Kolloquium, Essen, Germany.

Richardson, J. G., J. K. Kerver, J. A. Hafford, and J. S. Osoba (1952), Laboratory determination of relative permeability, *J. Pet. Technol.*, *4*(8), 187–196.

Riding, J. B. (2006), The IEA Weyburn CO_2 monitoring and storage project, in *Advances in the Geological Storage of Carbon Dioxide* [online], vol. 65, edited by S. Lombardi, L. K. Altunina, and S. E. Beaubien, pp. 221–230, Kluwer Acad., Dordrecht. [Available at http://rd.springer.com/chapter/10.1007/1–4020-4471-2_18, last accessed 5 Nov. 2013.]

Ringrose, P., M. Atbi, D. Mason, M. Espinassous, Ø. Myhrer, M. Iding, A. Mathieson, and I. Wright (2009), Plume development around well KB-502 at the In Salah CO_2 storage site, *First Break*, *27*(1), 85–89.

Roof, J. G. (1970), Snap-off of oil droplets in water-wet pores, *SPE J.*, *10*(1), 85–90.

Rose, W., and W. A. Bruce (1949), Evaluation of capillary character in petroleum reservoir Rock, *Trans. AIME*, *186*, 127–142.

Sabirzyanov, A. N., A. P. Il'in, A. R. Akhunov, and F. M. Gumerov (2002), Solubility of water in supercritical carbon dioxide, *High Temp.*, *40*(2), 203–206.

Saraji, S., L. Goual, M. Piri, and H. Plancher (2013), Wettability of supercritical carbon dioxide/water/quartz systems: Simultaneous measurement of contact angle and interfacial tension at reservoir conditions, *Langmuir*, *29*, 6856–6866.

Saraji, S., M. Piri, and L. Goual (2014), The effects of SO_2 contamination, brine salinity, pressure, and temperature on dynamic contact angles and interfacial tension of CO_2/brine/quartz systems, *Int. J. Greenhouse Gas Control*, *28*, 147–155.

Sarmadivaleh, M., and S. Iglauer (2014), Capillary pressure measurements for CO_2, brine and Berea sandstone at reservoir conditions, paper presented at the 4th EAGE CO_2 Geological Storage Workshop, Stavanger, Norway, 22–24 Apr.

Schlömer, S., and B. M. Krooss (1997), Experimental characterisation of the hydrocarbon sealing efficiency of cap rocks, *Mar. Pet. Geol.*, *14*, 565–580.

Schowalter, T. T. (1979), Mechanics of secondary hydrocarbon migration and entrapment, *AAPG Bull.*, *63*(5), 723–760.

Schwartz, A. M. (1969), Capillarity—Theory and practice, *Ind. Eng. Chem.*, *61*(1), 10–21.

Shah, V., D. Broseta, and G. Mouronval (2008), Capillary alteration of caprocks by acid gases, paper presented at Symposium on Improved Oil Recovery SPE/DOE, Tulsa, Okla.

Shi, J.-Q., Z. Xue, and S. Durucan (2011), Supercritical CO_2 core flooding and imbibition in Tako sandstone—Influence of sub-core scale heterogeneity, *Int. J. Greenhouse Gas Control*, *5*(1), 75–87.

Siemons, N., H. Bruining, H. Castelijns, and K.-H. Wolf (2006), Pressure dependence of the contact angle in a CO_2-H_2O-coal system, *J. Colloid Interface Sci.*, *297*(2), 755–761.

Silin, D., L. Tomutsa, S. M. Benson, and T. W. Patzek (2011), Microtomography and pore-scale modeling of two-phase fluid distribution, *Transp. Porous Media*, *86*(2), 495–515.

Span, R., and W. Wagner (1996), A new equation of state for carbon dioxide covering the fluid region from the triple-point temperature to 1100 K at pressures up to 800 MPa, *J. Phys. Chem. Ref. Data*, *25*(6), 1509–1596.

Spiteri, E. J., R. Juanes, M. J. Blunt, and F. M. Orr Jr. (2008), A new model of trapping and relative permeability hysteresis for all wettability characteristics, *SPE J.*, *13*(3), 277–288.

Suekane, T., N. Zhou, and T. Hosokawa (2011), Maximization of capillary trapping ratio to injected CO_2 by means of co-injection, *Energy Procedia*, *4*, 4260–4266.

Sutjiadi-Sia, Y., P. Jaeger, and R. Eggers (2008), Interfacial phenomena of aqueous systems in dense carbon dioxide, *J. Supercrit. Fluids*, *46*, 272–279.

Tanino, Y., and M. J. Blunt (2013), Laboratory investigation of capillary trapping under mixed-wet conditions, *Water Resour. Res.*, *49*, 4311–4319, doi:10.1002/wrcr.20344.

Thomas, L. K., D. L. Katz, and M. R. Tek (1967), Threshold pressure phenomena in porous media, paper presented at the SPE 42nd Annual Fell Meeting, Soc. of Pet. Eng., Houston, Tex.

Tokunaga, T. K., and J. Wan (2013), Capillary pressure and mineral wettability influences on reservoir CO_2 capacity, *Rev. Mineral. Geochem.*, *77*, 481–503.

Tokunaga, T. K., J. Wan, J.-W. Jung, T. W. Kim, Y. Kim, and W. Dong (2013), Capillary pressure and saturation relations for supercritical CO_2 and brine in sand: High-pressure Pc(Sw) controller/meter measurements and capillary scaling predictions, *Water Resour. Res.*, *49*, 4566–4579, doi:10.1002/wrcr.20316.

Tonnet, N., D. F. Broseta, and G. Mouronval (2010), Evaluation of petrophysical properties of a carbonate-rich caprock for CO_2 geological storage purposes, paper presented at SPE EUROPEC/EAGE Annual Conference and Exhibition, Soc. of Pet. Eng., Barcelona, Spain.

Treiber, L. E., and W. W. Owens (1972), A laboratory evaluation of the wettability of fifty oil-producing reservoirs, *Soc. Pet. Eng. J.*, *12*(6), 531–540.

Tsuji, S., Y. Liang, M. Kunieda, S. Takahashi, and T. Matsuoka (2013), Molecular dynamics simulations of the CO_2-water-silica interfacial systems, *Energy Procedia*, *37*, 5435–5442.

Tucker, O., P. Garnham, P. Wood, W. Berlang, and I. Susanto (2013), Development of an offshore monitoring plan for a commercial CO_2 storage pilot, *Energy Procedia*, *37*, 4317–4335.

US National Institute for Occupational Safety and Health (NIOSH) (2014). [Available at http://www.cdc.gov/niosh/idlh/7783064.html, last accessed 3 Oct. 2014.]

Waldmann, S., A. Busch, K. van Ojik, and R. Gaupp (2014), Importance of mineral surface areas in Rotliegend sandstones for modeling CO_2-water-rock interactions, *Chem. Geol.*, *378–379*, 89–109.

Wang, S., and A. F. Clarens (2012), The effects of CO_2-brine rheology on leakage processes in geologic carbon sequestration, *Water Resour. Res.*, *48*, W08518, doi:10.1029/2011WR011220.

Wang, S., I. M. Edwards, and A. F. Clarens (2013a), Wettability phenomena at the CO_2-brine-mineral interface: Implications for geologic carbon sequestration, *Environ. Sci. Technol.*, *47*(1), 234–241.

Wang, S., Z. Tao, S. Persily, and A. F. Clarens (2013b), CO_2 adhesion on hydrated mineral Surfaces, *Environ. Sci. Technol.*, *47*(20), 11,858–11,865.

Watts, N. L. (1987), Theoretical aspects of cap-rock and fault seals for single- and two-phase hydrocarbon columns, *Mar. Pet. Geol.*, *4*, 274–307.

Welge, H. J. (1949), Displacement of oil from porous media by water or gas, *Trans. AIME*, *179*(1), 133–145.

Wenk, H.-R., M. Voltolini, M. Mazurek, L. R. Van Loon, and A. Vinsot (2008), Preferred orientations and anisotropy in shales: Callovo-Oxfordian shale (France) and Opalinus clay (Switzerland), *Clays Clay Miner.*, *56*(3), 285–306.

Wenzel, R. N. (1949), Surface roughness and contact angle, *J. Phys. Colloid Chem.*, *53*(9), 1466–1467.

Wesch, A., N. Dahmen, K. Ebert, and J. Schön (1997), Grenzflächenspannungen, Tropfengrößen und Kontaktwinkel im Zweiphasensystem H_2O/CO_2 bei Temperaturen von 298 bis 333 K und Drücken bis 30 MPa, *Chem. Ingenieur Tech.*, *69*(7), 942–946.

Whyman, G., E. Bormashenko, and T. Stein (2008), The rigorous derivation of Young, Cassie-Baxter and Wenzel equations and the analysis of the contact angle hysteresis phenomenon, *Chem. Phys. Lett.*, *450*, 355–359.

Wildenschild, D., and A. P. Sheppard (2013), X-ray imaging and analysis techniques for quantifying pore-scale structure and processes in subsurface porpus medium systems, *Adv. Water Resour.*, *51*, 217–246.

Wollenweber, J., S. A. Alles, A. Kronimus, A. Busch, H. Stanjek, and B. M. Krooss (2009), Caprock and overburden processes in geological CO_2 storage: An experimental study on sealing efficiency and mineral alterations, *Energy Procedia*, *1*(1), 3469–3476.

Wollenweber, J., S. Alles, A. Busch, B. M. Krooss, H. Stanjek, and R. Littke (2010), Experimental investigation of the CO_2 sealing efficiency of caprocks, *Int. J. Greenhouse Gas Control*, *4*(2), 231–241.

Wunderlich, R. W. L. E. (1991), Obtaining samples with preserve wettability in *Interfacial Phenomena in Petroleum Recovery*, edited by N. R. Morrow, Marcel Dekker, N. Y.

Xu, T., Y. K. Kharaka, C. Doughty, B. M. Freifeld, and T. M. Daley (2010), Reactive transport modeling to study changes in water chemistry induced by CO_2 injection at the Frio-I Brine Pilot, *Chem. Geol.*, *271*(3–4), 153–164.

Yang, D., Y. Gu, and P. Tontiwachwuthikul (2008), Wettability determination of the reservoir brine—Reservoir rock system with dissolution of CO_2 at high pressures and elevated temperatures, *Energy Fuels*, *22*(1), 504–509.

Young, T. (1805), An essay on the cohesion of fluids, *Philos. Trans. R. Soc. London*, *95*, 65–87.

Yu, L., and N. C. Wardlaw (1986), The influence of wettability and critical pore-throat size ratio on snap-off, *J. Colloid Interface Sci.*, *109*(2), 461–472.

Yuan, Y., and T. R. Lee (2013), Contact angle and wetting properties, in *Surface Science Techniques, Springer Series in Surface Sciences*, vol. 51, edited by G. Bracco and B. Holst, pp. 3–34, Springer, Berlin.

Zemke, K., A. Liebscher, and M. Wandrey (2010), Petrophysical analysis to investigate the effects of carbon dioxide storage in a subsurface saline aquifer at Ketzin, Germany (CO2SINK), *Int. J. Greenhouse Gas Control*, *4*(6), 990–999.

Zhuravlev, L. T. (2000), The surface chemistry of amorphous silica. Zhuravlev model, *Colloids Surf. A*, *173*, 1–38.

Zweigel, P., E. Lindeberg, A. Moen, and D. Wessel-Berg (2004), Towards a methodology for top seal efficacy assessment for Underground CO_2 Storage, paper presented at the 7th International Conference on Greenhouse Gas Control Technologies (GHGT-7), Vancouver, B. C., Canada.

Zuo, L., C. Zhang, R. W. Falta, and S. M. Benson (2013), Micromodel investigations of CO_2 exsolution from carbonated water in sedimentary rocks, *Adv. Water Resour.*, *53*, 188–197.